Tomas Bata University in Zlín
Faculty of Technology

Doctoral Thesis

Applied Rheology for Characterization of Polymeric Nanofiber Based Filters

Aplikovaná reologie pro charakterizaci
polymerních nanovlákenných filtrů

Wannes Sambaer

March 2012

Zlín, Czech Republic

Study program: P 2808 Chemistry and Material Technology

                      2808V006 Technology of Macromolecular Substances

Supervisor: Prof. Ing. Martin Zatloukal, Ph.D.

Consultant: Ing. Frederik Desplentere, Ph.D.

CONTENT

ABSTRACT

In the first part of this work, the current stage of knowledge in areas of nanofiber nonwoven production, applications, characterization with specific attention to air filtration modeling, creation of 3D filter models, importance of Brownian diffusion and aerodynamic slip has been reviewed based on the open research literature.

In the second part of this work, polymeric nanofiber based filters created by electrospinning process utilizing wire based rotation electrode have been investigated by using newly developed experimental and theoretical methods in order to understand the complicated link between filter morphology and mechanical properties. It has been found that the supporting textile type, utilized during electrospinning process, has a strong effect on the polyurethane nanofiber filter porosity and their mechanical characteristics even if the fiber diameter distributions of the manufactured filters were similar. A novel 3D filtration model for polymer nanofiber based filter (utilizing particle-fiber/particle-particle interactions, transition/free molecular flow regime, Brownian diffusion and realistic scanning electron microscope image based 3D structure model) has been proposed and successfully tested. It has been found that the particle-fiber friction coefficient has much higher effect on filtration efficiency of polymer nanofiber based filters than air velocity, viscosity, temperature, pressure and its decrease leads to higher pressure drop, lower filtration efficiency, lower quality factor and lower quality factor sensitivity to the increased collected particle mass.

ABSTRAKT

První část této práce shrnuje současný stav poznání v oblasti přípravy, charakterizace a aplikovatelnosti nanovlákenných netkaných textilií se specifickým důrazem na modelování procesu filtrace vzduchu, tvorbu 3D filtračních modelů, významnost Brownova difuzního pohybu a aerodynamického skluzu.

Druhá část této práce se zabývá výzkumem polymerních nanovlákenných filtrů (vyrobených elektrostatickým zvlákňováním pomocí drátové rotační elektrody) s využitím nově vyvinutých experimentálních a teoretických metod s cílem porozumět komplikovanému vztahu mezi morfologickými a mechanickými charakteristikami. Bylo zjištěno, že typ použité podpůrné textilie při elektrostatickém zvlákňování ovlivňuje jak porozitu vyrobených polyurethanových nanovlákenných filtrů tak jejich mechanické vlastnosti, a to i přesto, že distribuce průměrů vláken se prakticky nezměnila. Byl vyvinut a úspěšně otestován nový 3D filtrační model pro polymerní nanovlákenné filtry beroucí v úvahu interakce typu částice-vlákno/částice-částice, molekulární charakter toku, Brownův difuzní pohyb včetně realistické 3D struktury filtru vytvořené ze snímku skenovací elektronové mikroskopie. Bylo zjištěno, že koeficient tření mezi filtrovanými částicemi a povrchem polymerních vláken má mnohem větší vliv na filtrační účinnost polymerních nanovlákenných filtrů než rychlost proudění vzduchu, viskozita, teplota a tlak, přičemž jeho pokles má za následek zvýšení tlakové ztráty, nižší filtrační účinnost, nižší faktor filtrační kvality a nižší citlivost faktoru filtrační kvality na množství zachycených částic.

Klíčová slova: Polymerní nanovláknové filtry • Elektrostatické zvlákňování • 3D modelování procesu filtrace • Modelování aerodynamického skluzu

LIST OF PAPERS

The following papers are included in the present doctoral thesis:

PAPER I

The use of novel digital image analysis technique and rheological tools to characterize nanofiber nonwovens

Wannes Sambaer, Martin Zatloukal and Dusan Kimmer

Polymer Testing 2010, vol.29, no.1, p.82-94.

PAPER II

3D modeling of filtration process via polyurethane nanofiber based nonwoven filters prepared by electrospinning process

Wannes Sambaer, Martin Zatloukal and Dusan Kimmer

Chemical Engineering Science 2011, vol.66, no.4, p.613-623.

PAPER III

3D air filtration modeling for nanofiber based filters in the ultrafine particle size range

Wannes Sambaer, Martin Zatloukal and Dusan Kimmer

Submitted for publication in *Chemical Engineering Science* in 2011.

PAPER IV

3D clogging modeling of polyurethane nanofiber based filters by ultrafine aerosol particles

Wannes Sambaer, Martin Zatloukal and Dusan Kimmer

Submitted for publication in *Chemical Engineering Science* in 2012.

THEORETICAL BACKGROUND

1. Nanofiber Nonwoven Production and Applications

1.1 Nanofiber Nonwoven

Nanofiber nonwovens, also called nanofiber textiles or mat are nonwovens created from nanofibers. Nanofibers might be defined as *fibers with diameters in the order of 100 nanometers*. Those nanofibers can mainly be produced by electrospinning, also known as electrostatic spinning, and meltblowing, each extended with its own variations. A nonwoven is defined as "*a manufactured sheet, web or mat of directionally or randomly oriented fibers, bonded by friction, and/or cohesion and/or adhesion, excluding paper or products which are woven, knitted, tufted stitch bonded incorporating binding yarns or filaments, or felted by wet milling, whether or not additionally needled. The fibers may be of natural or man-made origin. They may be staple or continuous or be formed in situ.*" according to the International Organization for Standardization [1].

A typical SEM image of a standard nanofiber nonwoven produced by the electrospinning process, which will be discussed in the next section, is shown in Figure 1.
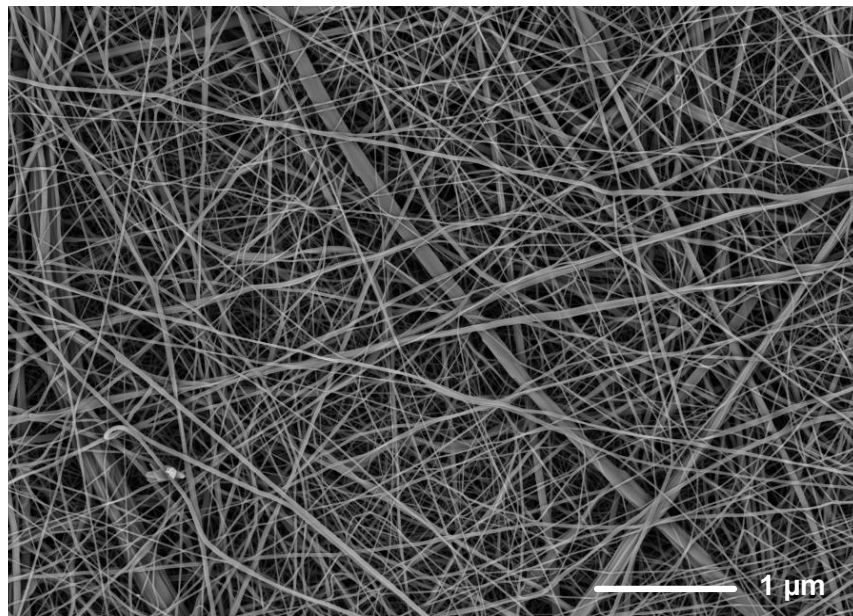

Figure 1:   An example of a nanofiber nonwoven produced by electrospinning from a polyurethane solution.

1.2 Electrospinning

There are many different techniques to create polymer fibers but only electrospinning and in some conditions meltblown technologies are used to produce fibers which can be classified as nanofibers.

The advantage of electrospinning is the ability to produce continuous thin fibers from a wide range of polymer solutions or polymer melts [2] with different morphological and mechanical properties. In the following sections the electrospinning process and possible obtained fibers as well as its equipment will be viewed in more detail.

Electrospinning Process

Despite popular belief electrospinning is not a new technique. The first documents regarding this technique can be found in the beginning of the last century. J. F. Cooly [3] and W.J. Morton [4] obtained a U.S. patent in February and July 1902, respectively. Illustrations of their principle are shown in Figure 2. Both sketches show a positive and negative electrode with a polymer solution, which is spun into fibers and accumulated on a collector.
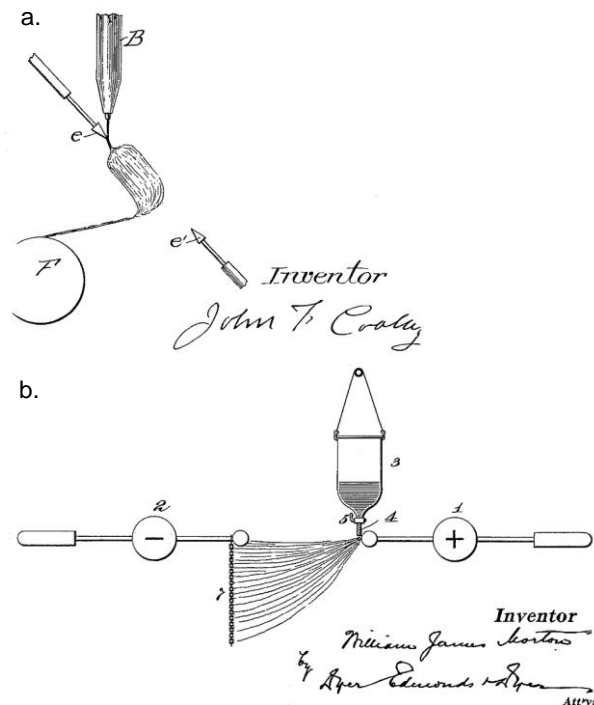

Figure 2:   Illustrations from the first two patents about electrospinning:
a. J. F. Cooly - U.S patent 692, 631[3] and
b. W.J. Morton - U.S patent 705,691[4].

Nowadays, the method of electrospinning is better understood and the equipment is better developed. The necessary parts for the production of nanofibers by electrospinning are simplified illustrated in Figure 3. These main components are the high voltage supply, the electrode, the polymer solution and the collector plate whether covered with a supporting textile or not.
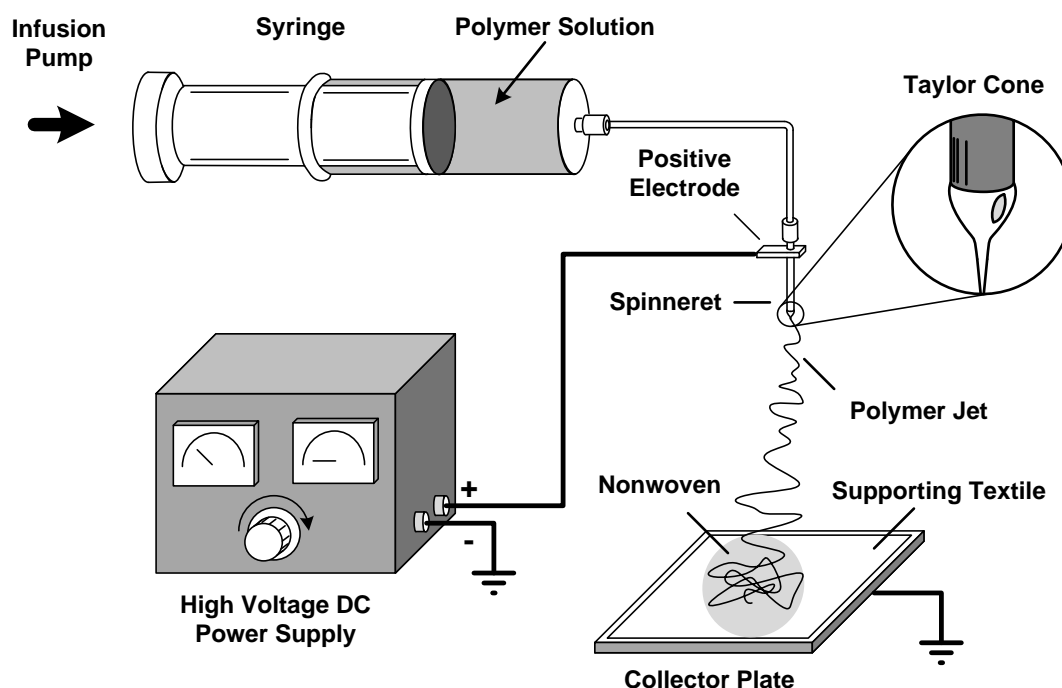

Figure 3: Illustration of the electrospinning principle. Figure based on [5].

The electrospinning process starts with the creation of a fiber or jet and was divided according Reneker et al. [6] in four stages. During the first stage the *jet is launched*, where the charging of a polymer solution droplet is essential. This droplet is pumped through the capillary or formed on an electrode, which is connected to the positive voltage as shown in Figure 3. A droplet is located at a certain distance from a grounded collector plate which can be covered with a supporting material. The droplet will deform due to the electrical field between the electrode and collector, which is created by the high voltage DC power supply. At a certain critical voltage the shape of the droplet will deform to a cone-like shape, so called Taylor cone, due to the migration of positive charged species to the surface and negative charged species to the core. During the transition of shape, extensional forces are induced which can lead to the formation of a straight segment of the jet on top of this cone. In this stage more fibers [7] or even branched fibers [8] can be initiated from a single droplet.

9

In the third stage an *elongation of the straight segment* will take place. The velocity in the jet increases when its position gets further away from the Taylor cone and as a result of this, the jet diameter decreases fast due to extension forces as well as due to evaporation of the solvent. This step is followed by the *development of instabilities* were the stretched straight segment becomes unstable and starts to bend. Together with the further evaporation of the solvent the *diameter* will *reduce* further. In the final step, the *solidification* of the fiber takes place, which is highly influenced by the vapor pressure of the solvent. When finally the nanofiber gets in contact with the collector, continues fibers will build up a nonwoven.

During the electrospinning process numerous of parameters have effect on the quality of the created nanofiber. These parameters can be related to the environment, collector (e.g. geometry or material), process settings (e.g. feed rate, applied voltage or gap distance) and/or the polymer solution. The requirements to make a spinnable polymer solution are fulfilled when the polymer has a high enough average molecular weight and an open chain-like geometry as well as a good solvability. Additionally, the polymer has to be solved in a high enough concentration of solvent, which has a suitable conductivity, surface tension and vapor pressure.

Nanofiber Structures

The thickness of a mat is easily to control by adjusting the collection time during the electrospinning process. Beside this, the structure of the fibers or nonwoven morphology can be adjusted by changing process and/or material parameters. When nanofibers are produced under optimal conditions, then the fiber will be continuous without defects called beads. However, the controlled production of these beads can lead to positive properties and is used in several applications (e.g. composite structures [9] and filters).

Significant number of various nanofiber and nanofiber structures can be created by using different materials and processing conditions. In the following figure (see Figure 4) some SEM images of normal and stretched polyurethane fibers (a-b), as well as fibers for filters (c-d) and some special type of fibers with surface porosity (e-f), carbon nanowebs (h) and hollow fibers (g) are demonstrated.
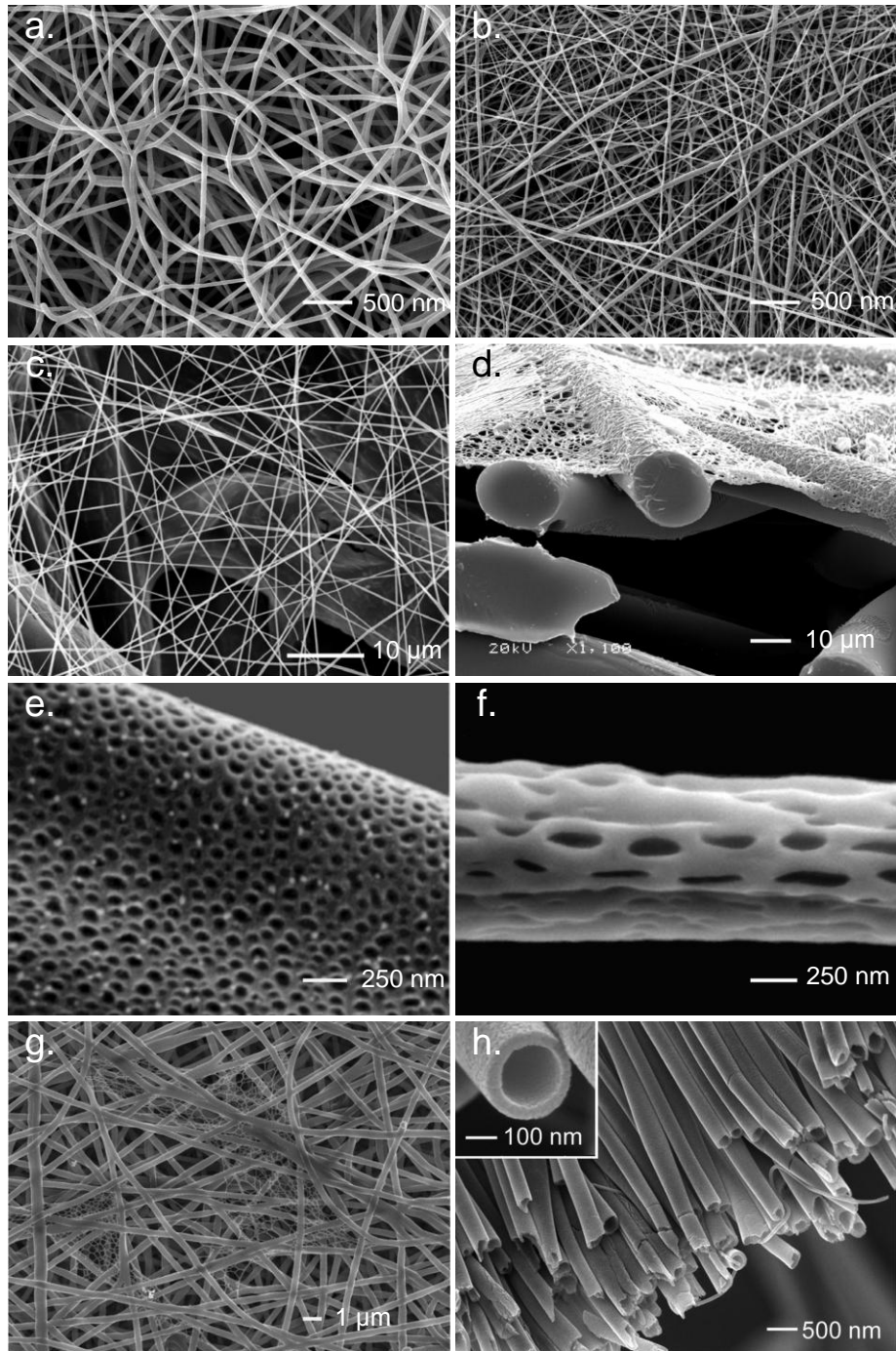
Figure 4:   Normal and stretched PUR fibers (a-b), filter morphology (c-d[11]) fibers with surface porosity (e[12]-f[13]), carbon nanowebs (h[14]) and hollow fibers (g[15]).

Electrospinning Equipment

Through this Ph.D. work the nanofiber based nonwovens created from polyurethane (PUR) solutions were prepared by electrospinning. For this purpose the commercially available NanoSpider[TM] (Elmarco s.r.o. Liberec, Czech Republic) has been utilized with a special adjusted wire rotational electrode. The fibers were collected on a moving supporting textile. A principle sketch of the used equipment, completed with the indication of the most important parts, is shown in Figure 5.
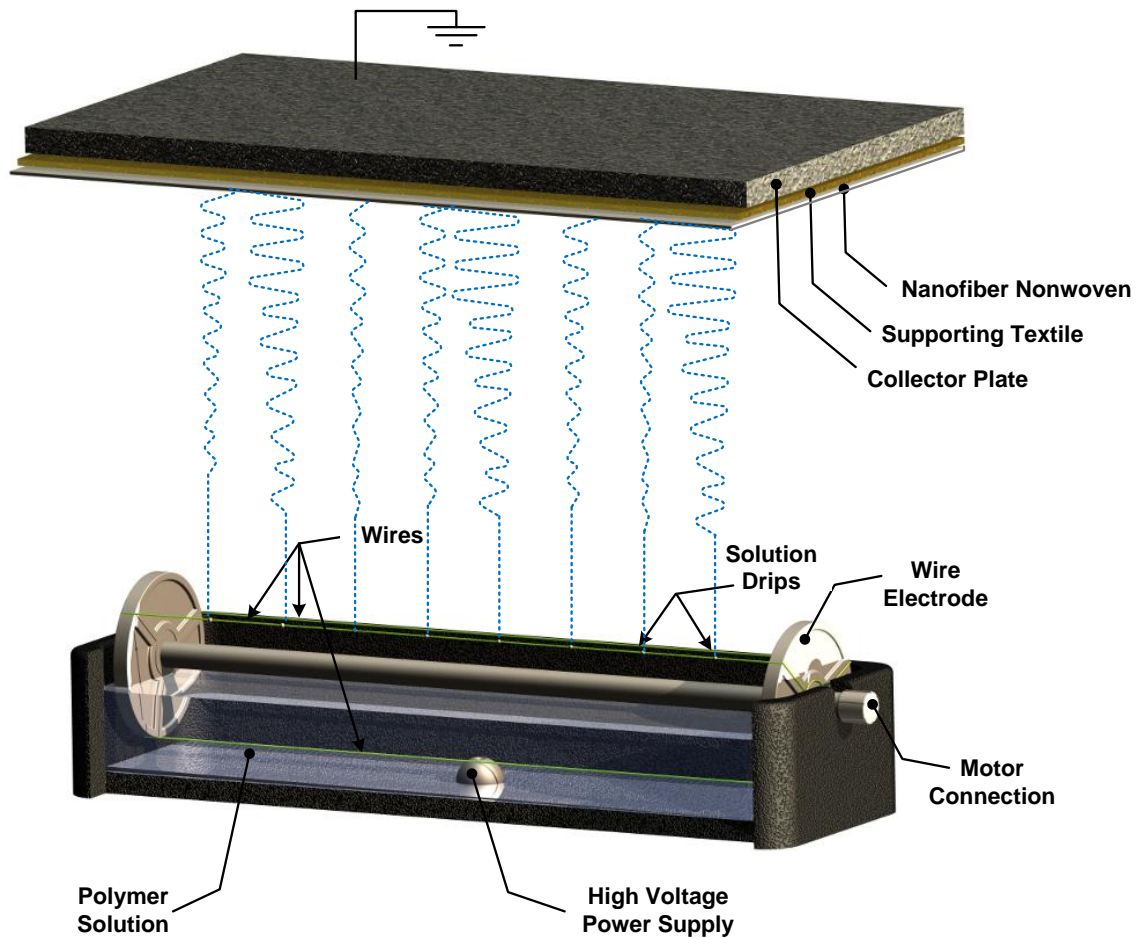

Figure 5: Electrospinning equipment with rotational wire electrode and moving support textile.

1.3 Nanofiber Applications

Nowadays, nanofibers are already used in a wide range of applications. Figure 6 gives a general overview [16] of the possible applications of nanofiber based nonwovens. The largest application group of nanofibers based nonwovens is the medical industry (e.g. drug delivery, tissue engineering and wound dressing) followed by filtration applications [17-18] and composite reinforcements. During this thesis the attention will be paid to the filter media characterization and filter performance.
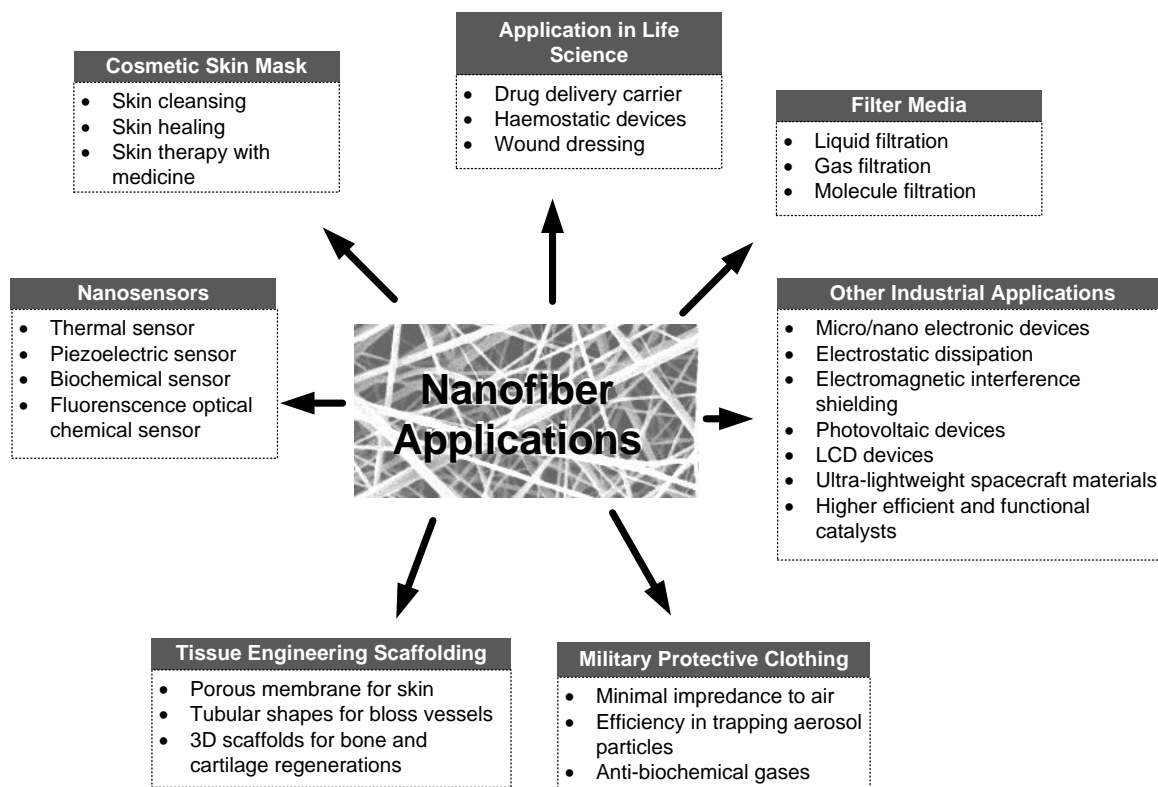
Figure 6: General overview from nanofiber applications. Figure based on [16].

Filtration Applications

Nanofiber nonwovens are promising materials, especially for filtration applications due to their small fiber diameters creating a larger surface area, which basically lead to higher filtration efficiency. In addition, the low resistance to airflow of the nonwovens induced by aerodynamic slips around the nanofibers leads to a desirable smaller pressure drop over the filter. Low mechanical properties of nanofiber nonwovens can be overcome if necessary by combination with a support textile or with other fibers having enhanced mechanical properties [19].

Practical examples of filtration applications are personal masks for inhalation protection, air cleaning in industrial effluents or electronic equipment, vacuum cleaners, air purifiers, engine filtration and in maintaining clean room manufacturing environments. Another interesting field is reactive textile fibers which are able to interact with chemicals in air.

The growing interest in filtration applications and there advantages are the main reasons for the focus in this Ph.D. thesis on nanofiber nonwovens designed for air filtration.

2. Characterization of Nanofiber Nonwovens

The characterization of nanofiber nonwovens is related to the specific application of the textile. Since this Ph.D. thesis addresses mainly filtration modeling through nanofiber based nonwoven structures, the filtration performance of the nonwoven will be viewed beside mechanical properties and morphological nanofiber nonwoven features.

2.1   Mechanical Properties

Mechanical properties of a nanofiber nonwoven are highly important in range of their characterization features. The basic information about those properties can be obtained from the stress-strain curve, which is able to be measured on nanofiber based structures with universal testing machines. Those testing equipment are also used to measure the properties for films and textile based materials [19]. However, the interpretation of the data has to be done carefully because several problems can arise when nanofiber mats are measured. The first problem can be the handling of the nonwoven samples, which is complicated due to its sensitivity. Another problem is the clamping method in universal test geometries, which can introduce breakage on an unrepresentative place in the sample resulting in wrong measurements. In order to solve this clamping problem, Huang et al. [21] described a methodology to reinforce the clamping areas of the test samples with tape. Additionally, the difference in porosity in the analyzed samples can lead to difficulties. Therefore, Schreuder-Gibson et al. [22] proposed and applied a method to normalize the data to a constant volume density of fibers in the sample. For this method the thickness of the samples has to be known which can introduce an additional problem in case it is measured with a micrometer due to the compressibility of the sample and uneven surface. It has been reported [22] that this way of measuring overestimates the mat volume. To overcome this difficulty McKee et al. [23] proposed an equivalent thickness based on the area, density and mass of the sample. It has to be mentioned that the effect of orientation of the fibers have to be kept in mind during these mechanical tests.

2.2 Morphological Properties

Morphological properties of the nanofiber based textiles are related to the form and structure of the nonwoven. The main morphological characteristics are porosity, fiber orientation, pore sizes and fiber diameters distribution.

The porosity α, which is unrelated with the material characteristics, is the amount of volume taken by pores in a fiber mat. The porosity can be defined in terms of apparent density of the nanofiber mat and the bulk density of the polymer expressed as [23]:

$$\alpha = 1 - \frac{\rho_{mat}}{\rho_{polymer}}$$
(Eq. 1)

This porosity can be measured with experimental techniques, such as liquid intrusion or liquid extrusion porosimetry. These two methods are based on the needed pressure to push a liquid through the nonwoven. Those techniques are additionally able to define the poresize distribution in an indirect way. In order to avoid these indirect measurements of the pore size distribution, voluminous research has been done in the last decennia to reveal proper methodologies by using digital image analysis. According Ptak and Cady [26] this technique is the most direct technique to measure the pore size distribution, but it can only be applied on structures with straight pores perpendicular to the filter surface. This novel way of analyzing structures can also reveal information about other morphological properties such as poreshape, fiber diameter distribution, fiber orientation, among others.

Image analyses were already used to measure pore characteristics for woven textiles with an erosion method [27] and for nonwoven geotextiles by a slicing method [28]. Ziabari et al. [29] developed a methodology, which is more focused on the poresize of thin electrospun nanofiber nonwovens. In their work the assumption is made that the porosity (a three dimensional feature) is equal to the percent of open air (a two dimensional feature). Their simplicity and direct features, which do not introduce systematic errors such as the assumption that the pores are circular represents their main advantages. In addition, they allow determination of complete pore size distribution curve.

Pourdeyhimi et al. [30] developed a technique to use image analysis to characterize the fiber orientation of real nonwoven fabrics. They also developed the basic methodology to determinate the fiber diameter distribution using Euclidian distance transform, which was later improved by Ziabari et al. [31]. They eliminated the effect of intersections on the distribution which leads to more accuracy of the measurements. Tomba et al. [32] developed an artificial vision system for the automatic measurement of interfiber pore characteristics and fiber diameter distribution in nanofiber based nonwovens. The novelty of their work is that an artificial visual inspection system based on Multivariate Image Analysis (MIA) has been used to determinate the fibers which has to be analyzed. This system has been coupled with a measurement algorithm to perform the measurements of fiber and pore distributions. Facco et al. [33] presented a machine vision system for automatic characterization of the quality properties of nanofiber assemblies using digital image analysis. This technique was determined to estimate the pore size and fiber diameter distribution and permeability of a nanofiber membrane.

In order to use digital image analysis a valuable image has to be firstly created, which can be done in different ways depending on the wanted quality and resolution. In the case of nanofiber nonwovens, optical microscopy cannot be used due to limitation of the wavelength of light (450-600 nm). A better method is to use scanning electron microscopy (SEM) or transmission electron microscopy (TEM) where the wavelength is much smaller (6pm). These last two techniques can give images with a much higher resolution, 1-20 nm/px and 0.1 nm/px for SEM and TEM, respectively. The disadvantage of all this mentioned microscopy techniques are that they give only a two dimensional surface view of the fibers and pores. Also the shape in the depth direction cannot be seen properly and therefore, the measurements of the porosity can highly defer between different techniques. To avoid these disadvantages, atomic force microscopy (AFM) might be used. This technique can measure in the third dimension by the use of a needle following the fiber surface with an accuracy of 1 nm.

It has to be mentioned that not only the resolution of the picture has to be acceptable but a more important feature is the lightning of the picture. Ghasemi-Mobarakeh [25] related the threshold levels, based on the average and standard deviation of the

grayscale histogram, of a SEM image with a certain depth of the image in order to determine the porosity of various layers of nanofibers mat. Later Semnani et al. [33] used this method to predict the cell infiltration for various cell sizes, shapes and configurations.

2.3   Filtration Testing

Because of the use of nanofiber based nonwovens in filtration applications, the filtration performance properties are highly important. The main purpose for applying a filtration test on a structure based on a single layer or a complete filter is to evaluate the quality of the filter by defining the filtration efficiency and/or pressure drop. The conditions to test these parameters are prescribed in numerous standards. Beside the size of the pores and diameters of the fibers, the performance of a filter in practice (e.g. temperature, pressure, humidity, aging, charge and chemical degradation) can additionally influence its characteristics.

Sizes of common particle types which are of interest to filter are shown according their size in Figure 7. This Ph.D. thesis is mainly focused on the filtration of ultra-fine particles, defined within a range of 10 to 800 nm.
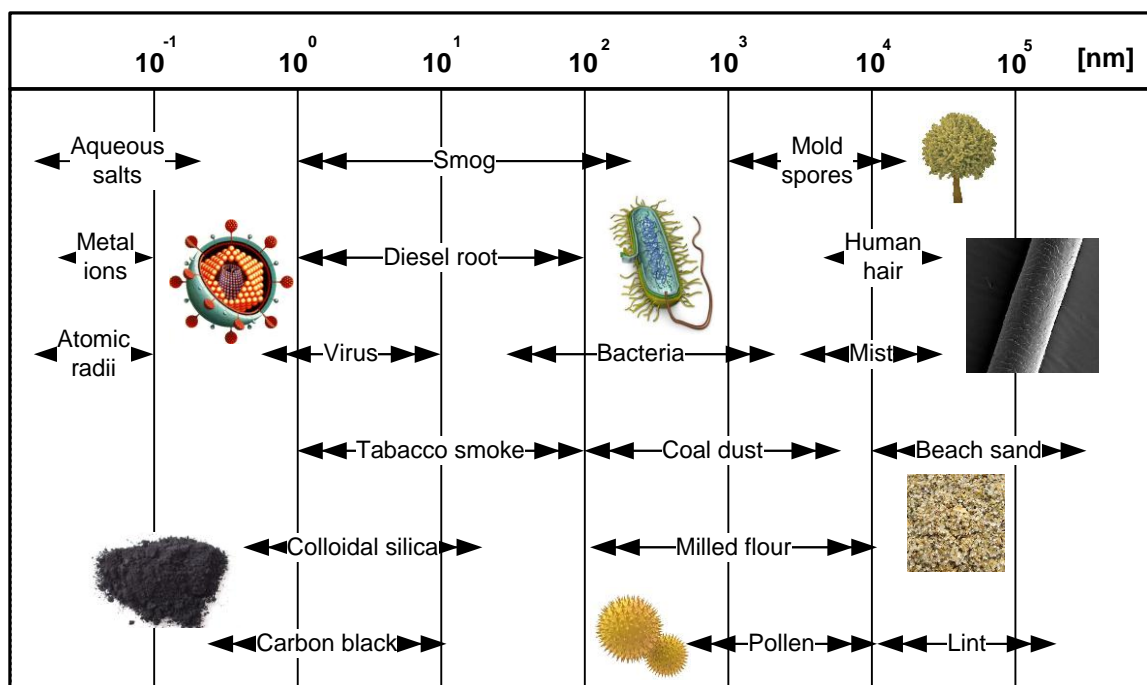

Figure 7: An overview from particle sizes. Figure based on [35].

Filtration Efficiency

A number of available test methods and methodologies that evaluate experimentally the filtration efficiency already exist. First of all, various types of filtration efficiency have to be distinguished. Generally, *filtration efficiency* is simply the ratio between the amount of removed contaminant by the filter media and the used particles [56]. This can be measured by weight, number of particles or volume. *Single pass efficiency* is the particle contaminant, which is a specific particle size or range, passing only once through the filter. Its efficiency calculation is based on the weight. A second type, *cumulative efficiency* is a multi-pass test where the efficiency is measured at various intervals during a filter life test. *Fractional efficiency* is a term which is generally used for filtration efficiency for particle sizes or particle group sizes. The last type is *multi-pass efficiency*, where particle-analyzers are used to determine the filtration efficiency for a certain particle size. These efficiencies are measured at selected intervals and the efficiency is cumulative calculated.

In practice, the most important types and standards for filtration efficiency rating [35] are: *micron rating*, *MERV* (Minimum Efficiency Reporting Value) rating, *HEPA* (High Efficiency Particulate Air) and *ULPA* (Ultra Low Penetration Air) ratings and the *maximum penetration particle size* (MPPS). With those ratings it is possible to classify and compare filters with each other according their quality factor or filtration performance.

Pressure Drop

The second important parameter beside filtration efficiency is the pressure drop which is created due to the resistance to the flow during the airflow at a certain flow rate through the filter. The needed pressure is in general related to the energy needed to filter particles out of a fluid.

Quality Factor

A good filter has to filter as much as possible particles, which easily can be done by making the filter media thicker. However, this poses the disadvantage of a pressure drop increase related to the thickness and will make the filter unusable due to the high effort needed to pass the air through it. Therefore a good compromise is necessary between the filtration efficiency and the pressure drop. This compromise can be

quantified by the quality factor also called as filtration index. The quality factor represents the ratio of the filtration efficiency and pressure drop as:

$$QF = \frac{-\ln(1-P)}{\Delta p},$$
(Eq. 2)

where P is the fraction of aerosol penetrated and Δp the pressure drop. Good filters give a high efficiency and low pressure drop Δp, thus larger values of quality factor indicate higher quality of the filter media [36].

Filter Life Testing

Beside the quality factor of a filter the filter lifetime is another important parameter characterizing the filter media according the time the filter can be used. The filter life time can be measured in two different ways. In the first case, the time is measured which is needed to reach a definite pressure drop over the filter. This pressure drop level is related to the quality factor and indicated that from this point the filtration process quality is too low. In the latter case the filter is rated on its dust holding capabilities by measuring the trapped dust level.

3. Air Filtration Modeling through Nanofiber Nonwovens

3.1   Basic Filtration Mechanisms

In order to get better understandings regarding the working principles of filters simulation models are developed to predict the filtration efficiency and pressure drop through the filter. Generally, there are four fundamental filtration mechanisms [37]: surface straining, depth straining, depth filtration and cake filtration. In the first mechanism, *surface straining*, particles which are larger than the pore size are blocked while particles which are smaller than the pores can pass through the filter media. In the second mechanism, *depth straining*, the depth of the filter media is much larger than the size of the pores. This leads to the effect that particles go through the structure until they get stuck at a place where the pore diameter is smaller than its size. In the third mechanism, *depth filtration*, extra mechanisms which allow the filter to trap particles with a smaller size then the pore size are acting. The last type of filtration is *cake filtration,* also called as surface filtration, were the filter cake created by caught particle on top of the filter is becoming the filter media and the nonwoven is used as support to hold the cake. This type of filters is easily cleanable by changing the stream flow direction.

The particle range a nanofiber based structures can capture is very large. It can vary from 10 µm (large particles) down to engineered nanoparticles having the size of just several nanometers.

This Ph.D. thesis mainly focuses on nanofiber based filtration where the depth filtration mechanism predominantly takes place. In the depth filtration mechanism, particles which are bigger than the pore size as well as particles smaller than the pores can be caught. This is possible due to some extra mechanisms (sieving, interception, impaction, diffusion, electrostatic attraction and gravity) taking place in the filter media. The principles of these mechanisms have been simplified illustrated in Figure 8.
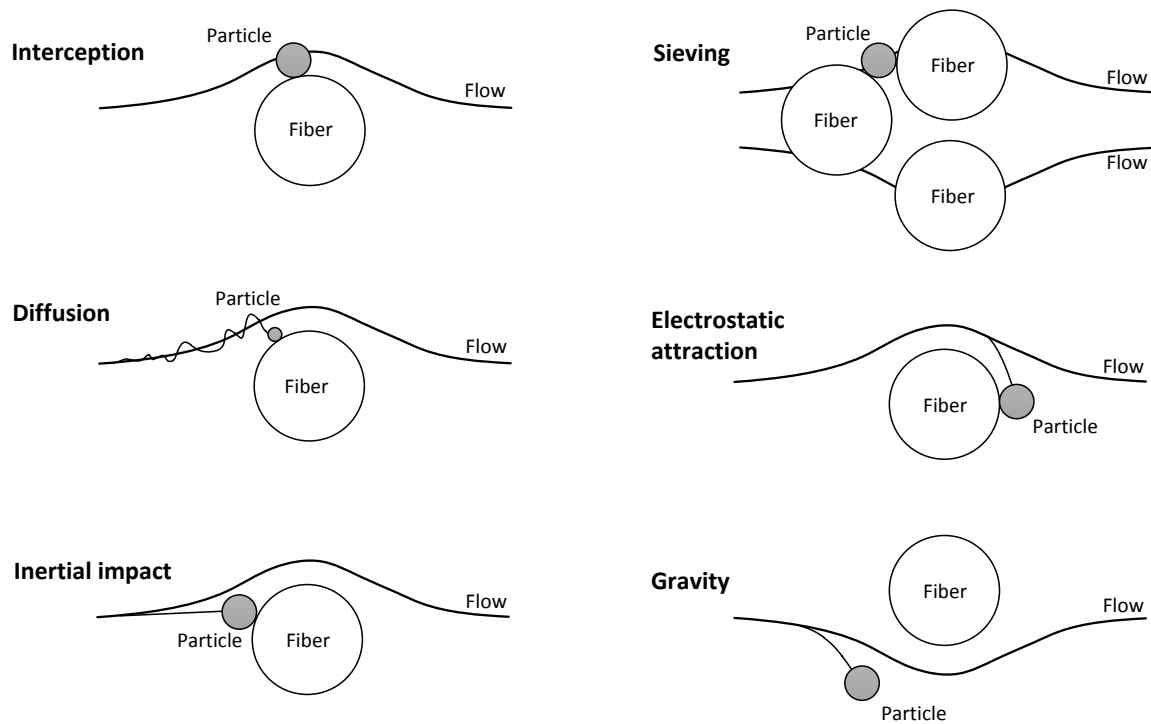
Figure 8:   Classification of six filtration mechanisms: Interception, Diffusion, Inertial impact, Sieve, Electrostatic attraction and Gravity.

The illustrated filtration mechanisms are divided in two main groups: *mechanical capture mechanisms* and *attraction mechanisms*. The first group of mechanisms works without the influence of attraction forces between particles and fibers while the latter principle is mainly based on these kinds of attractions. The most obvious way of filtration is *sieving* and occurs when a particle is larger than the pore size. In case a particle passes through a pore created by two or more fibers, the particle can still be caught by *interception*. Hereby, the particle touches the fiber while it follows its stream line around the fiber. This effect was defined by Lastow and Podgorski [38] as "*a particle is intercepted by a fiber when the distance from the center of mass of the particle to the fiber surface is equal or less than the radius of the particle*". In case there is an impact force which is large enough to deviate the particle from its original streamline then the particle can be caught by *inertial impaction*. This catching mechanism has been defined by Hinds [39] as "*a particle, because of its inertia, is unable to adjust quickly enough to the abruptly changing streamlines near to the fiber and crosses those streamlines to hit the fiber*". In the case of small particles (<500 nm) *Brownian diffusion,* which is composed of the diffusional deposition combined with the airflow, is playing a dominant role. Due to the random path, the probability to get

in contact with a fiber is increasing and will lead to a higher probability to be caught. The fifth described mechanism, classified under the attraction mechanisms is called *electrostatic attraction*. In this mechanism particles are attracted to the fiber due to electric or electrostatic charge being present on the fiber. Beside the described five main effects, *gravity* can also have an influence but has in general a negligible effect on the filtration efficiency in the range of small particle sizes.

When all these filtration mechanisms are acting during the filtration process a weaker filtration region will still remain. In a certain range, within the small particle sizes, the diffusion mechanism is not large enough and there is not enough momentum for inertial effects which leads to difficulties to filter this range of particle sizes. This can be clearly seen in the filtration efficiency curve plotting the efficiency as a function of the particle size. This phenomenon results in a typical V-shape as illustrated in Figure 9. The maximum penetration particle size (MPPS) is located on the position where the total collection efficiency reaches a minimum. This point can be used as a characteristic value to describe the filtration efficiency and to calculate the quality factor when the pressure drop in known.
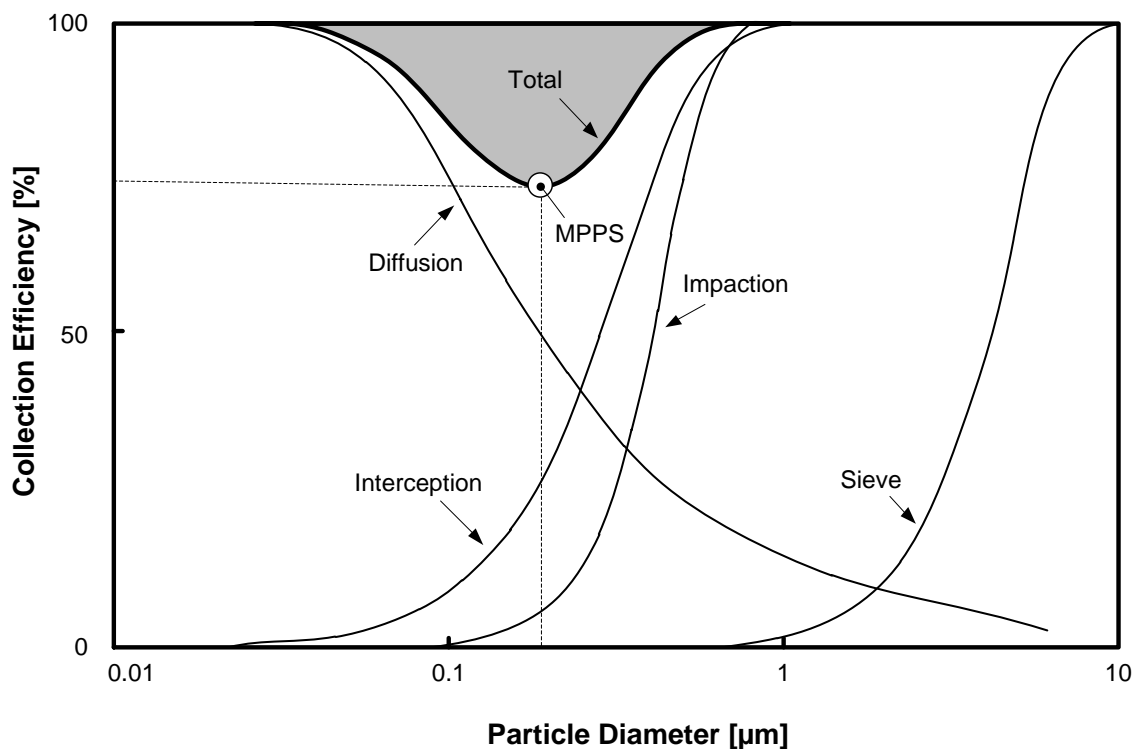

Figure 9: Typical example of the V-shape in the filtration efficiency curve.

3.2   Filtration Models

In order to predict theoretically the filtration efficiency and the pressure drop through a nonwoven several of theories were established based on the Stokes flow for a single fiber and fiber patterns.

Kuwabara [40] and Happel [41] were in 1959 independently the first to develop a mathematical theory (cell model) to predict the collection efficiency of fibrous filters in the continuum flow regime, each with different boundary conditions. Those cell models have been widely used in the literature because its application is relatively easy. Other researchers improved and adjusted later Kuwabara his model by considering the so-called "fiber array" models, and obtained different expressions for pressure drop and particle collection efficiency for different fibrous media [43]. Different models were developed in order to calculate the filtration efficiency as a combination of filtration mechanisms for single fiber theories (e.g. interception, inertial impaction and Brownian diffusion of the particles). In addition to the theoretical models, pure empirical equations were developed to predict the pressure drop over a filter media. The most known and used empirical equations are obtained by Davis [42] and Brown [43]. The empirical equation of Davis has been validated within a range of fiber diameters between 1.6 µm and 80 µm with a solid volume fraction between 0.6 % and 30 %. Later the application area of the equation has been extended by Werner and Clarenburg [44] for fiber within a diameter of 98 nm and 1.54 µm with porosity between 3.9 % and 84 %. The disadvantage of the empirically adjusted expressions is being inaccurate for a wide range of parameters. For this reason, these models are among others reasons not applicable for nanofiber based structures where aerodynamic slip is highly present.

It has to be mentioned that numerous models were created to obtain the pressure drop across clean fibrous HEPA filters [45-49] and non-HEPA filters [50-52], but only a few research studies was performed to calculate the pressure drop across an aerosol loaded fibrous filter [53]. Therefore, Bergman et al. [54] used the Davis model for clean filters extended with a model describing the pressure drop due to the particles deposit with the assumption that the particle load is constant through the filter thickness. A different approach was suggested by Novick et al. [55] where the overall

pressure drop has been defined by the combination of pressure drops over the clear filter and the cake.

Aerodynamic Slip

The basic theories established for single fiber theory and fiber array model are not valid for structures with small fibers at norm temperature and pressure (NTP) due to aerodynamic slip. The conditions which are assumed in the Stoke flow are not valid due to not taken into account of the molecular nature of air, also called "aerodynamic slip" [43]. This effect must be considered for small fibers whose size is comparable with the mean free path of air molecules. When aerodynamic slip occurs, the tangential velocity at the fiber surface is not zero and is related to the tangential stress. This stress depends on the nature of the reflection of molecules at the fiber surface based on the Knudsen number, defined by:

$$Kn = 2\lambda / D_f ,$$ (Eq. 3)

where λ is the mean free path of air and D_f the fiber diameter. Based on this Knudsen number, four flow regimes around the fiber are defined [43]: the *continuum regime* (Kn ≤ 10^{-3}), the *slip regime* (Kn ≤ 0.25), the *free molecular regime* (Kn ≥ 10) and a *transitional regime* (0.25 < Kn < 10). The effect of the Knudsen number on the flow paths is demonstrated in Figure 10, where the change in path line curvature is demonstrated for three different Knudsen numbers. As can be observed in case of a high Knudsen number (see Figure 10c) there is pure slip around the fiber surface. This condition is valid for really small fibers working in a low viscosity fluid under low pressure as stated by Maze et al. [56]. Because this thesis is dealing with nanofiber structures the aerodynamic slip has to be kept in mind during the modeling.
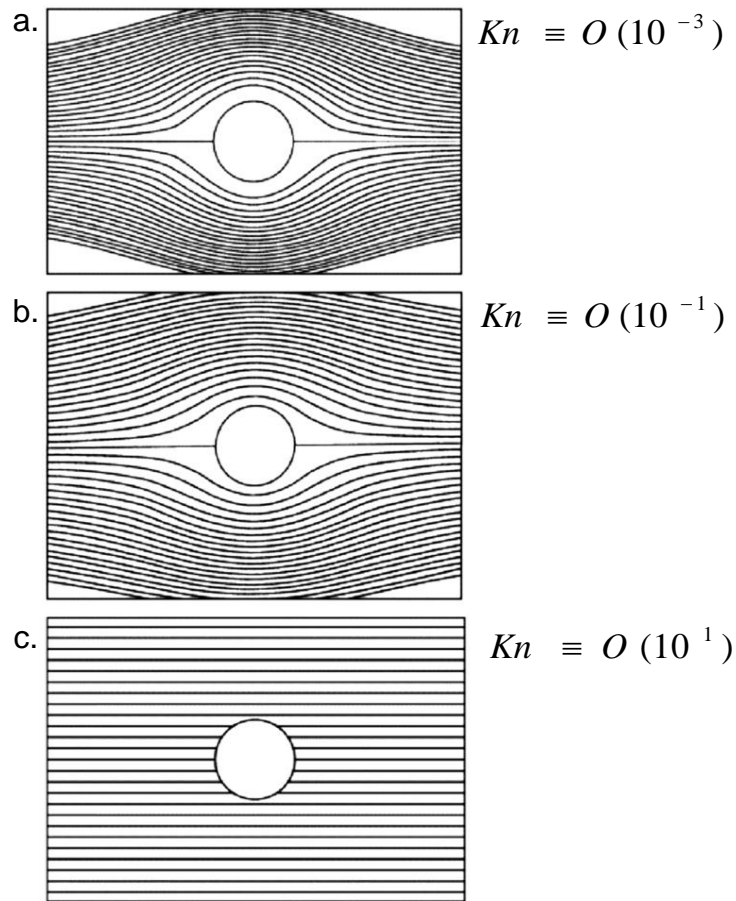
$a. \qquad Kn \equiv O\,(10^{-3})$

$b. \qquad Kn \equiv O\,(10^{-1})$

$c. \qquad Kn \equiv O\,(10^{1})$

Figure 10: Knudsen number dependence on the path lines [56]:

a. low Kn-number, b. middle Kn-number, c. high Kn-number.

Brownian Motion

Beside aerodynamic slip, Brownian motion plays an additional significant role for small particles which are filtered by the nanofiber nonwovens. The Brownian motion of nanoparticles is well described in the work of Maze et al. [56]. They solved a set of differential equations which result in directly applicable equations describing the distance and velocity vector for a certain time interval predicted by the Brownian diffusion with several input parameters. Figure 11 shows an example of those Brownian paths according their equations for a 20 and 30 nm in size particle for one millisecond in the x-y plane in stagnant air starting from the origin. When the attention is paid to filtration of small particles, the Brownian motion has to be considered because the diffusion motion will be dominant.
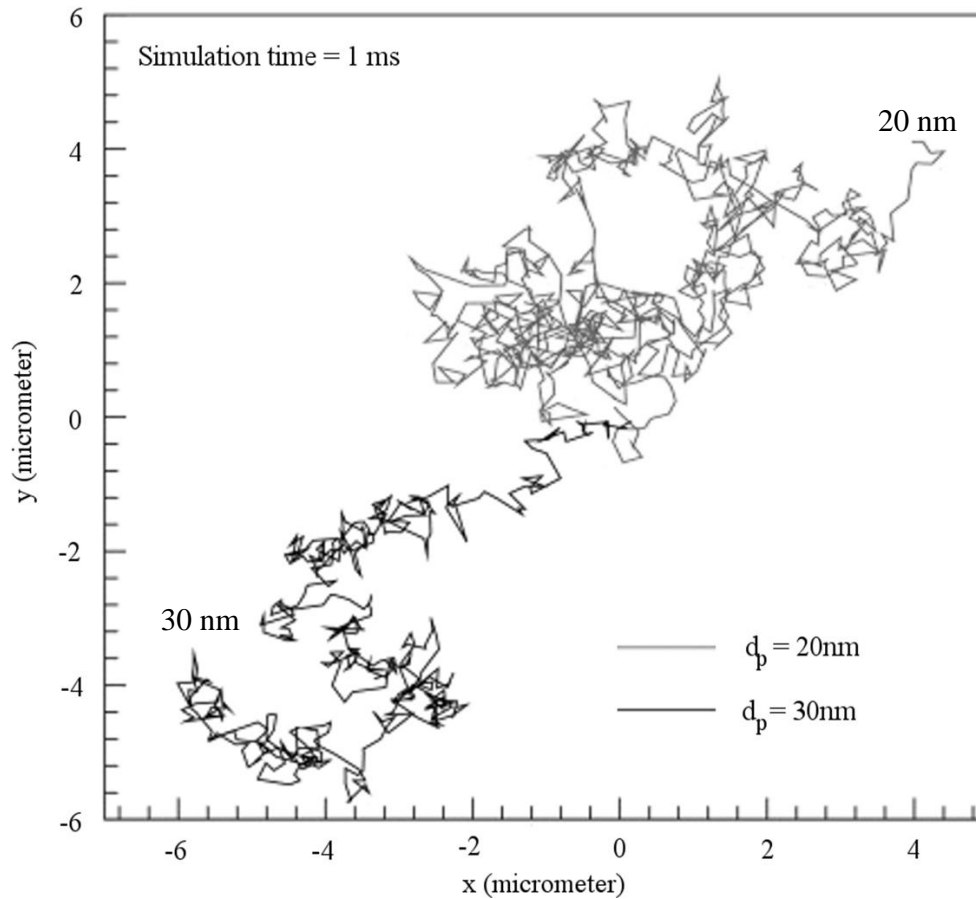
Figure 11: Trajectory of 20 and 30 nm particles in the x-y plane within the first millisecond of their travel from the origin in stagnant air [56].

Filtration Efficiency and Pressure Drop

The filtration efficiency depends generally on several parameters as there are, the structure of the filter (packing, fiber diameter, thickness, material, etc.) and the operation conditions where the filter is working (velocity, pressure, temperature, etc.) as well as the properties of the particles (size, distribution, material, density, etc.).

As previously described, the general filtration models are not valid in the region of small fibers due to the aerodynamic slip. Therefore, Hosseini and Tafreshi [57] did interesting work to predict the pressure drop and the filtration efficiency on own created simplified virtual 3D geometries of microstructure of electrospun fibrous materials which were challenged with aerosol particles in a range of 25 to 1000 nm (see Figure 12). The main advantage of their 3D simulation model is that unlike the previous studies based on oversimplified 2D geometries, no empirical correction factors are needed. Their model includes particle collection due to interception and Brownian diffusion, as well as the slip effect at the nanofiber surface.
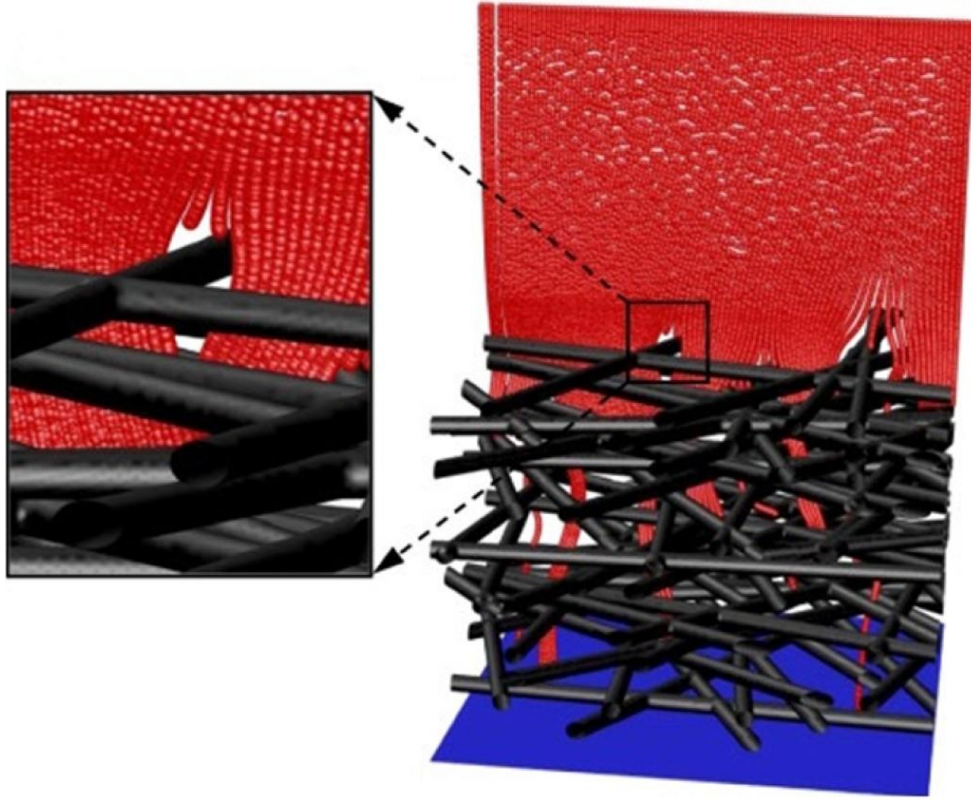
27

Figure 12: Simulation of particle filtration in an electrospun nanofibrous filter [57].

In another work of them [58], they solved numerically the Stokes flow equation in a void space between virtual created fibers with slip flow boundary conditions. The results of these calculations were compared with existing permeability expressions used for nanofiber media and utilized to establish a correction factor for those expressions.

Rebaï et al. [59] predicted the pressure drop and the filtration efficiency virtual for random microfiber networks by using the lattice Boltzmann approach.

Another way to take the slip of the particles around the fibers into account is given by McNenly et al. [60]. They modified the fluid viscosity and slip boundary conditions for simple geometries for Couette and Poiseuille flow. Therefore, they introduced a Knudsen number dependence (from 0.01 to 10) of the viscosity. Additionally, a slip model for the two flow types, where the air viscosity is reduced with increased Knudsen number (more slip), was proposed.

Pich [61] showed the effect of the different Knudsen number based regimes on the pressure drop over a filter with low solid volume fraction. It has been found that the pressure drop is decreasing with higher Knudsen numbers due to aerodynamic slip.

An alternative way to predict the pressure drop through a nonwoven has been obtained by the derivation of simple equations. The calculation of the pressure drop is possible by several models which are valid for continuous flows. This pressure drop can be calculated as a function of the air viscosity η, filter thickness t, face velocity U, fiber diameter d_f and a parameter as function of the Solid Volume Fraction (SVF) [39]. The following basic equation (see Eq. 4) is for every model the same but the definition of the parameter f(α) (where α is the SVF) defers from model to model.

$$\Delta p = f(\alpha) \frac{\eta t U}{d_f^2} \qquad \text{(Eq. 4)}$$

Clogging of Fibrous Filters

The previous described theories are generally not taking the interaction and accumulation of particles into account. However, several researchers have built up models which are taking clogging of fibrous filters into account based on experimental research [62-65]. The analyses of the deposition morphology were already successfully established for fiber structures [66-69] and tube geometries [70-72]. The accumulation of the particles is divided into three basic steps [72]. In the first step, particles come into contact with the surface of the filter media, named as capillary deposition. This is followed by an accumulation of particles, called as capillary clogging due to sticking to the surface and by interception of already caught particles. In the final step, particles are only caught by interception by other particles which lead to a prominent increase in cake growth.

The contact between particles with size between 10 nm and 5 µm has been experimentally found by Wang and Kasper [73] and Pawu and Braaten [74] to be fully sticking. For larger particles bending and breaking of particle chains has been evaluated by Huang et al. [75].

Beside different shapes and fiber morphologies, the influence of a possible electric charge present on the fibers has also been investigated [68].

Until now these filtration simulations of clogging of filters and cake formation by micro-size particles has mainly been done on microfiber structures or for tube geometries representing a pore but not for nanofiber based structures. Therefore, the

effect of particle-particle interaction, within an ultra-fine size range, initiating cake formation will be studied in this Ph.D. work.

3.3   Filter Media Model

In order to model the particle flow through a nonwoven a filter media model is required. This model can be created in two [76, 77] or three dimensions, depending on the complexity of the nanofiber nonwoven and the assumptions which have been made in the filtration model due to this possible simplifications. In this Ph.D. thesis the use of full 3D simulations has been chosen due to the complex structure of the nanofiber nonwovens.

There are known several techniques to transform a real porous structure in a 3D model, e.g. Magnetic Resonance Imaging (MRI) [78, 79]), X-ray microtomography [80, 81] or Digital Volumetric Imaging (DVI). Jaganathan and co-workers [82] developed a methodology to create three-dimensional structures using an integrated approach utilizing automated serial sectioning technique. Figure 13 shows an example of such a 3D model obtained by Digital Volumetric Imaging (DVI) technique. X-ray microtomography can also be used to create a three dimensional model from a small piece of nonwoven. This principle [83, 84] uses X-ray beams at various angles through successive layers of a rotating specimen. These described methods have the ability to create 3D models from real objects like nonwovens but these advanced techniques have some critical disadvantages: they are expensive, time consuming and mainly they have a limited resolution (480nm/pixel for DVI) which unfortunately makes properly scanning of a nanofiber structure impossible.

Figure 13: 3-D reconstructed DVI image from a nonwoven

(800 x 800 x 600 voxels, with resolution 1.77 µm/pixel) [85].

Due to this problem to create a proper 3D model based on a real structure, it is not surprising that various researchers have developed virtual models, to get a better understanding in the filtration mechanism of nanofiber based nonwovens. Those filter media models are based on morphological properties of the nanofiber nonwoven, for example: porosity, orientation, fiber diameter, fiber length, etc. The constructed cylindrical fiber representation can be randomly distributed in one, two or three dimensions as illustrated in Figure 14. A nonwoven is mostly described by a random 2D model [86].

Figure 14: Random virtual structures in one-, two- and three- dimensions [86]

These virtual models have been used in several researches dealing with filtration modeling of nonwovens [57-58, 76, 82, 84, 86]. Likely, this way of using virtual cannot take some of the real nonwoven features into account (e.g. defects, fiber curvature and variation in fiber thickness). Therefore, there is a need for a new method which is able to generate 3D models based on real structures instead of using morphological parameters as input to build up virtual filter media models.

GOALS OF THE DOCTORAL STUDY

The main goal of this Ph.D. thesis work is to develop new types of experimental and theoretical techniques in order to reveal the complicated link between morphology, mechanical properties and filtration efficiency of polymeric nanofiber based filters created by a wire rotation electrode based electrospinning process. The individual Ph.D. thesis work aims are provided below:

- ✓ Investigation of the effect of supporting textile type utilized during the electrospinning process on the mechanical and structural characteristics of the nanofiber nonwovens using a Sentmanat extensional rheometer, to overcome difficulties connected with problematic manipulation of extremely small fibers, and very sensitive force transducer requirements.

- ✓ Development of both, SEM image analysis techniques for automatic determination of pore size diameter distributions for polymeric nanofiber based filters as well as a new approach for real 3D nanofiber mat model construction from their scanning electron microscopy (SEM) images.

- ✓ Development and testing of full 3D particle filtration model using the 3D structure model representing real filter structure considering slip/transition/free molecular flow regime, particle–fiber and particle-particle interactions, air/particle slip, sieve and homogenous flow field.

- ✓ Investigation the effect of air velocity, viscosity, temperature, pressure and particle–fiber friction coefficient on the polymer nanofiber filter efficiency, quality factor and cake formation.

SUMMARY OF THE PAPERS

In the first part of this work (Paper I), polymeric nanofiber based filters created by electrospinning process utilizing wire based rotation electrode have been investigated by using newly developed experimental methods and digital image analysis techniques in order to understand the complicated link between filter morphology and mechanical properties. The latter part (Papers II, III and IV) is focused on the development and testing of a novel 3D filtration model for polymeric nanofiber based filters (utilizing particle-fiber/particle-particle interactions, transition/free molecular flow regime, Brownian diffusion and realistic scanning electron microscope image based 3D structure model) in order to understand the effect of filter morphology, particle-fiber friction coefficient, air velocity, viscosity, temperature and pressure on the filtration efficiency and quality factor. Short summaries and main results of the four papers are presented below.

PAPER I

The use of novel digital image analysis technique and rheological tools to characterize nanofiber nonwovens

In this work, polyurethane solved in dimethylformamide has been electrospun under one set of conditions using five different supporting textiles. The mechanical properties of these nanofiber mats were measured by the Sentmanat extensional rheometer, and the pore size distribution was calculated by a newly proposed digital image analysis methodology. This methodology was applied on nanoscale SEM images taking macroscopic features of the nonwovens into account.

It has been found that based on the performed experimental work and proposed novel digital image analysis technique the supporting textiles have a very high effect on mechanical properties of nanofiber mats (even if their fiber diameter distributions are similar), which can be explained by different porosity of the prepared samples.

PAPER II

3D modeling of filtration process via polyurethane nanofiber based nonwoven filters prepared by electrospinning process

In this work, a nanofiber nonwoven based polyurethane filter has been produced using electrospinning process. A new methodology to create simple 3D structure model from SEM image of the filter, which represents a real filter structure, has been proposed. In the following step, full 3D particle filtration modeling using such a 3D structure model has been utilized. This model takes slip/transition/free molecular flow regime, particle– fiber interactions, air/particle slip at the fiber surface, sieve and homogenous flowfield in consideration. The obtained theoretical predictions for the filtration efficiency have been compared with the corresponding experimental data. A good agreement between both data sets of filtration data has been obtained, especially at the particle size range for which the applied model assumptions are valid.

In the next step of this work a theoretical study has been done to investigate the effect of different factors such as air velocity, viscosity, temperature, pressure and particle–fiber friction coefficient for the produced polyurethane nanofiber based filter. It has been revealed that the change of the particle–fiber friction coefficient (which can be done by for example surface modification) has one of the highest effects on the filtration efficiency, within the range of all tested parameters and their values.

PAPER III

3D air filtration modeling for nanofiber based filters in the ultrafine particle size range

In this work, 3D filtration model for nanofiber based filters (utilizing particle-fiber interactions and realistic SEM image based 3D structure model) has been proposed and tested. For the model validation purposes, two polyurethane nanofiber layers prepared by the electrospinning process (having identical average fiber diameter but different average pore size) were combined to create 2 pairs of nanofiber based filters; each pair consist of two filters having comparable mass area and thickness. Filtration efficiency characteristics of prepared filters were determined experimentally in the ultrafine particle size range (20-400 nm). It has been found that the proposed model is able to reasonably predict the measured filtration efficiency curves for all tested filter samples.

PAPER IV

3D clogging modeling of polyurethane nanofiber based filters by ultrafine aerosol particles

In this work, realistic SEM image based 3D filter model, transition/free molecular flow regime, Brownian diffusion, aerodynamic slip, particle-fiber as well as particle-particle interactions together with a novel Euclidian distance map based methodology to calculate the pressure drop has been utilized for a polyurethane nanofiber based filter prepared via electrospinning process in order to more deeply understand the filter clogging, filtration cake formation and its role on the final filter efficiency. The model predictions have been found to be in good agreement with the corresponding experimental data justifying the used assumptions. By using the proposed theoretical approach for the 3D filter clogging modeling, it has been found that the decrease in the fiber-particle friction coefficient leads to higher pressure drop, lower filtration efficiency, lower quality factor and lower quality factor sensitivity to the increased collected particle mass due to deeper particle penetration in the filter and creation of smaller pores.

CONCLUSIONS

Based on the performed experimental work and proposed novel digital image analysis technique for nanoscale SEM pictures (taking macroscopic structure features into account) has been found that supporting textiles have a very high effect on mechanical properties of polyurethane nanofiber nonwovens prepared by the electrospinning process (even if their fiber diameter distributions were similar), which can be explained by different porosity of the prepared samples.

Firstly, a new methodology to create simple 3D structure model from SEM image of the filter has been proposed. This created 3D filter media model, representing the real filter, has been used in a newly developed full 3D particle filtration model considering slip/transition/free molecular flow regime, particle–fiber/particle-particle interactions, air/particle slip at the fiber surface, sieve and homogenous flow field. The obtained theoretical predictions for the filtration efficiency have been compared with the corresponding experimental data and good agreements between both data sets have been obtained.

Secondly, the effect of different factors such as air velocity, viscosity, temperature, pressure and particle–fiber friction coefficient has been theoretically investigated for the produced polyurethane nanofiber based filter. It has been revealed that the change of the particle–fiber friction coefficient (which can be done by particle–surface modification for example) has one of the highest effects on the filtration efficiency within the range of all tested parameters and their values, especially for nanoparticles having diameter less than 200 nm for the studied conditions and filter structure.

Thirdly, a novel Euclidian distance map based methodology to calculate the pressure drop through the 3D filter model has been proposed and tested with corresponding experimental data. It has been found that even if the utilized theoretical approach tends to over predict the pressure drop by approximately 35%, the filter samples ordering according to pressure drop is predicted correctly.

Finally, based on the performed theoretical analysis, it has been revealed that the decrease in the fiber-particle friction coefficient leads to higher pressure drop, lower filtration efficiency, lower quality factor and lower quality factor sensitivity to the increased collected particle mass due to more weaker particle penetration in the filter,

creation of bigger pores and generation of lower pressure drop in comparison with lower particle-fiber friction coefficient filters. Moreover, it has been revealed that even if the particle-fiber friction coefficient is different, the cake morphology is very similar.

ACKNOWLEDGEMENTS

First and foremost, I would like to express my gratitude to my supervisor, Professor Martin Zatloukal for giving me the opportunity to start my doctoral study at the Tomas Bata University in Zlin and for all help and untiring support during the last four years.

Besides, I would also like to thank Dusan Kimmer, which is the co-author of all the presented papers, for his support with respect to filter samples preparation and experimental characterization.

Moreover, I would like to thank Ondrej Pokluda for the help and advice he have me during the programming process of the modeling software in C++ and C#. I am sure I would not stand where I am standing now without his help and advice.

Beside this professional gratitude I would like to thanks my family which supported me in my study and always stood behind my choice to study abroad in Czech Republic. Also I want to thank my friends Franky and Hana for giving me a Belgian home in Zlin. I am also very thankful to my future wife Marta for believing and supporting me during all times. Additionally, I would like to thank all my Czech and foreign friends and colleague researchers for filling my days with nice and interesting discussions.

Finally, because I am not able to life from friendship and love alone I want to thank Tomas Bata University in Zlin as well as Martin Zatloukal and the university collage KHBO in Belgium, especially Eric Debrabandere en Frederik Desplentere, for the financial support during my study period.

REFERENCES

[1] ISO 9092:1988 Textiles - Nonwovens - Definition, International Organization for Standardization, Geneva, Switzerland, stage 2011-09-29.

[2] LYONS, J., LI, C., KO, F. Melt-electrospinning part I: Processing Parameters and Geometric Properties. *Polymer* 2004, vol. 45, no. 22, p. 7597-7603.

[3] Apparatus for Electrically Dispersing Fluids. Deviser: COOLY, J. F., *U.S patent 692 631*, 1902-02-04.

[4] Method of Dispersing Fluids. Deviser: MORTON, W.J., *U.S patent 705 691*, 1902-07-29.

[5] ELLISON, C.J. Melt blown nanofibers: Fiber diameter distribution and onset of fiber breakup, *Polymer* 2007, vol. 48, no. 11, p. 3306-3316.

[6] RENEKER, D.H. and FONG H. *Polymeric Nanofibers,* An American Chemical Society Publication, 2006, ISBN 9780841239197.

[7] LARSEN, G., SPRETZ, R., VELARDE-ORTIZ, R. Use of coaxial gas jackets to stabilize Taylor cones of volatile solutions and to induce particle-to-fiber transitions, *Advanced Materials* 2004, vol. 16, no. 2, p. 166-169.

[8] YARIN, A.L., KATAPHINAN, W., RENEKER, D.H., Branching in electrospinning of nanofibers, *J. Appl. Phys.* 2005, vol. 98, no. 6, art. 064501.

[9] PATANAIK, A., JACOBS, V., ANANDJIWALA, R.D. Performance evaluation of electrospun nanofibrous membrane, *J. Membrane. Sci.* 2010, vol. 352, no. 1-2, p. 136-142.

[10] HOMAEIGOHAR, S.S., BUHR, K., EBERT, K. Polyethersulfone electrospun nanofibrous composite membrane for liquid filtration, *J. Membrane. Sci.* 2010, vol. 365, no. 1-2, p. 68-77.

[11] GRAFE, T., GRAHAM K. Polymeric Nanofibers and Nanofiber Webs: A New Class of Nonwovens, *International Nonwovens Technical Conference (Joint INDA – TAPPI Conference)*, Atlanta, Georgia, September 24-26, 2002.

[12] CASPER, C.L., STEPHENS, J.S., TASSI, N.G., CHASE, D.B. and RABOLT, J.F. Controlling surface morphology of electrospun polystyrene fibers: effect of humidity and molecular weight in the electrospinning process, *Macromolecules* 2004, vol. 37, no. 2, p.573-578.

[13] KIM, G.-M, MICHLER, G.H., PÖTSCHKE, P. Deformation processes of ultrahigh porous multiwalled carbon nanotubes/polycarbonate composite filbers prepared by electrospinning, *Polymer.* 2005, vol. 46, no. 18, p. 7346-7351.

[14] LI, D., XIA, Y.N. Direct fabrication of composite and ceramic hollow nanofibers by electrospinning, *Nano Letters* 2004, vol. 4, no. 5, p. 933-938.

[15] KIMMER, D., SLOBODIAN, P., PETRAS, D., et al. Polyurethane/Multiwalled Carbon Nanotube Nanowebs Prepared by an Electrospinning Process, *J. Appl. Polymer. Sci.* 2009, vol. 111, no. 6, p.2711-2714.

[16] HUANG, Z.M., ZHANG, Y.Z., KOTAKI, M., et al. A review on polymer nanofibers by electrospinning and their applications in nanocomposites, *Compos. Sci. Technol.* 2003, vol. 63, no. 15, p. 2223-2253.

[17] BHARDWAJ, N., KUNDU, S.C. Electrospinning: A fascinating fiber fabrication technique, *Biotechnology Advances* 2010, vol. 28, no. 3, p. 325-347.

[18] LU, P. and DING, B. Applications of Electrospun Fibers, *Recent Patents on Nanotechnology* 2008, vol. 2, p. 169-182.

[19] PODGORSKI, A., BALAZY, A. and GRADON, L. Application of nanofibers to improve the filtration efficiency of the most penetrating aerosol particles in fibrous filters, *Chem. Eng. Sci.* 2006, vol. 61, no.20, p. 6804-6815.

[20] ANDRADY, A.L., Science and Technology of Polymer Nanofibers, 1st ed., Wiley-Interscience, 2008, 404 p. ISBN 0471790591.

[21] HUANG, Z.M., ZHANG, Y.Z, RAMAKRISHNA, S., et al. Electrospinning and mechanical characterization of gelatin nanofibers, *Polymer* 2004, vol. 45, no. 15, p. 5361-5368.

[22] SCHREUDER-GIBSON, H. and GIBSON, P. Application of electrospun nanofibers in current and future materials. In *Polymer Nanofibers,* Oxford University Press (USA) 2006**,** ACS Symposium Series*,* ISBN 9780841220362.

[23] MCKEE, M.G., PARK, T., UNAL, S., YILGOR, I., LONG, T.E, Electrospinning of linear and highly branched segmented poly(urethane urea)s, *Polymer* 2005, vol. 46, no. 7, p.2011-2015.

[24] POURDEYHIMI, B., DENT, R. Measuring fiber diameter distribution in nonwovens, *Textile Research Journal* 1999, vol. 69, no. 4, p. 233-236.

[25] GHASEMI-MOBARAKEH, L., SEMNANI, D., MORSHED, M. A novel method for porosity measurement of various surface layers of nanofibers mat using image analysis for tissue engineering applications, *J. Appl. Polymer. Sci.* 2007, vol. 106, no. 4, p. 2536-2542.

[26] PTAK, T.J., CADY, D. Filter Media Pore Size Analysis, *Separation Technology* 1995, vol. 9, no. 5, p. 37-45.

[27] AYDILEK, A.H., OGUZ, S.H., EDIL, T.B. Digital image analysis to determine pore opening size distribution of nonwoven geotextiles, *J. Comput. Civil Eng.* 2002, vol. 16, no. 4, p. 280-290.

[28] AYDILEK, A.H., EDIL, T.B. Evaluation of Woven Geotextile Pore Structure Parameters Using Image Analysis, *Geotech. Test. J.* 2004*,* vol. 27, no. 1, p. 99-110.

[29] ZIABARI, M., MOTTAGHITALAB, V., HAGHI, A.K. Evaluation of electrospun nanofiber pore structure parameters, *Korean J. Chem. Eng.* 2008,vol. 25, no. 4, p. 923-932.

[30] POURDEYHIMI, B., DENT, R. Measuring fiber orientation in nonwovens, *Textile Research Journal* 1999, vol. 69, no. 3, p. 185-192.

[31] ZIABARI, M., MOTTAGHITALAB, V., HAGHI, A.K. Distance transform algorithm for measuring nanofiber diameter, *Korean J. Chem. Eng.* 2008, vol. 25, no. 4, p. 905-918.

[32] TOMBA, E., FACCO, P., ROSO, M., et al. Artificial Vision System for the Automatic Measurement of Interfiber Pore Characteristics and Fiber Diameter Distribution in Nanofiber Assemblies, *Ind. Eng. Chem. Res.* 2010, vol. 49, no. 6, p. 2957-2968.

[33] FACCO, P., TOMBA, E., ROSO, M., MODESTI, M., BEZZO, F., BAROLO, M. Automatic characterization of nanofiber assemblies by image texture analysis, *Chemometr Intell. Lab.* 2010, vol. 103, no. 1, p. 66-75.

[34] SEMNANI, D., GHASEMI-MOBARAKEH, L., MORSHED, M., et al. A Novel Method for the Determination of Cell Infiltration into Nanofiber Scaffolds Using Image Analysis for Tissue Engineering Applications, *Journal of Applied Polymer Science* 2009, vol. 111, no. 1, p. 317-322.

[35] HUTTEN, I.M., *Handbook of Nonwoven Filter Media*, 1st ed., Elsevier, 2007, 473 p., ISBN 1-8561-7441-7.

[36] WANG, J., KIM, S.C., PUI, D.Y. Investigation of the Figure of Merit for Filters with a Single Nanofiber Layer on a Substrate, *Journal of Aerosol Science* 2008, vol. 39,no. 4, p. 323-334.

[37] SUTHERLAND, K., PURCHAS, D. B. *Handbook of filter Media,* 2nd ed., Elsevier 2002, ISBN: 18-561-737-55.

[38] LASTOW, O., PODGORSKI, A. Airflow through filters-beyond single-fiber theory. In SPURNY, K.R., (ed) *Advances in Aerosol Filtration*. Lewis Publisher, 1st ed., CRC-Press 1997, ISBN 08-737-183-01.

[39] HINDS W.C. *Aerosol Technology: Properties, Behavior, and Measurement of Airborne Particles,* 2nd ed., Wiley-Interscience 1999, ISBN 04-711-941-01.

[40] KUWABARA, S. The forces experienced by randomly distributed parallel circular cylinders of spheres in a viscous flow at small Reynolds number, *J. Phys. Soc. Japan* 1959, vol. 14, no. 4, p. 527-532.

[41] HAPPEL, J. Viscous flow relative to array of cylinders, *Aiche Journal* 1959, vol. 5, no. 2, p. 174-177.

[42] DAVIS, C.N., *Air Filtration*, Londen, Academic Press Inc. 1973, ISBN: 01-220-566-04.

[43] BROWN, R.C. *Air Filtration: An Integrated Approuch to the Theory and Applications of Fibrous Filters*, 1st ed., Pergamon Press 1993, ISBN 00-804-127-40.

[44] WERNER, R.M., CLARENBURG, L.A. Aerosol filters. Pressure drop across single-component glass fiber filters, *Ind. Eng. Chem. Process Des. Dev.*1965, vol. 4, no. 3, p. 288-293.

[45] BERGMAN, W.,TAYLOR, R.D., MILLER, H.H., BIERMANN, A.H., HEBARD, H.D.,DAROZA, R.A., LUM, B.Y. Enhanced filtration program at LLL - a progress report, *15th DOE NACC* 1978, p. 1058–1099.

[46] VENDEL, J., MULCEY, P., LETOURNEAU, P. Aerosol penetration inside HEPA filtration media, *21st DOE/NRC NACC* 1990, p. 799–808.

[47] LETOURNEAU, P., RENAUDIN, V., VENDEL, J. Effects of the particle penetration inside the filter medium on the HEPA filter pressure drop, *22nd DOE/NRC NACC* 1992, p. 128–142.

[48] NOVICK, V.J., KLASSEN, J.F., MONSON, P.R. and LONG, T.A. Predicting mass loading as a function of pressure difference across prefilter/HEPA filter systems, *22nd DOE/NRC NACC* 1992, p. 554–573.

[49] THOMAS, D., CONTAL, P., RENAUDIN, V., PENICOT, P., LECLERC, D., VENDEL, J. Modelling pressure drop in HEPA filters during dynamic filtration, *J. Aerosol Sci.* 1999, vol. 30, no. 2, p. 235–246.

[50] BROWN, R.C., and WAKE, D. Loading filters with monodisperse aerosols: macroscopic treatment, *J. Aerosol Sci.* 1999, vol. 30, no. 2, p. 227–234.

[51] SAKANO, T., OTANI, Y., NAMIKI, N., EMI, H. Particle collection of medium performance air filters consisting of binary fibers under dust loaded conditions, *Sep. Purif. Technol.* 2000, vol. 19, no. 1-2, p. 145–152.

[52] MIGUEL, A.F. Effect of air humidity on the evolution of permeability and performance of a fibrous filter during loading with hygroscopic and non-hygroscopic particles, *J. Aerosol Sci.* 2003, vol. 34, no. 6, p. 783–799.

[53] LEUNG, W.W.F., HUNG, C.H. Investigation on pressure drop evolution of fibrous filter operating in aerodynamic slip regime under continuous loading of sub-micron aerosols, *Sep. Purif. Technol.* 2008, vol. 63, no. 3, p. 691-700.

[54] BERGMAN, W. TAYLOR, R.D., MILLER, H.H. *15th DOE Nuclear Air Cleaning Conference*, 1978, CONF-780819, Boston.

[55] NOVICK, V.J., MONSON, P.R., ELLISON, P.E., *J. Aerosol Sci.* 1992, vol. 23 p.657-665.

[56] MAZE, B., VAHESI TAFRESHI, H., WANG, Q., POURDEYHIMI, B. A simulation of unsteady-state filtration via nanofiber media at reduced operation pressures, *J. Aerosol Sci.* 2007, vol. 38, no. 5, p. 550-571.

[57] HOSSEINI, S.A., TAFRESHI, H.V. 3-D simulation of particle filtration in electrospun nanofibrous filters, *Powder Technol.* 2010, vol. 201, no. 2, p. 153–160.

[58] HOSSEINI, S.A., TAFRESHI, Modeling permeability of 3-D nanofiber media in slip flow regime, *Chem. Eng. Sci.* 2010, vol. 65, no. 6, p. 2249-2254.

[59] REBIA, M., DROLET, F., VIDAL, D., et al. A Lattice Boltzmann approach for predicting the capture efficiency of random fibrous media, *Asia Pas. J. Chem. Eng.* 2011, vol. 6, no. 1, p. 29-37.

[60] MCNENLY, M.J., GALLIS, M.A., BOYD, I.D. Empirical slip and viscosity model performance for microscale gas flow, *Int. J. Numer. Meth. Fl.* 2005, vol. 49, no. 11, p. 1169-1191.

[61] PICH, J. Pressure characteristics of fibrous aerosol filters, *J. Colloid Interf. Sci.* 1971, vol. 37, no. 4, p. 912-917.

[62] BILLINGS, C.E., Effects of particle accumulation in aerosol filtration, *PhD Thesis*, California Institute of Technology, Pasadena, USA, 1966.

[63] KANAOKA, C., and HIRAGI, S., Pressure drop of air filter with dust load, *J. Aerosol Sci.* 1990, vol. 21, no. 1, p. 127-137.

[64] WITTEN, T., SANDER, L. Diffusion-limited aggregation, *Phys Rev.* 1983, vol. 27, no. 9, p. 5686.

[65] PAYATAKES, A.C. and GRADON, L., Dendritic deposition of aerosol by convective Brownian diffusion for small, intermediate and high particle Knudsen numbers, *American Int. Chem. Eng. J.* 1980, vol. 26, no. 3, p. 443-454.

[66] THOMAS, D., PENICOT P., CONTAL P., LECLERC, D. and VENDEL, J, Clogging of fibrous filters by solid aerosol particles: Experimental and modelling study, *Chem. Eng. Sci.* 2001, vol. 56, no. 11, p. 3549-3561.

[67] CHEUNG, C.S., CAO, Y.H. and YAN, Z.D., Numerical Model for particle deposition and loading in electret filter with rectangular split-type fibers, *Computation mechanics* 2005, vol. 35, no. 6, p. 449-458.

[68] KANAOKA, C., HIRAGI, S. and TANTHAPANICHAKOON, T. Stochastic simulation of the agglomerative deposition process of aerosol particles on an electret fiber, *Powder Technol.* 2001, vol. 118, no. 1-2, p. 97-106.

[69] KARADIMOS, A. and OCONO, R. The effect of the flow field recalculation on fibrous filter loading: a numerical simulation, *Powder Technol.* 2003, vol. 137, no. 3, p. 109-119.

[70] CHANG, Y., HUANG, Y., LUO, Z. and ZHANG, G. A study on particle deposition morphology within a constricted tube in the presence and absence of the detachment mechanism, *Sep. Purif. Technol.* 2008, vol. 63, no. 3, p. 566-576.

[71] HUANG, B., TURTON R., PARK J., FAMOURI, P, and BOYLE, E.J. Dynamic model of the riser in circulating fluidized bed, *Powder Technol.* 2006, vol. 163, no. 1-2, p. 23-31.

[72] ELMOE, T.D., TRICOLI, A., GRUNWALDT, J, PRATSINIS, S., Filtration of nanoparticles: Evolution of cake structure and pressure-drop, *J. Aerosol Sci.* 2009, vol. 40, no. 11, p. 965-981.

[73] WANG H.C. and KASPER G. Filtration efficiency of nanometer-size aerosol-particles, *J. Aerosol Sci.* 1991, vol. 22 , no. 1, p. 31–41.

[74] PAWU K.T. and BRAATEN D.A. New perspectives on rebound and re-entrainment processes, *Aerosol Sci. Tech.* 1995, vol. 23, no. 1, p. 72–79.

[75] HUANG, B., TURTON R., PARK J., FAMOURI P, and BOYLE E.J. Dynamic model of the riser in circulating fluidized bed, *Powder Technol.* 2006, vol. 163, no. 1-2, p. 23-31.

[76] HOSSEINI, S.A., TAFRESHI, H.V. Modeling particle filtration in disordered 2-D domains: A comparison with cell models, *Sep. Purif. Technol.* 2010, vol. 74, no. 2, p. 160-169.

[77] ZHOU, B., TRONVILLE, P., RIVERS, R. Generation of 2-Dimensional Models for CFD Simulation of Fibrous Filter Media with Binder, *Fibers and Polymers* 2009, vol. 10, no. 4, p. 526-538.

[78] LEHMANN, M.J., HARDY, E.H., MEYER, J., and KASPER, G. MRI as a key tool for understanding and modeling the filtration kinetics of fibrous media, *Magn. Reson. Imaging* 2005, vol. 23, no. 2, p. 341.

[79] SCHWEERS, E. and LÖFFLER F. Realistic modeling of the behaviour of fibrous filters through consideration of filter structure, *Powder Technol.* 1994, vol. 80, no. 3, p. 191–206.

[80] FAESSEL, M., DELISÉE, C., BOS, F. and CASTÉRA, P., 3D modelling of random cellulosic fibrous network X-ray tomography and image analysis, *Composite Sci. Tech.* 2005, vol. 65, no. 13, p. 1931–1940.

[81] LUX, J., AHMADI, A., GOBBÉ, C. and DELISÉE, C. Macroscopic thermal properties of real fibrous materials: Volume averaging method and 3D image analysis, *Int. J. Heat. Mass. Transfer* 2006, vol. 49, no. 11-12, p. 1958-1973.

[82] JAGANATHAN, S., TAFRESHI, H.V., POURDEYHIMI, B. Modeling liquid porosimetry in modeled and imaged 3-D fibrous microstructures, *Journal of Colloid and Interface Science* 2008, vol. 326, no. 1, p. 166-175.

[83] BLOCH, J.-F, Paper Structure Characteristics Using X-Ray Microtomography, *AFSS Ninth World Filtration Congress*, April, 2004.

[84] THIBAULT, X., CLOETENS, P., BLOCH, J -F, PEYRIN, F. Non-Woven Characterization Using X-Ray Synchrotron Radiation Micro-tomography, *AFSS Ninth World Filtration Congress*, April, 2004.

[85] JAGANATHAN, S., TAFRESHI, H.V., POURDEYHIMI, B. A Case Study of Realistic Two-Scale Modeling of Water Permeability in Fibrous Media, *Seperation Science and Technology* 2008, vol. 43, no. 8, p. 1901-1916.

[86] TOMADAKIS, M.M. and ROBERSTON, T.J. Viscous permeability of random fiber structures: Comparison of electrical and diffusion estimates with experimental and analytical results, *J. Compos. Mater.* 2005, vol. 39, no. 2, p. 163-188.

PAPER I

Polymer Testing

Test Method

The use of novel digital image analysis technique and rheological tools to characterize nanofiber nonwovens

Wannes Sambaer [a], Martin Zatloukal [a,*], Dusan Kimmer [b]

[a] Polymer Centre, Faculty of Technology, Tomas Bata University in Zlin, TGM 275, 762 72 Zlin, Czech Republic
[b] SPUR a.s., T. Bati 299, 764 22 Zlin, Czech Republic

ARTICLE INFO

ABSTRACT

Polyurethane (PU) solved in dimethylformamide (DMF) was electrospun under one set of conditions using five different supporting textiles. The mechanical properties of the nanofiber mats were measured by the Sentmanat extensional rheometer, and the pore size distribution was calculated by a newly proposed digital image analysis methodology applied on nanoscale SEM images taking macroscopic features of the nonwovens into account. It has been found that supporting textiles have a very high effect on mechanical properties of nanofiber mats (even if their fiber diameter distributions are similar), which can be explained by different porosity of the prepared samples.

© 2009 Elsevier Ltd. All rights reserved.

1. Introduction

In recent years, nanofiber-related research work, publications and patents have grown rapidly in areas of biological, medical, filtration, sensors, composites and catalysis applications [1–3]. One of the most popular techniques for nanofiber production is electrospinning where the polymer solution is stretched by the electrostatic force acting between two electrodes with simultaneous evaporation of the solvent [4,5]. In this case, the produced nanofibers are accumulated on a grounded collector, which is covered by the supporting textile. It has been found that the final properties of the produced nanofiber nonwovens depends on the material-related properties, such as polymer type, viscosity, electrical conductivity [6], surface tension of the solvent, as well as on the processing-related characteristics, such as applied voltage [7], distance between collector and electrode, humidity [8,9], pressure [10] and temperature [10] in the chamber. One of the most important characteristic of polymeric nanofiber webs are their mechanical properties and, therefore, it is not surprising that considerable effort has been paid to experimentally determining these characteristics by using conventional tensile machines or more sophisticated equipment such as an atomic force microscope cantilever (AFM) or bending tests [8,11–15]. Even if many useful conclusions about the link between processing parameters and produced nanofiber webs can be extracted from the open literature, to our knowledge, there is no research related to the role of the supporting textile type (where the nanofibers are collected during the electrospinning process) on the product properties. Therefore, in this work, the role of the supporting textile type on the mechanical and structural characteristics of the nanofiber nonwovens will be investigated in detail. For this purpose, firstly, a specific procedure to measure mechanical properties of the nanofiber webs by using a Sentmanat extensional rheometer [16–18] will be utilized to overcome difficulties connected with problematic manipulation of extremely small fibers, and very sensitive force transducer requirements. Secondly, a novel digital image analysis technique (which is based on the theoretical approach proposed in [19–21]) will be developed and used for the detailed structure nanofiber web analysis.

* Corresponding author.
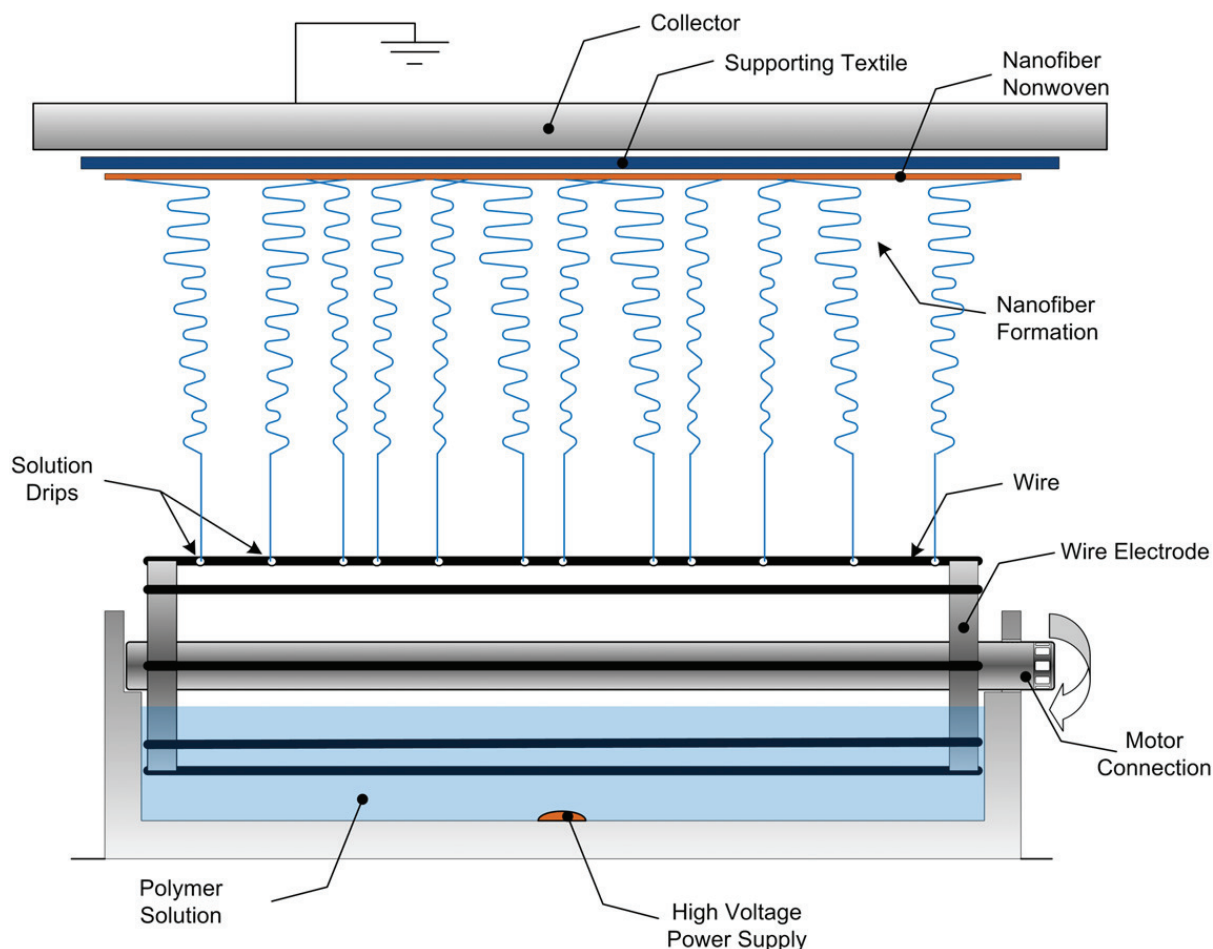 E-mail address: mzatloukal@ft.utb.cz (M. Zatloukal).

Fig. 1. Scheme of the electrospinning process.

2. Experimental and theoretical analysis

2.1. Material

A polyurethane (PU) solution based on 4,4′methylene-bisphenylisocyanate, poly(3-methyl-1,5-pentanediol)-alt-(adipic, isophtalic acid) and 1,4 butanediol (molar ratio 6:1:5) solved in dimethylformamide (DMF) was synthesized. The prepared solution was suitable for electrospinning and had a PU concentration of 11.5 wt%, viscosity of 0.99 Pa s and conductivity of 151 μS/cm (adjusted by tetraethylamonium bromide).

2.2. Sample preparation by electrospinning process

PU nanofibers were prepared from the above mentioned PU solution with a commercially available NanoSpider™ machine (Elmarco s.r.o. Liberec, Czech

Table 1
Detailed characteristics of the used supporting textiles.

Textile	% Poly(m-aramid)	Staple length (mm)	Fineness (dtex)	Fibre diameter (μm)
311	89.9%	51	1.7	12.5
318	35.0%	51	1.7	12.5
319	98.8%	51	1.7	12.5
	% Poly(p-aramid)	Staple length (mm)	Fineness (dtex)	Fibre diameter (μm)
311	90.0%	–	1.7	12.7
318	63.8%	50	2.2	13.8
319	–	–	–	–
	% Stainless steel	Staple length (mm)	Fineness (dtex)	
311	1.2%	–	400	
318	1.2%	51	400	
319	1.2%	51	400	
PPNW	Melt blown PP 30 g/m^2	Freshening Polyfix N		
PPPE	Melt blown PP + PE foil	Freshening Polyfix N		

I.2
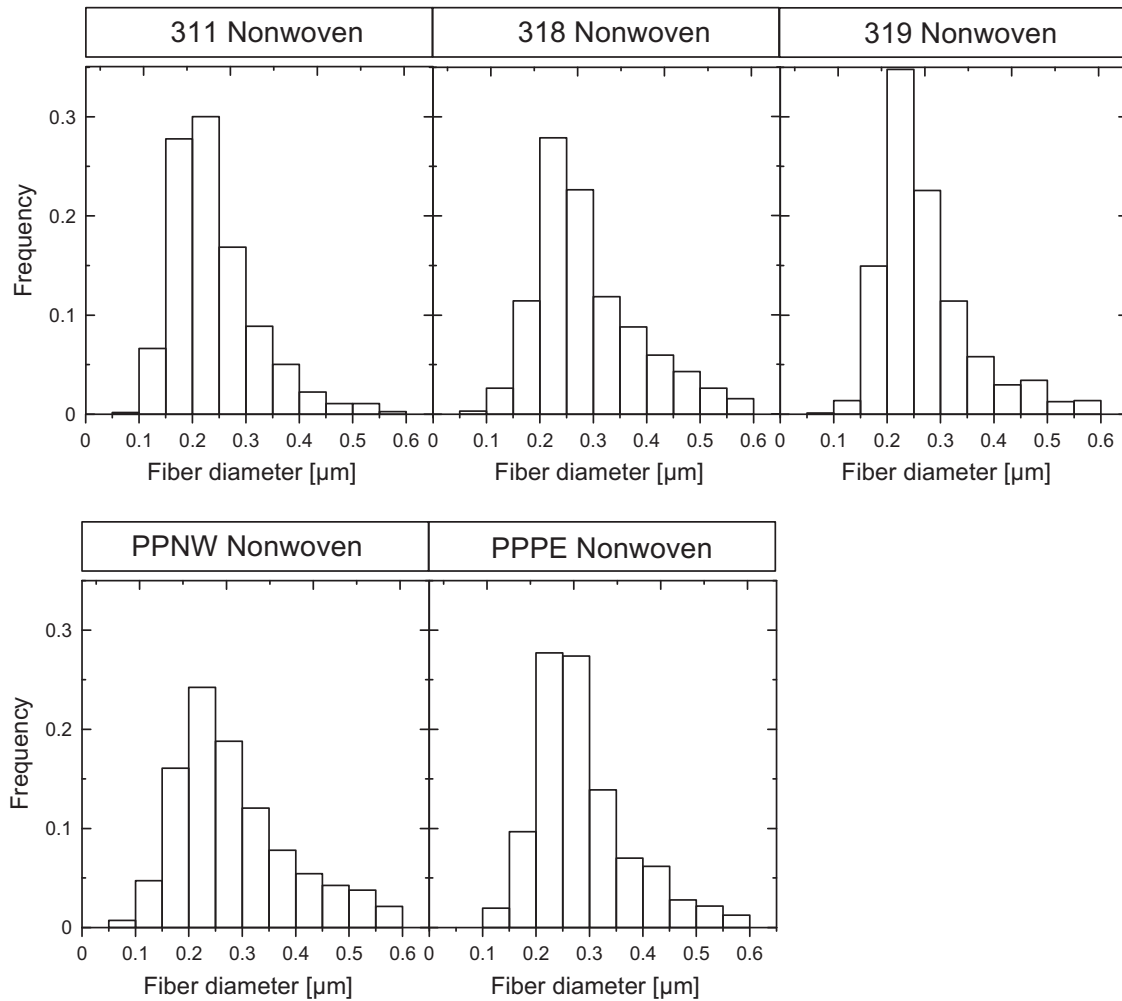
Fig. 2. Fiber diameter distributions for all investigated nanofiber nonwovens.

Republic, http://www.elmarco.com/) equipped with one rotational electrode (see Fig. 1) and five different supporting textiles. Three of them were based on meta and para aramid fibers containing 1.2% of stainless steel fibers (which were woven through these textiles) whereas the other two were based on melt-blown polypropylene with and without polyethylene foil (see Table 1 for more details). The experimental conditions were: relative humidity 28%, temperature 27.5 °C, electric voltage between wire rotational electrode and grounded collector (electrode) 75 kV, distance between electrodes 180 mm, rotational electrode speed 7 rpm and speed of supporting textile collecting nanofibers was 0.16 m/min. Samples for further analyses were taken from the middle part of the produced nanofiber textiles having the fiber diameter distribution as depicted in Fig. 2.
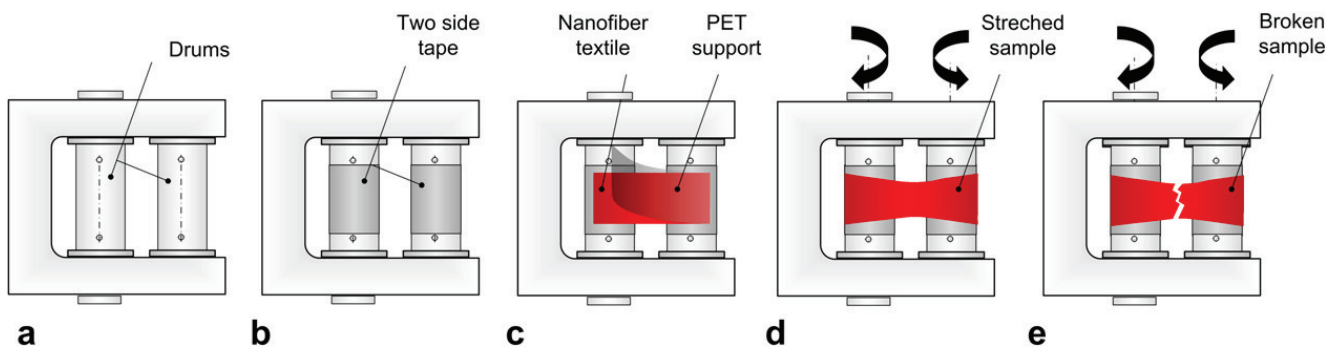
Fig. 3. Visualized methodology for the tensile testing of the nanofiber nonwoven by using Sentmanat extensional rheometer. a) SER unit, b) SER with double-sided adhesive tape, c) Nanofiber web deposition on the SER unit, d) Sample stretching, e) Sample at break.

I.3
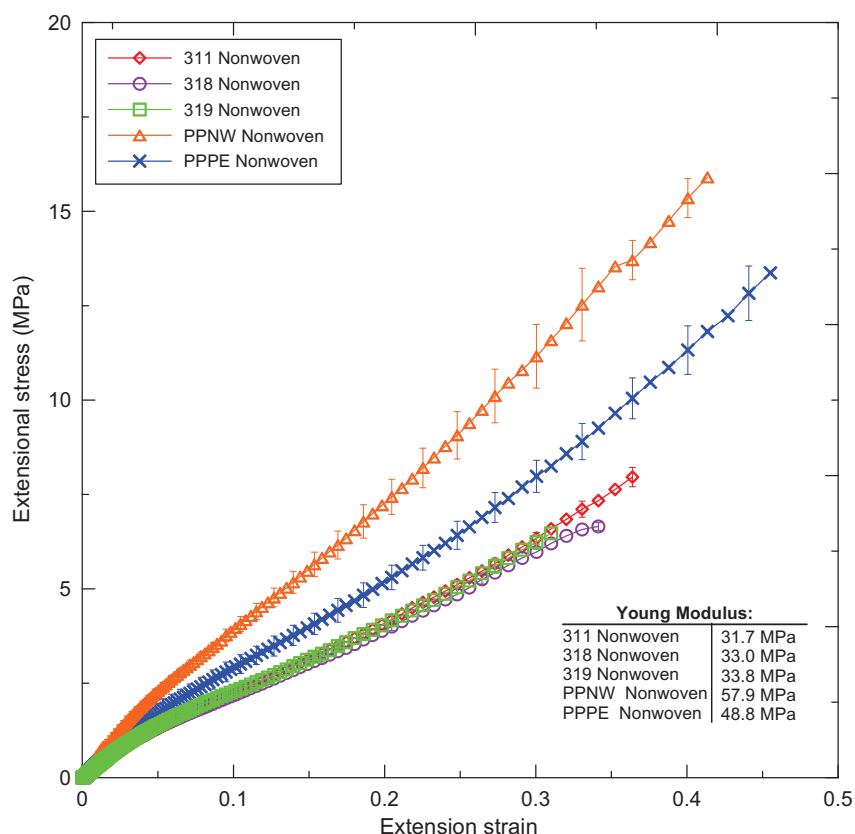
Fig. 4. Measured extensional stress as a function of extensional strain for all investigated nonwoven samples.
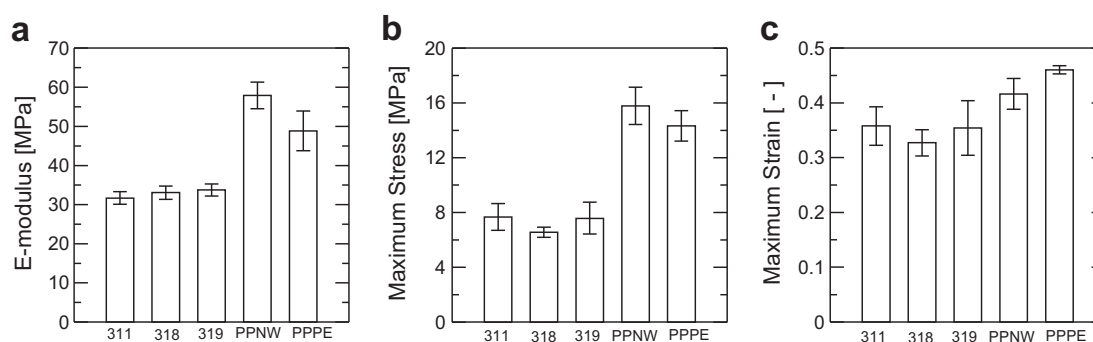
Fig. 5. Summarized tensile strength characteristics for all investigated nonwoven samples. a) E-modulus, b) Stress at break, c) Strain at break.

Table 2
Summarization of mechanical properties for different PU nanofiber nonwovens produced on different supporting textiles.

Sample name		E-modulus	Max Stress	Max Strain
		[MPa]	[MPa]	[–]
311 nonwoven	Average	31.7	7.7	0.358
	Deviation	1.6	1.0	0.035
	Fault	5.1%	12.7%	9.8%
318 nonwoven	Average	33.0	6.6	0.3
	Deviation	1.7	0.4	0.024
	Fault	5.2%	5.5%	7.3%
319 nonwoven	Average	33.8	7.6	0.4
	Deviation	1.5	1.2	0.0
	Fault	4.5%	15.4%	14.0%
PPNW nonwoven	Average	57.9	15.8	0.416
	Deviation	3.4	1.4	0.028
	Fault	5.9%	8.7%	6.7%
PPPE nonwoven	Average	48.8	14.3	0.460
	Deviation	5.1	1.1	0.008
	Fault	10.4%	7.8%	1.7%

2.3. Tensile testing

An Advanced Rheometric Expansion System (ARES) rotational rheometer equipped with Sentmanat Extensional Rheometer (SER) Universal Testing Platform [16–18], Fig. 3a, (which is normally used for polymer melt extensional viscosity/strength characteristics determination) was used in this work to determine mechanical properties of the prepared nanofiber textiles. For this purpose, the following strategy has been proposed. Firstly, double-sided adhesive tape was stuck on both SER drums (Fig. 3b). Secondly, the very thin nanofiber textile (deposited on PET foil) was attached on this tape and then the PET foil was carefully removed (Fig. 3c). Finally, the sample was stretched at a constant extensional strain rate of 0.01 s^{-1} (Fig. 3d) until the sample breaks (Fig. 3e). The
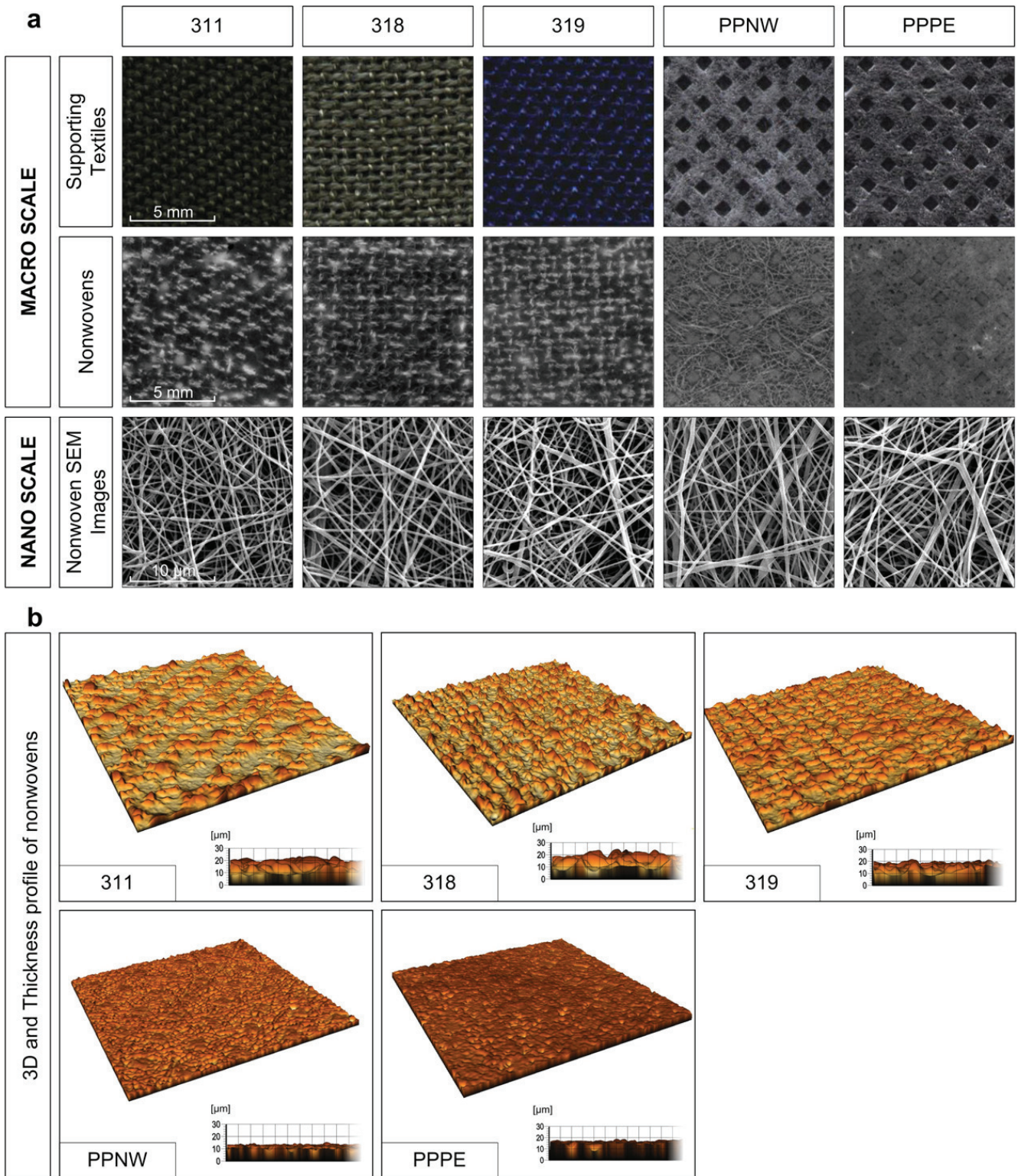
I.4

Fig. 6. Visualization of the utilized supporting textiles and obtained nanofiber nonwovens through electrospinning process. a) Macroscale top view of the used supporting textiles and obtained nanofiber nonwovens together with nanoscale views. b) Visualized macroscale view of 3D structure and thickness profile for obtained nanofiber nonwoven.

obtained tensile curves (extensional stress as a function of extensional strain) and basic characteristics such as Young's modulus and stress/strain at break are depicted in Figs. 4 and 5 and summarized in Table 2 for all tested samples. As it can be seen, there is a big difference between the mechanical properties of the nanofiber nonwovens due to different supporting textiles that were used during the electrospinning process. In more detail, PU nanofiber samples where the melt blown PPNW and PPPE supporting textiles were used have much higher

I.5
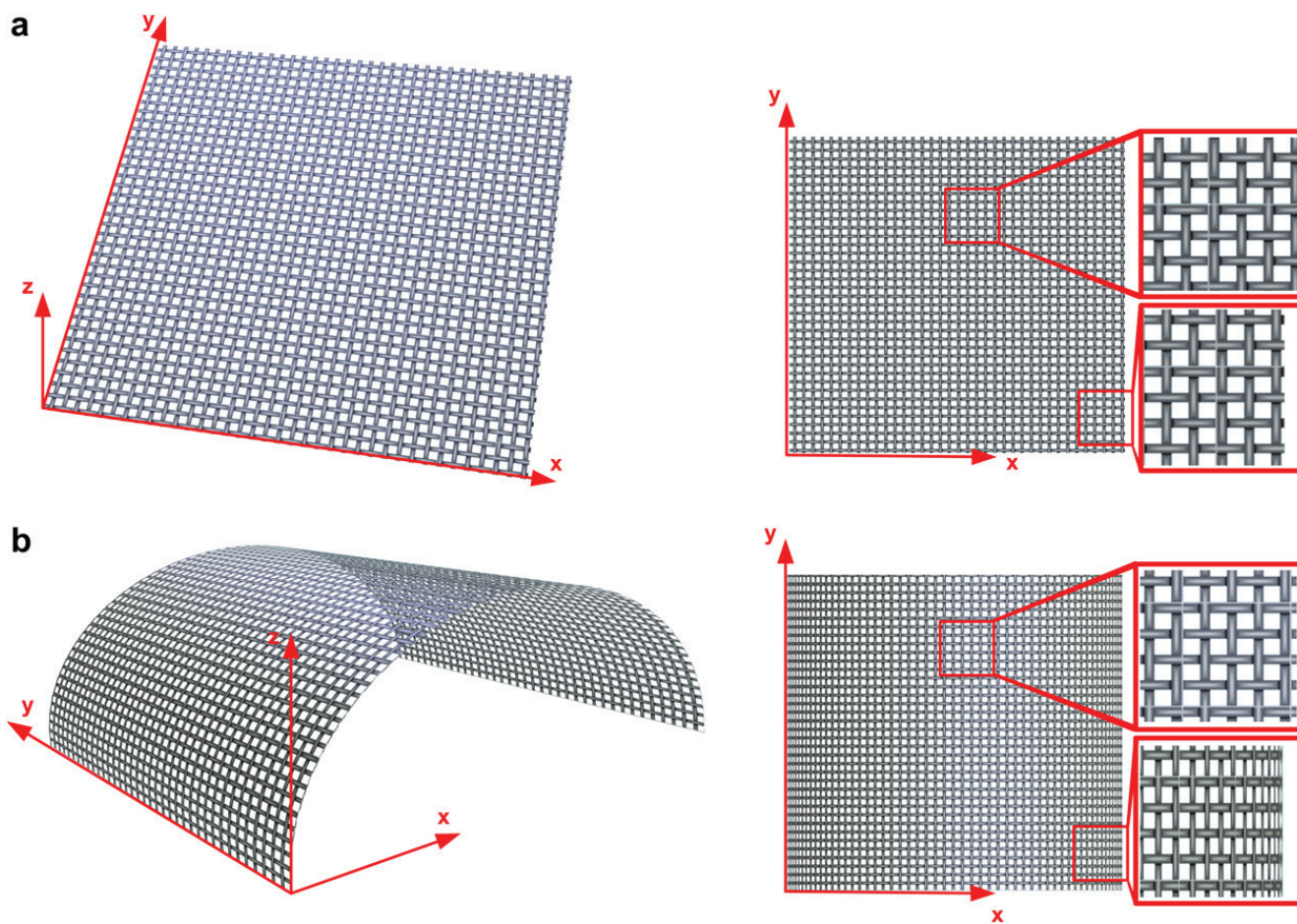
Fig. 7. Effect of the surface bending on the artificial change of the pore sizes if only top view is considered. a) Flat sample surface, b) Bended sample surface.

Young's modulus and stress/strain at break in comparison with PU nanofiber samples which have been produced on supporting textiles 311, 318 and 319 (based on aramid). From this experimental data, it is obvious that the supporting textile used during the electrospinning process has crucial impact on the final mechanical properties of the PU nanofiber nonwoven material. An interesting question is why the supporting textile has such a high effect on the final mechanical properties of the produced

nonwovens having similar and/or comparable fiber diameter distribution (see Fig. 2). In order to understand this phenomenon in more detail, we have developed and used a novel digital image analysis technique to determine pore size distribution for all tested samples, which is introduced in the next section.

With respect to mechanical testing by using SER, it should be mentioned that the main advantage of this 'rheology based' methodology is the possibility to measure
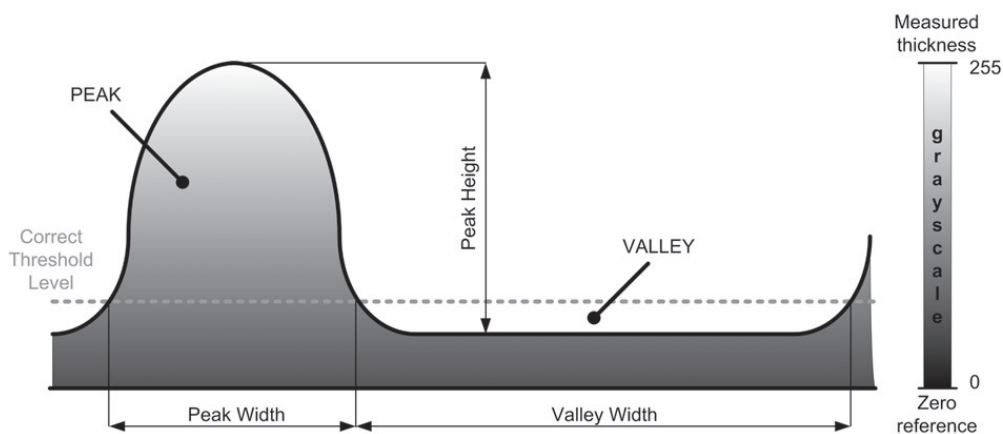
Fig. 8. Definition of 3D structure characteristics such as peak height, peak width and valley width for 'correct' threshold level calculation.

I.6
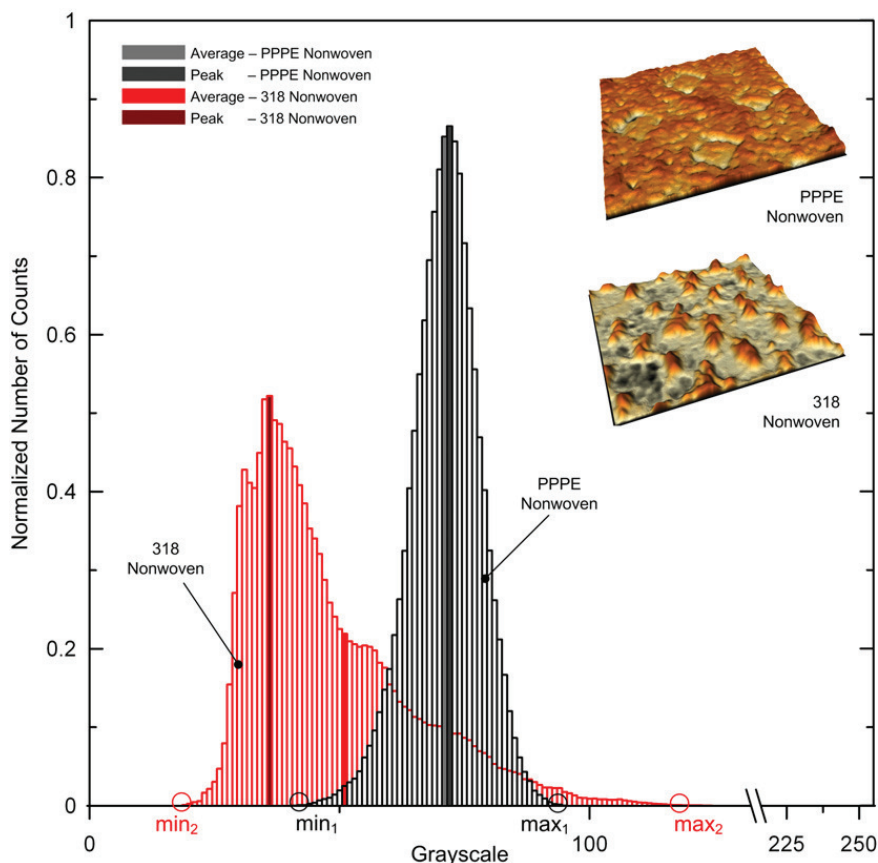
Fig. 9. Normalized greyscale histogram for PPPE and 318 nonwovens.

very fine structures with low experimental error due to the utilization of very sensitive torque/normal force trans-ducers, which are normally present on standard rotational rheometers for polymer melt rheology evaluation. More-over, the measurements can be done at different exten-sional strain rates and temperatures by using the conventional rheometer oven, which is difficult or impos-sible to do by using standard methodologies.

2.4. Nanofiber based nonwovens structure analysis

In Fig. 6a, macroscale as well as nanoscale views of both supporting textiles and corresponding PU nanofiber based nonwovens are provided. It is clearly visible that the specific 3D character of the supporting textile texture is 'copied' into the PU nanofiber based nonwovens as it is visible on the macroscale pictures. In more detail, it is clearly visible that the use of the aramid based support-ing textiles during the electrospinning process causes creation of highly 3D textured nonwovens (with high number of peaks and valleys), whereas the use of melt blown supporting textiles leads to generation of more 2D textures (the thickness profile of PU nonwovens is more even in this case), as visible in Fig. 6b. This 3D nature of the nonwoven texture may cause an artificial pore size density increase as demonstrated in the example Fig. 7. In this Figure, 2D top views of two identical virtual rectan-gular textiles (having different 3D textures) are provided.

In Fig. 7a, the textile having identical pore sizes and flat surface is depicted. On the other hand, the Fig. 7b shows top view of exactly same textile which is bent i.e. surface is not flat. Even if the pore sizes are identical in both cases, due to the textile bending (peak occurrence), artificial decrease of the pore sizes can occur, as visible in Fig. 7b. This means that the 3D nature of any analyzed nanofiber based nonwovens has to be taken into account for detailed structure analysis, especially if a Scanning Electron Microscope (SEM) picture representing the top view of the sample is utilized. Note that all SEM pictures used in this work were obtained by using field emission scanning electron microscopy (Vega II LSU, Tescan, Czech republic). The analyzed nanoscale pictures had a resolu-tion of 9009 × 9009 px where one pixel represents a square of 10 by 10 nm.

2.4.1. 3D correction for nanoscale SEM pictures

At the beginning, it is necessary to relate greyscale level of the macroscale pictures with the real sample thickness. To do that, the nonwoven samples were scanned with black paper on top to increase the contrast of the picture. The black color of the paper (greyscale number is equal to 0) was taken as a zero-reference thickness of the nanofiber textile whereas the brightest point (greyscale number up to 255) was calibrated as the maximum thickness, which was measured with a micrometer on the real nonwoven sample. By using these two calibration points, the whole
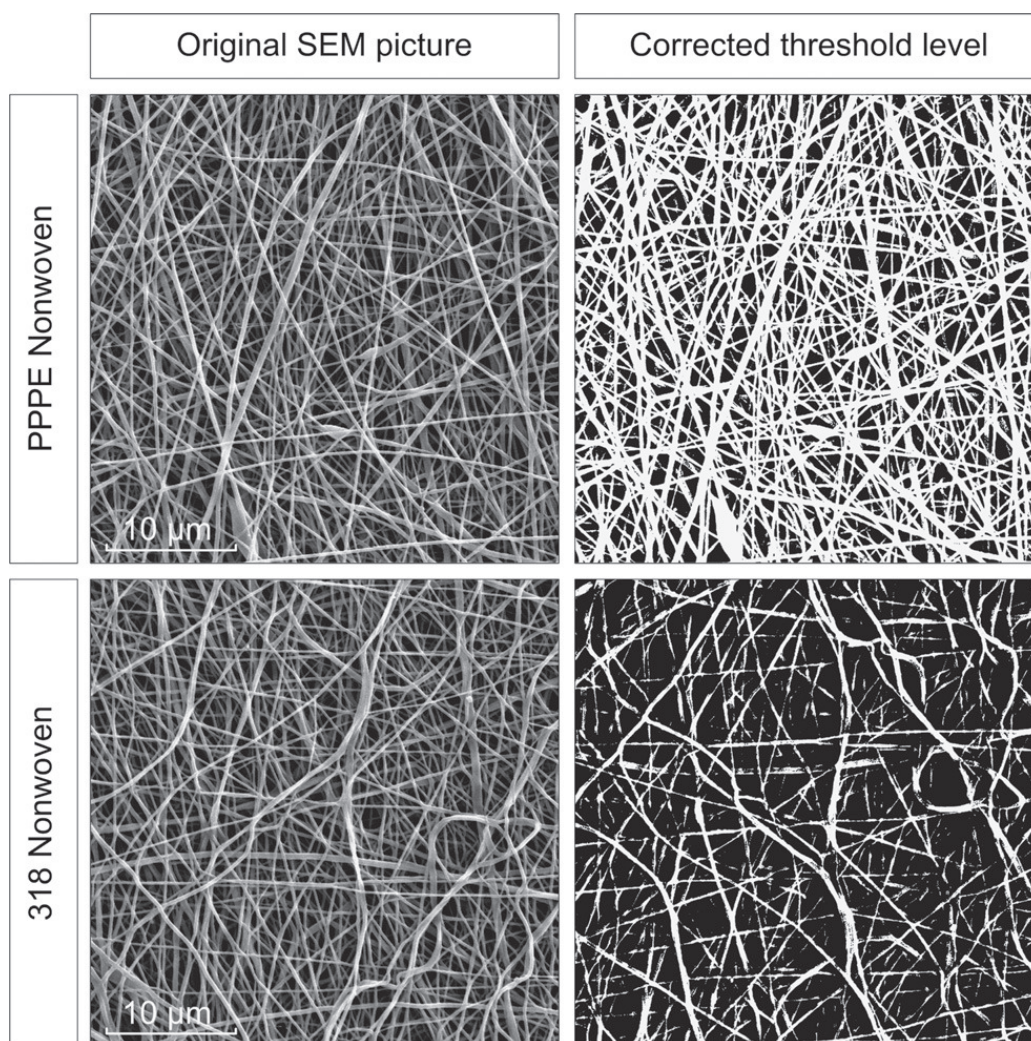
Fig. 10. SEM pictures for flat PPPE and 3D 318 nonwoven samples before and after 'correct' threshold level χ application.

range of the greyscale values has been related to the thickness, considering a linear relationship between these two variables.

The basic principle of the 3D correction is modification of 2D SEM pictures to emphasize all structure details at one real depth level, which will be the same for all investigated samples. This can be done by defining the 'correct' threshold level χ (pixels having greyscale value higher or lower than threshold level value becomes white or black, respectively) for each 2D SEM picture by using the following 3D structure characteristics: the peak height, β, and the peak and valley width ratio α (graphical definition of these parameters is provided in Fig. 8). All these parameters can be determined from the calibrated macroscale picture greyscale histogram as is demonstrated in the following example. Fig. 9 shows two different greyscale histograms (pixel greyscale value distribution) for a macroscale flat structure (PPPE sample) and a 3D structure (318 sample). Each histogram is characterized by the following values: minimum, *min*, maximum, *max*, the most frequent, *P*, and average, μ, greyscale numbers. By using these parameters, the 'correct' threshold level χ (which can vary only between

0 and 255) can be determined from the peak height β (Eq. (1)) and the peak and valley width ratio α (Eq. (2)) according to Eq. (3).

$$\beta = \max - \min \tag{1}$$

$$\alpha = \frac{P}{\mu} \tag{2}$$

$$\chi = \frac{\beta}{\alpha} \tag{3}$$

where the average greyscale number μ is defined as following:

$$\mu = \frac{\sum_{i=0}^{255} iC_i}{\sum_{i=0}^{255} C_i} \tag{4}$$

Here, i is the greyscale number and C_i represents number of counts for the ith greyscale number.

It also should be mentioned that original SEM pictures may have different lightening depending on the operator and microscopy type. In order to have comparable SEM
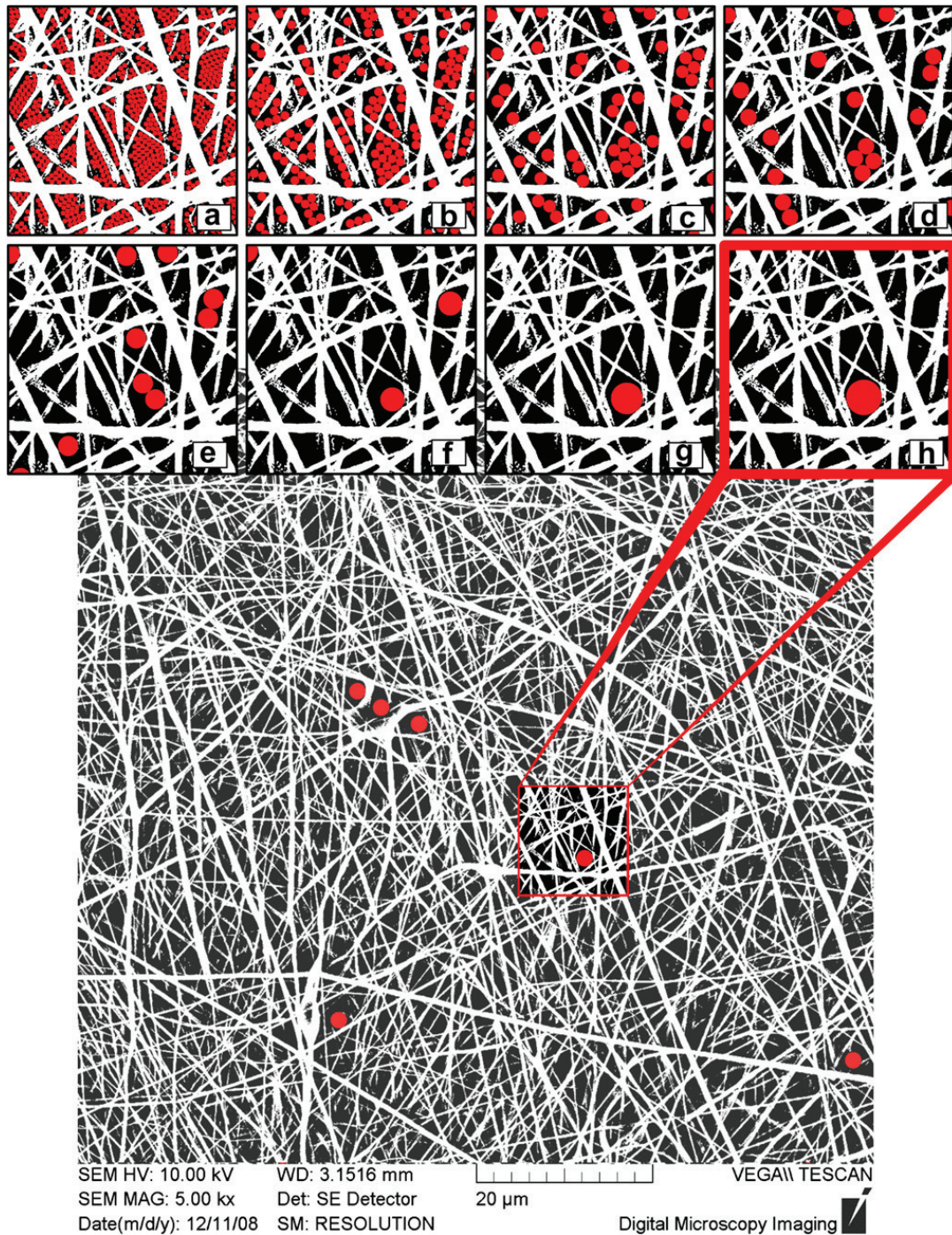
I.8

Fig. 11. Visualization of pore size distribution analysis for PPNW nonwoven sample for different circle diameters: $D_A = 250$ nm, $D_B = 450$ nm, $D_C = 650$ nm, $D_D = 850$ nm, $D_E = 1050$ nm, $D_F = 1250$ nm, $D_G = 1650$ nm, $D_H = 1850$ nm.

picture lightening, firstly, average greyscale level for each picture has been evaluated from the greyscale histogram. Secondly, the obtained individual average greyscale values for each picture have been averaged to get one total greyscale value average. Finally, the lightness for all SEM pictures has been changed in such a way, that all the pictures have the same average greyscale number, which is equal to the total greyscale value average. After this procedure, the 'correct' threshold level χ has been applied for all SEM pictures to perform pore size distribution

analysis, which is described below in more detail (see Fig. 10 that shows SEM pictures for flat PPPE and 3D 318 samples before and after 'correct' threshold level χ application).

2.4.2. Pore size distribution analysis

In this part, novel Scanning Electron Microscope (SEM) picture digital image analysis technique for determination of pore size distribution for nanofiber based nonwovens is introduced. This method is based on the recent work of

I.9
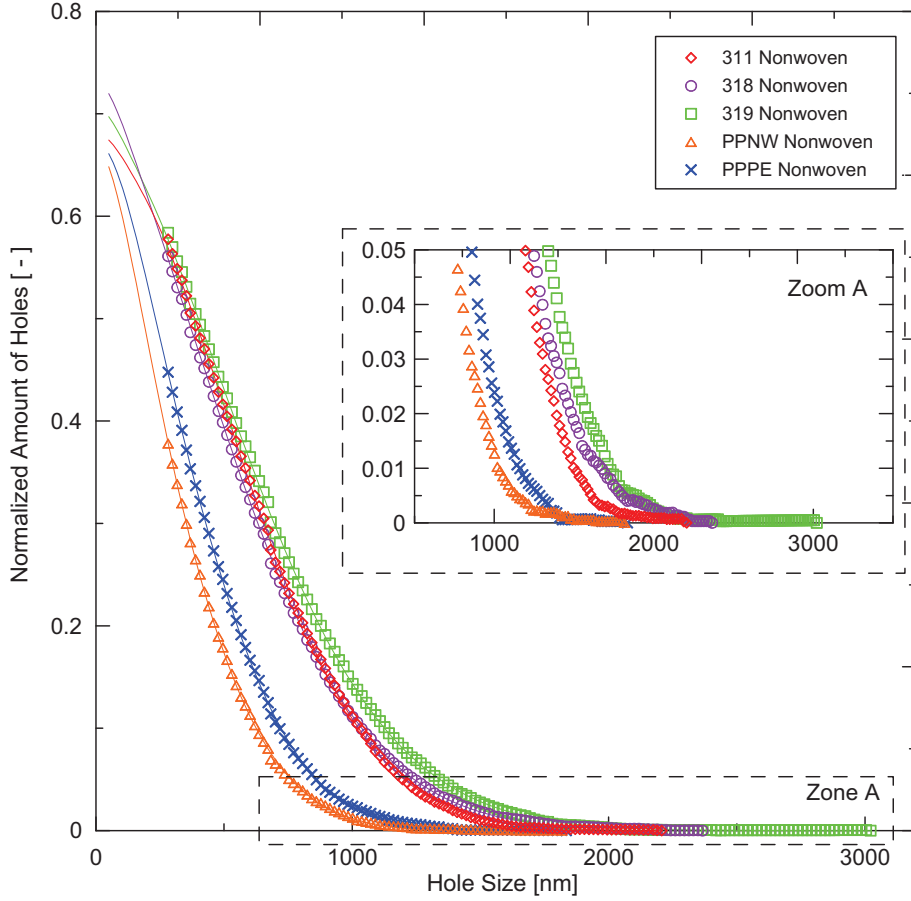
Fig. 12. Normalized amount of holes as a function of the hole size for all samples where symbols represents raw data and lines represents prediction of double stretched exponential (Kohlrausch–Williams–Watts) function.

Ghasemi-Mobarakeh and Semnani et al. [20,21], who analyze the pores by using different cells with three different characteristic sizes (10, 20 and 30 μm) that could infiltrate the fiber based product. In this work, we have generalized this approach considering virtually unlimited number of cells (depends on particular computer memory allocation capability of the PC used) having sizes from units of nanometers to hundreds of μm which can pass through the fiber nonwoven, and also taking the 3D macroscopic shape of the nanofiber based textile properly into account through application of 'correct' threshold level χ. In Fig. 11, a part of the graphical results are shown to demonstrate how the methodology works. After this procedure is done, the number of circles has been counted and normalized for each sample and plotted versus circle diameter, which represents the pore/hole size in this case (see Fig. 12). In order to calculate pore/hole size distribution curve, the derivatives from the Fig. 12 has to be calculated. To do that effectively and precisely, the data in Fig. 12 were fitted by a combination of two stretched exponential functions (Kohlrausch–Williams–Watts, KWW, function) having the following form:

$$N(D) = A_1 \exp\left[-\left(\frac{D}{\tau_1}\right)^{\beta_1}\right] + A_2 \exp\left[-\left(\frac{D}{\tau_2}\right)^{\beta_2}\right] \quad (5)$$

where $N(D)$ is normalized number of holes, D is the hole size in nm and A_1, A_2, β_1, β_2, τ_1 and τ_2 are fitting constants.

As can be seen in Fig. 12, the chosen model (solid line in this Figure) describes the discrete data very well and, thus, the normalized derivative $dN(D) = d$(normalized number of holes)/d(hole size) can be easily calculated from Eq. (5) by using the following expression:

$$\frac{dN(D)}{} = \frac{A_1 \exp\left[-\left(\frac{D}{\tau_1}\right)^{\beta_1}\right]\frac{\beta_1}{\tau_1}\left(\frac{D}{\tau_1}\right)^{\beta_1-1} + A_2 \exp\left[-\left(\frac{D}{\tau_2}\right)^{\beta_2}\right]\frac{\beta_2}{\tau_2}\left(\frac{D}{\tau_2}\right)^{\beta_2-1}}{A_1 \exp\left[-\left(\frac{D_s}{\tau_1}\right)^{\beta_1}\right] + A_2 \exp\left[-\left(\frac{D_s}{\tau_2}\right)^{\beta_2}\right]}$$

$$(6)$$

where D_s is a constant equal to the smallest (circle/hole) diameter that can be detected in the picture. The obtained pore size distribution curves for all investigated samples are depicted in Fig. 13. For the pore size distribution curves evaluation, D_{z+1} hole size average (which is sensitive to the highest pores in the analyzed structure), which is defined below has been used

$$D_{z+1} = \frac{\int_{D_s}^{\infty} D^3 dN(D) dD}{\int_{D_s}^{\infty} D^2 dN(D) dD} \quad (7)$$

Based on the pore size distribution curves depicted in Fig. 13, it can be concluded that the use of melt blown supporting textiles during electrospinning process leads
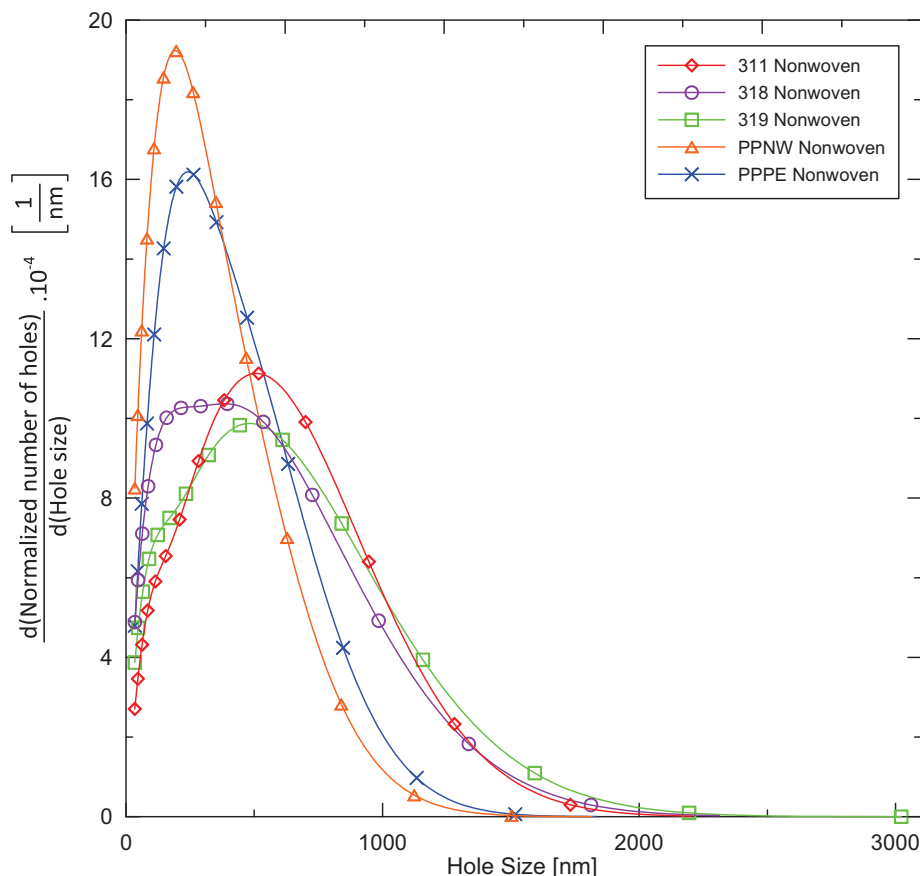
I.10

Fig. 13. Calculated pore size distribution for all investigated nonwoven samples.

to nanofiber based structures (PPNW and PPPE samples) having much smaller pores than structures prepared by the use of the aramid based supporting textiles (311, 318, 319 samples). For experimental determination of the amount of air in the mats, the air or porosity factor $\overline{\alpha} = 1 - (\rho_f/\rho_{PU})$ has been utilized, where ρ_f and ρ_{PU} are densities of fibers and bulk PU, respectively. The density of the fibers was determined from 10 different measurements of the weight and the volume for each sample. Volume has been calculated from the rectangle sample area (width = 12.7 mm, length = 50 mm) and sample thickness. Note that percentage amount of the air has also been theoretically evaluated from area calculation between all nanofibers by using the circles having the smallest possible size, i.e. one pixel size, for all investigated samples. Theoretically, as well as experimentally, determined amounts of air are summarized for all samples in Table 3. Clearly, the samples having the smallest pores (PPNW and PPPE) contain less air than samples having the higher pores (311, 318, 319). It can also be seen that the error of measured amount of air is much higher than the theoretical one due to thickness measurement difficulties (small sample thicknesses and high elasticity). The airfactor difference between investigated samples prepared from the same PU solution can explain their big differences in mechanical properties because the amount of PU material in each sample is different. This is visible in Figs. 14 and 15 where the

maximum stress at break together with E-modulus is plotted as a function of D_{z+1} hole size average and percentage amount of air.

3. Conclusions

Based on the performed experimental work and proposed novel digital image analysis technique for nanoscale SEM pictures (taking macroscopic structure features into account) has been found that supporting textiles have very high effect on mechanical properties of polyurethane nanofiber nonwovens prepared by the electrospinning process (even if their fiber diameter distributions were similar), which can be explained by different porosity of the prepared samples.

Table 3
Theoretically as well as experimentally determined airfactor for all investigated nonwoven samples.

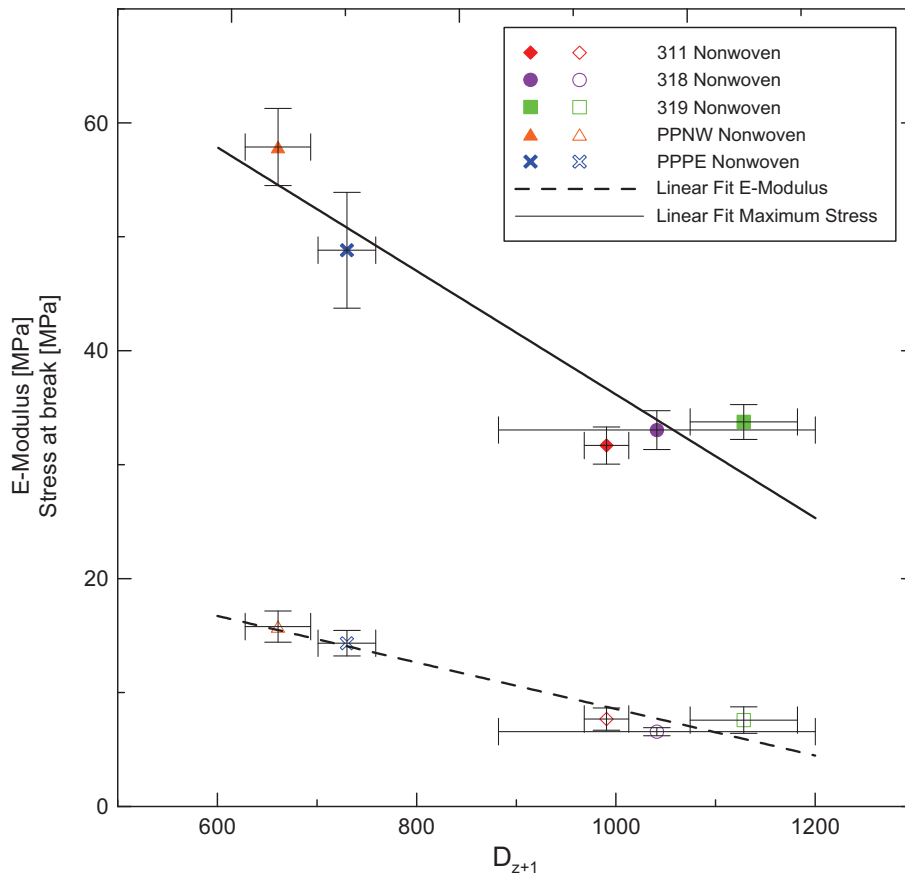| Nonwoven	Experimental Airfactor	Theoretical Airfactor
311	84.9% ± 3.7%	79.1% ± 1.3%
318	83.9% ± 4.1%	68.7% ± 0.2%
319	83.8% ± 4.5%	73.5% ± 1.7%
PPNW	75.5% ± 2.9%	34.1% ± 0.9%
PPPE	79.0% ± 9.4%	43.5% ± 0.5%

I.11

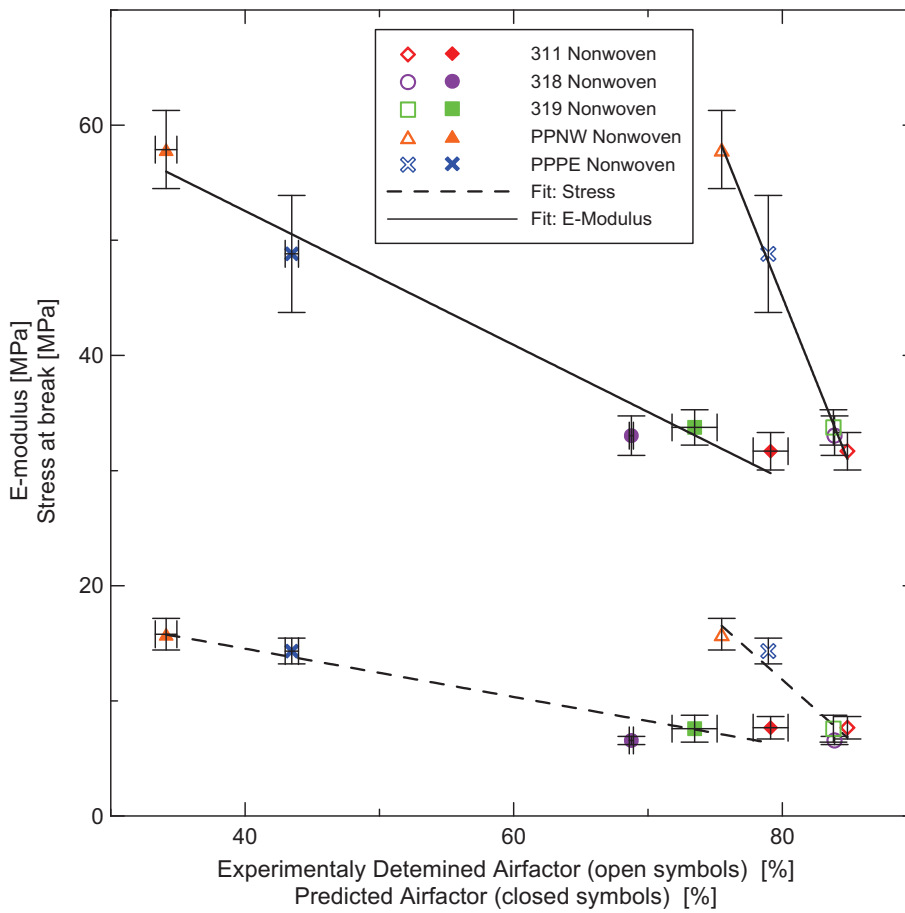**Fig. 14.** E-modulus and stress at break as a function of D_{z+1} hole size average.

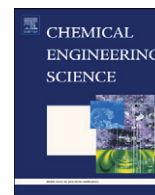**Fig. 15.** E-modulus and stress at break as a function of airfactor.

I.12

Acknowledgments

References

[1] Z.M. Huang, Y.Z. Zhang, M. Kotiki, S. Ramakrishna, Compos. Sci. Technol. 63 (2003) 2223–2253.
[2] M.S. Khil, Di Cha, H.Y. Kim, I.S. Kim, N. Bhattarai, J. Biomed. Mater. 67B (2003) 675–679.
[3] S.H. Kim, Y.S. Nam, T.S. Lee, W.H. Park, Silk, Polym. J. 35 (2003) 185–190.
[4] D. Li, Y. Xia, Adv. Mater. 16 (2004) 1151–1170.
[5] D. Kimmer, P. Slobodian, D. Petras, M. Zatloukal, R. Olejnik, P. Saha, J. Appl. Polym. Sci. 111 (2009) 2711–2714.
[6] T. Uyar, Flemming Besenbacher, Polymer 49 (2008) 5336–5343.
[7] D. Fallahi, M. Rafizadeh, N. Mohammadi, B. Vahidi, Polym. Int. 57 (2008) 1363–1368.
[8] E.P.S. Tan, C.T. Lim, Compos. Sci. Technol. 66 (2006) 1102–1111.
[9] S. Megelski, J.S. Stephens, D.B. Chase, J.F. Rabolt, Macromolecules 35 (2002) 8456.
[10] S. de Vrieze, T. van Camp, A. Nelvig, B. Hagstrom, P. Westbroek, K. de Clerck, J. Mater. Sci. 44 (2009) 1357–1362.
[11] X. Wang, Y. Yan, M.J. Yost, S.A. Fann, S. Dong, X. Li, J. Biomed. Mater. Res. Part A 130–135 (2006).
[12] Lu-Qi Liu, D. Tasis, M. Prato, H.D. Wagner, Adv. Mater. 19 (2007) 1228--1233.
[13] E.P.S. Tan, S.Y. Ng, C.T. Lim, Biomaterials 26 (2005) 1453–1456.
[14] C.L. Casper, J.S. Stehens, N.G. Tassi, D.B. Chase, J.F. Rabolt, Macromolecules 37 (2004) 573–578.
[15] X.F. Wang, X.M. Chen, K.H. Yoon, D.F. Fang, B.S. Hsiao, B. Chu, Environ. Sci. Technol. 39 (2005) 7684–7691.
[16] M.L. Sentmanat, B.N. Wang, G.H. McKinley, J. Rheol. 49 (2005) 585.
[17] M.L. Sentmanat, Rheol. Acta 43 (2004) 657.
[18] M.L. Sentmanat, US Patent No.6, 578, 413, (2003).
[19] M. Ziabari, V. Mottahitalab, A.K. Haghi, Korean J. Chem. Eng. 25 (2008) 923–932.
[20] L. Ghasemi-Mobarakeh, D. Semnani, M. Morshed, J. Appl. Polym. Sci. 106 (2007) 2536–2542.
[21] D. Semnani, L. Ghasemi-Mobarakeh, M. Morshed, Mohammad-Hossein Nasr-Esfahani, J. Appl. Polym. Sci. 111 (2009) 317--322.

I.13

PAPER II

3D modeling of filtration process via polyurethane nanofiber based nonwoven filters prepared by electrospinning process

Wannes Sambaer [a], Martin Zatloukal [a,*], Dusan Kimmer [b]

[a] Polymer Centre, Faculty of Technology, Tomas Bata University in Zlin, TGM 275, 762 72 Zlin, Czech Republic
[b] SPUR a.s., T. Bati 299, 764 22 Zlin, Czech Republic

ARTICLE INFO

ABSTRACT

Full 3D particle filtration modeling at low pressures considering slip/transition/free molecular flow regime, particle–fiber interactions, air/particle slip, sieve and homogenous flow field has been performed for the polyurethane nanofiber filter prepared by electrospinning process and the obtained theoretical predictions for the filtration efficiency have been compared with the corresponding experimental data. Moreover, the effect of air velocity, viscosity, temperature, pressure and particle–fiber friction coefficient on the produced polyurethane nanofiber filter efficiency has been investigated in more details. In order to take all real structure features of the nanofiber filter into account (such as varying fiber diameter, curvature along its length, inhomogeneity and mat defects), a new approach for 3D nanofiber mat model construction from corresponding SEM images has been proposed and utilized.

© 2010 Elsevier Ltd. All rights reserved.

1. Introduction

During the past decades, significant progress has been done in the area of filtration science and technology (Andrady, 2008; Hosseini and Tafreshi, 2010a, b; Fotovati et al., 2010; Sambaer et al., 2010; Ashari and Tafreshi, 2009; Tafreshi et al., 2009; Jaganathan and Tafreshi, 2008; Jaganathan et al., 2008; Zobel et al., 2007; Wang et al., 2006a, b, 2007; Maze et al., 2007; McNenly et al., 2005; Pich, 1966; Li and Ahmadi, 1992; Ounis and Ahmadi, 1990; Ounis et al., 1991; Altmann and Ripperger, 1997; Rubin, 1977; Brown, 1993; Thomas and Yoder, 1956; Sinclair, 1970), which follows increased needs of many advanced industries dealing with electronics, medical, pharmaceutical and biology to maintain clean room manufacturing environments (Andrady, 2008; Brown, 1993). Nanofiber mats, having fiber diameter typically in order of tens and hundred nanometers, are very well suited for air filtration because low solidity and acceptable mechanical strength can be obtained. Moreover, due to nanoscale fiber diameter dimension, air slip flow occurs at the fiber surface, which lowers filtration pressure and increases efficiency of impaction, interception and diffusion due to increased contact of air and particles with the fiber surface (Andrady, 2008; Hosseini and Tafreshi, 2010a; McNenly et al., 2005; Brown, 1993). Even if the filters with nanofibers have relatively simple engineering construction, their aerosol collection efficiencies are not easily predictable because of the inability to precisely measure the detailed filter properties (Andrady, 2008). Thus, it is not surprising

that filtration modeling has been recently utilized on the virtual simplified nanofiber mats in order to understand their behavior in more detail (Hosseini and Tafreshi, 2010a, b). However, utilization of virtual idealized nanofiber mats in filtration modeling considering constant diameter along the fiber, neglecting their curvature, inhomogeneous features and possible defects may not sufficiently represent real nanofiber mats and thus, predictive capabilities of such models could be significantly reduced. In order to overcome this possible limitation, a new approach for real 3D nanofiber mat construction from their scanning electron microscopy (SEM) images is proposed here as the first step. This methodology is applied for manufactured polyurethane (PU) nanofiber nonwoven based filter prepared by the electrospinning process. In the next stage, full 3D particle filtration modeling using the 3D structure model representing real filter structure has been utilized considering slip/transition/free molecular flow regime, particle–fiber interactions, air/particle slip, sieve and homogenous flow field. The obtained theoretical predictions for the filtration efficiency have been compared with the corresponding experimental data. Finally, the effect of air velocity, viscosity, temperature, pressure and particle–fiber friction coefficient on the produced polyurethane nanofiber filter efficiency have been investigated.

2. Filter sample preparation and characterization

2.1. Material

A polyurethane solution in dimethylformamide (DMF) based on 4,4′methylenebis(phenylisocyanate) (MDI), poly(3-methyl-1,5-pentanediol)-alt-(adipic, isophtalic acid) (PAIM) and 1,4 butanediol

* Corresponding author. Tel.: +420 57 603 1320.
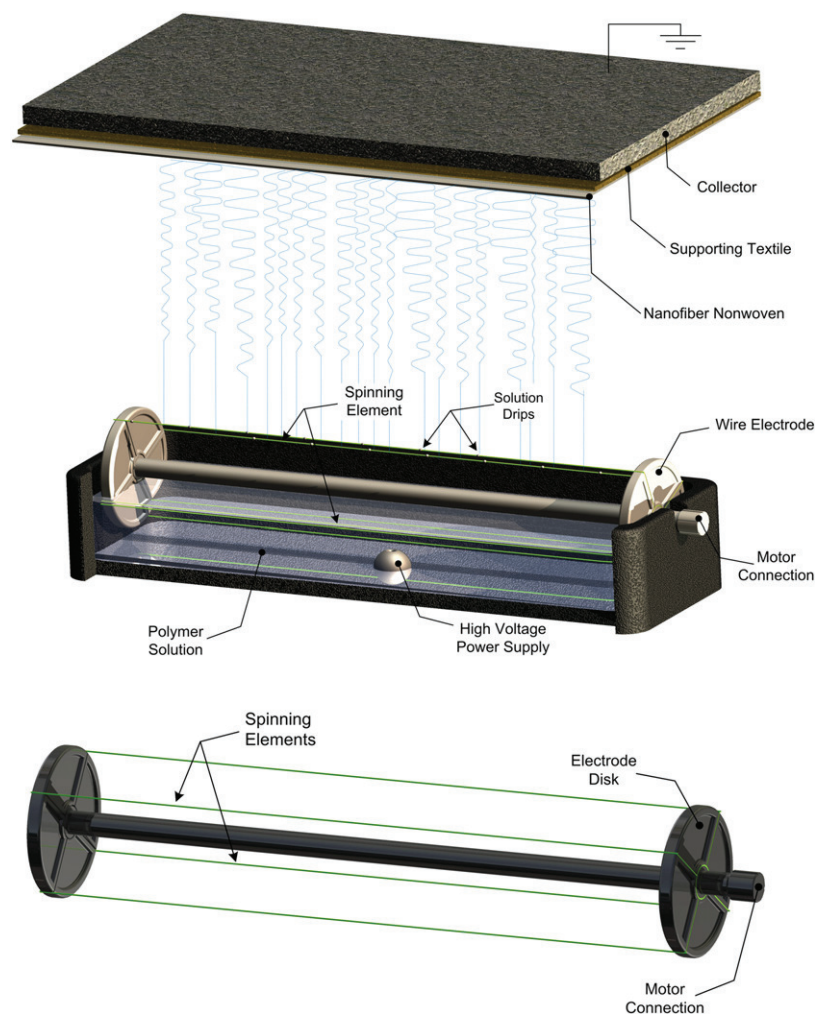E-mail address: mzatloukal@ft.utb.cz (M. Zatloukal).

Fig. 1. Scheme of the electrospinning process (at the top) using rotating electrode with cotton cord spinning elements (at the bottom).

(BD) was synthesized in molar ratio 9:1:8 at 90 °C for 5 h (per partes way of synthesis starting with preparation of prepolymer from MDI and PAIM and followed by addition of BD, remaining quantity of MDI). The prepared solution, suitable for electrospinning process, had a PU concentration of 13.5 wt%, viscosity of 1.53 Pa s and conductivity of 146.2 μS/cm (adjusted by tetraethylammonium bromide).

2.2. Filter sample preparation by electrospinning process

Nanofiber nonwoven based filter sample was prepared from polyurethane solution with a commercially available NanoSpider™ machine (Elmarco s.r.o. Liberec, Czech Republic, http://www.elmarco.com/) equipped with patented rotating electrode with 4 cotton cords spinning elements (PCT/CZ2010/000042) as shown in Fig. 1. The experimental conditions were: relative humidity 36%, temperature 22 °C, electric voltage (applied into PU solution) 75 kV, distance between electrodes 180 mm, rotational electrode speed 7 rpm and speed of supporting textile collecting nanofibers was 0.16 m/min. Nanofibers were collected on polyester fabric with square ordering of electroconductive fiber Resistat 9601, area mass 95 g/m^2, electroconductive thread distance was 5 mm. Samples for further analyses were taken from the middle part of the 40 cm wide fabric coated with layer of nanofibers.
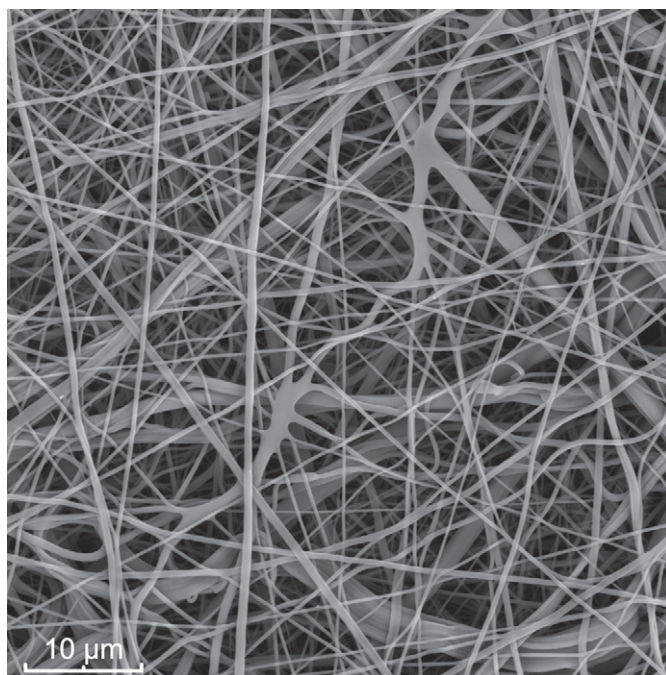

Fig. 2. SEM image of the PUR nanofiber mat produced by electrospinning process.

II.2

2.3. Filter sample characterization

Nanofiber based filter, prepared through the electrospinning process, has been characterized by the Scanning Electron Microscope (Vega II, Tescan, Czech republic), as visible in Fig. 2. The obtained SEM picture has consequently been used for the fiber diameter/pore size distribution determination using recently proposed digital image analysis technique (Sambaer et al., 2010). The obtained basic characteristics for the analyzed filter samples are summarized in Fig. 3(a) and (b); the produced filter sample has average fiber diameter size (293 nm), number average and biggest pore sizes (473 and 3478 nm, respectively), mass area (3.14 g/m^2) and thickness (20 μm) determined from SEM side view sample image.

2.4. Filtration efficiency

Experimental particle penetration efficiency of fabrics was determined according to EN 779 standard at the constant air flow rate 5.7 cm/s. Aerosol particles were produced from di-ethyl-hexyl-sebacate by a pneumatic aerosol generator. Size distribution of particles was measured before and after the fabric with the optical particle analysers—particle counters LAS X, manufactured by Particle Measuring Systems (USA), for small particles 0.1–0.4 μm and APS, manufactured by TSI (USA), for bigger particles 1.2–8.3 μm. The measurement results were reported as the collecting efficiency of fabric (%). The measured filtration efficiency curve is depicted in Fig. 3(c) (air flow rate 5.7 cm/s, pressure drop 316 Pa).

3. 3D structure model development from SEM pictures

The following strategy has been proposed for the realistic 3D model representation of produced PU based nanofiber electrospun mat.

First, the original SEM sample image of the filter (see Fig. 2 as an example) is converted to a black and white image by applying a proper threshold level (equal to average grayscale value as suggested in (Ghasemi-Mobarakeh et al., 2007)) in order to emphasize only the top fibers from the others.

Second, using the converted black and white image, fiber centerlines pixels (which are always connected to each other) are determined by the algorithm developed by Ignacio et al. (2010) (see Fig. 4). The continuous centerline curves for each individual fiber (or its part) are determined by the grouping of those centerline pixels having only two neighbor pixels (i.e.
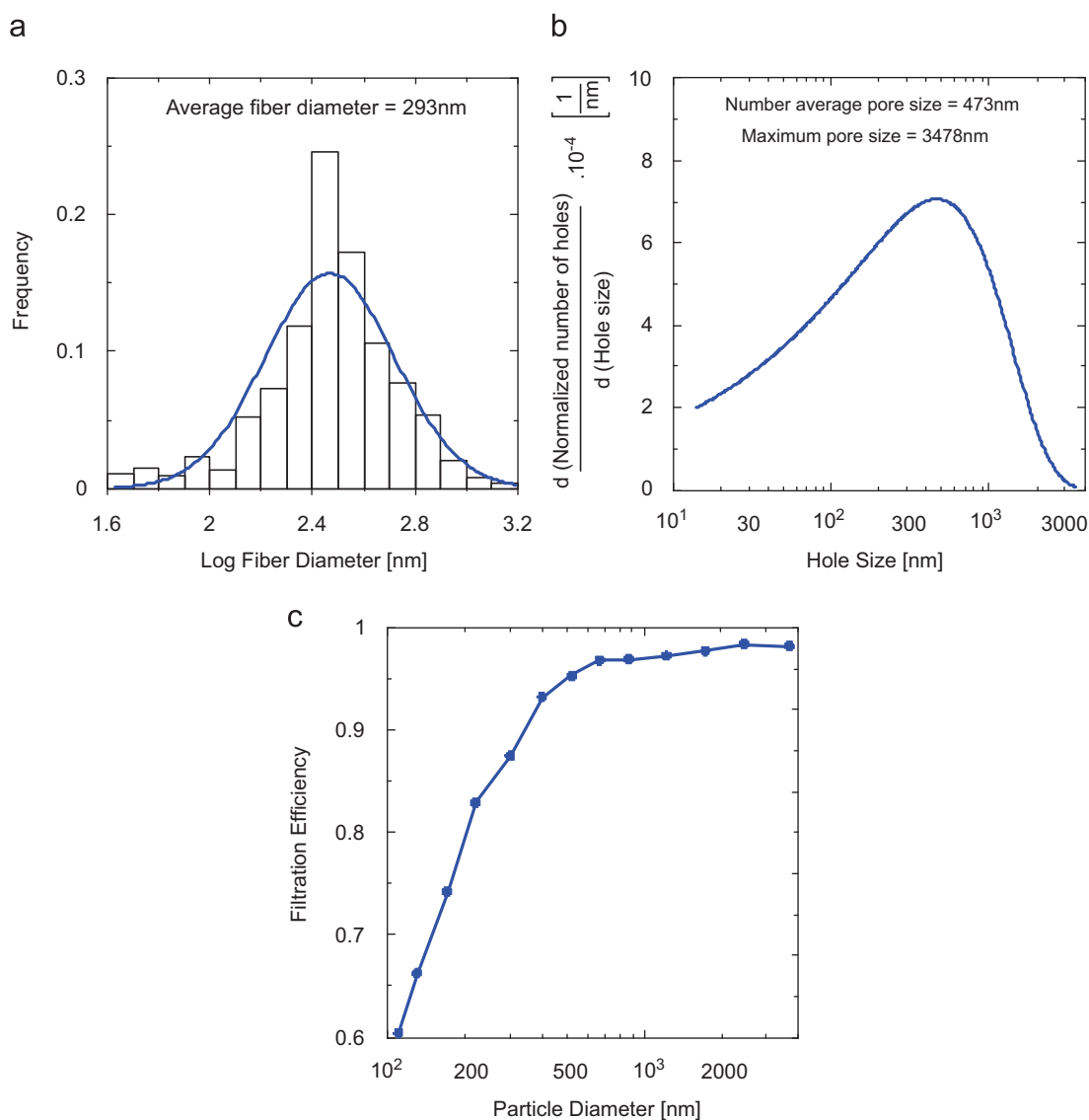

Fig. 3. Basic characteristics for PUR nanofiber mat: (a) Fiber diameter distribution; (b) pore size distribution and (c) filtration efficiency.
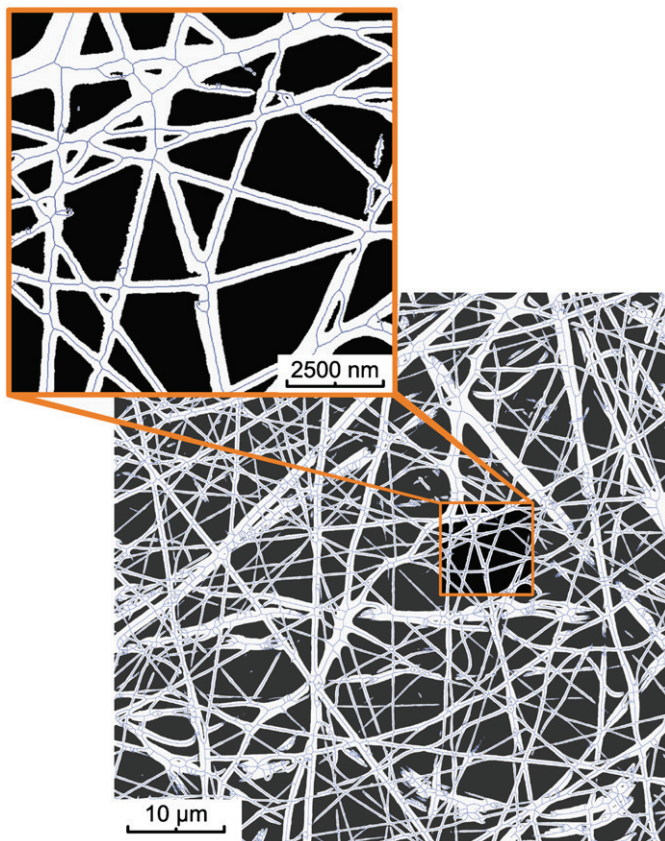
II.3

Fig. 4. Visualization of the converted black and white SEM image of the PUR nanofiber mat (depicted in Fig. 2) together with particular fiber centerlines.
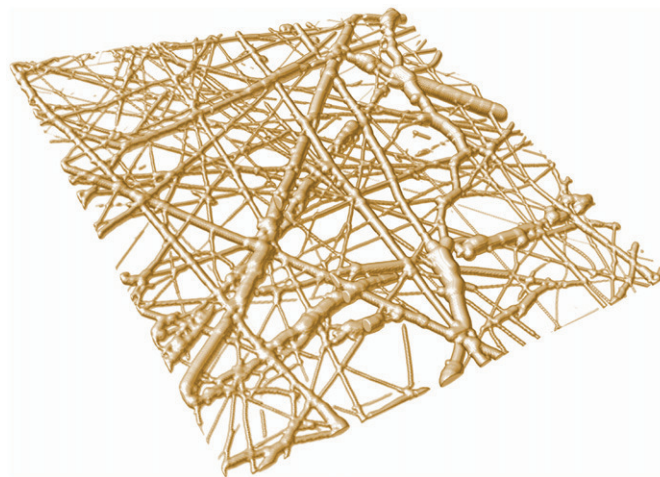

Fig. 5. Visualization of one 3D nanofiber layer created from the converted black and white SEM image (depicted in Fig. 4).

fiber (or its part) to which they belong. This makes proposed model utilization in the particle filtration modeling very simple and effective.

It should also be mentioned that in order to build the 3D structure model from SEM picture successfully, the following requirements for the SEM image has to be fulfilled:

- The perpendicular rather than angled view should be preferred. This minimize the light reflection at the fiber edges, which can disturb the global threshold process during converting the grey scale SEM image to binary image leading to creation of artificial structures.
- Top fibers should be lighter (ideally having constant grayscale value) than bottom fibers and background. This allows precise extraction of top fibers only from SEM image for consequent creation of one 3D layer without creation of artificial structures. For this purpose, Back-Scattered Electron (BSE) detector for electron microscopy scanning can be utilized.

4. Flow field calculation

In general, four different flow regimes around the fibers exist depending on the fiber diameter and gas thermal and pressure conditions (Hosseini and Tafreshi, 2010a; Brown, 1993; Maze et al., 2007): continuum flow regime ($K_n < 10^{-3}$), slip-flow regime ($10^{-3} < K_n < 0.25$), transition regime ($0.25 < K_n < 10$) and free molecule regime ($K_n > 10$), where K_n is Knudsen number representing the ratio of the gas molecules mean free path and fiber diameter (see Eq. (6) for exact definition). Due to the fact that PU based nanofiber filters (prepared in this work by electrospinning process with average fiber diameter about 300 nm) operate at low pressure drops only, hydrodynamics conditions lies in the slip/transition/free molecular flow regime. Maze et al. (2007) concluded that for such flow condition, the influence of the fibers on the flow field is negligible because of significant slip occurrence at the fiber surface, thus uniform gas flow field can be considered in this work, as visible in Fig. 7.

In order to calculate particle position at each time step due to drag force exerted by the flow and the Brownian forces (assuming a constant air flow), all the time intervals Δt are divided into two parts by a single random coefficient (which is constant for each particle) $U \in [0;1[$ in order to shift the Brownian motion sampling. The following solution taken from (Maze et al., 2007) has been utilized for these two time intervals:

branching is eliminated on the centerline curve). This reduces the complexity of the 3D structure model significantly because each fiber is represented by the limited number of sections. Moreover, it helps to recognize the sieve during the particle filtration modeling (because different fibers or their parts can be easily identified) and the distance calculation between different fibers/fiber parts (which is required for the force balance between the fiber and filtered particle) can be easily determined through direct availability of normal direction with respect to particular centerline curve (represented by the simple line for example in the most simplest case).

Third, 3D shape of each fiber section is created by the rotation of particular average diameter circle along every corresponding centerline pixel in the depth direction. The particular average diameter circle is determined from the number of different circles, which are localized in the particular centerline pixels and locally represents the fiber section diameters. In other words, all fiber sections are viewed in the proposed 3D structure model as mutually connected tubes having different diameters (see Fig. 5).

Full 3D nanofiber based nonwoven filter model is created by stacking limiting number of individual 3D nanofiber layers on each other with particular space between them in such a way that the mass area and final thickness of the 3D filter model is equal to the real sample (see Fig. 6). The proper and realistic representation of the fiber curvature, varying fiber diameter and specific shape of the cross section points are the main advantages of the proposed 3D structure model. Moreover, the 3D model is simply given by x, y, z centerline pixel coordinates (for one layer, all pixels lies on one plain) having information about the fiber diameter and particular
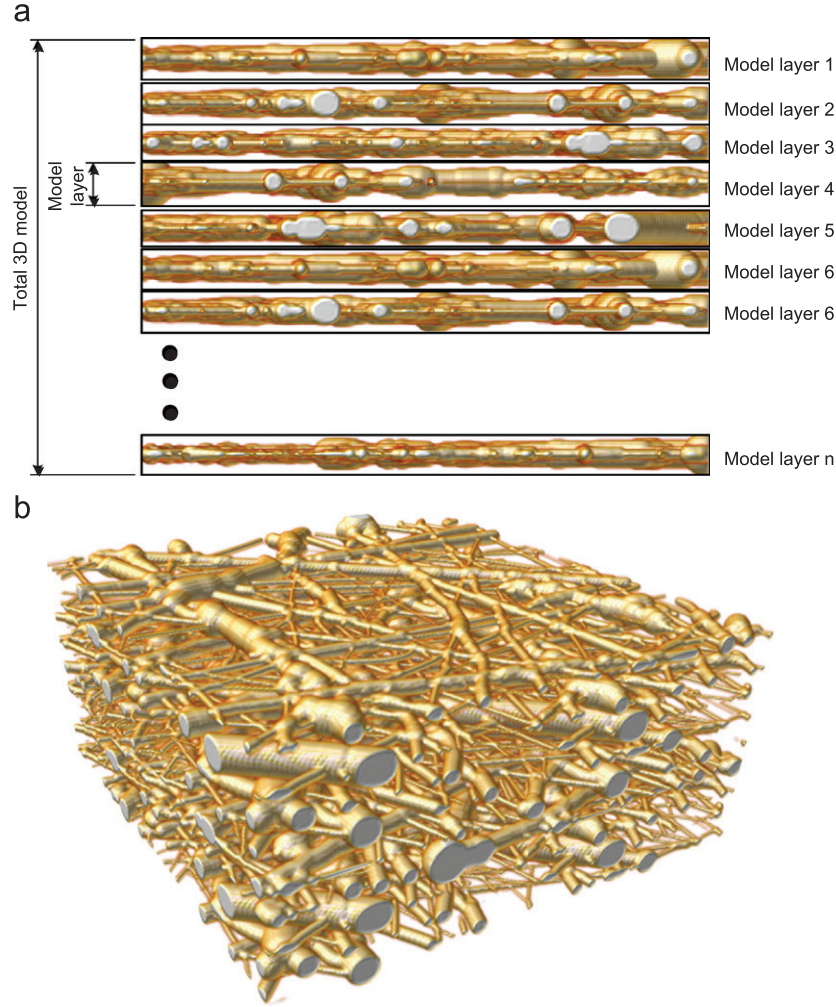
II.4

Fig. 6. Full 3D model for PUR nanofiber mat: (a) Side view and (b) perspective view (number of layers=10).

Time interval $[j\Delta t; (j+U)\Delta t]$.

$$v_{i_p}((j+U)\Delta t) = \left(v_{i_p}(j\Delta t) - v_{i_f} - \frac{F_{b_i}}{\beta}\right)e^{(-\beta U\Delta t)} + \frac{F_{b_i}}{\beta} + v_{i_f}, \tag{1}$$

$$x_{i_p}((j+U)\Delta t) = \left(\frac{v_{i_p}(j\Delta t) - v_{i_f} - \frac{F_{b_i}}{\beta}}{\beta}\right)(e^{(-\beta U\Delta t)} - 1)$$
$$+ \left(\frac{F_{b_i}}{\beta} + v_{i_f}\right)U\Delta t + x_{i_p}(j\Delta t), \tag{2}$$

Time interval $[(j+U)\Delta t; (j+1)\Delta t]$.

$$v_{i_p}((j+1)\Delta t) = \left(v_{i_p}((j+U)\Delta t) - v_{i_f} - \frac{F_{b_{i+1}}}{\beta}\right)e^{(-\beta(1-U)\Delta t)} + \frac{F_{b_{i+1}}}{\beta} + v_{i_f}, \tag{3}$$

$$x_{i_p}((j+1)\Delta t) = \left(\frac{v_{i_p}((j+U)\Delta t) - v_{i_f} - \frac{F_{b_{i+1}}}{\beta}}{\beta}\right)(e^{(-\beta(1-U)\Delta t)} - 1)$$
$$+ \left(\frac{F_{b_{i+1}}}{\beta} + v_{i_f}\right)(1-U)\Delta t + x_{i_p}((j+U)\Delta t), \tag{4}$$

where v_{i_f} and v_{i_p} are, respectively, the fluid and particle velocities in the x, y or z direction,

$$\beta = \frac{18\eta}{d_p^2 \rho_p C_c} \tag{5}$$

is the relaxation frequency of the particle, d_p and ρ_p are the particle diameter and density, respectively, η is liquid viscosity, $C_c = 1 + K_n(1.275 + 0.4e^{(-1.1/Kn)})$ is an empirical Cunningham slip correction factor, K_n is the fiber Knudsen number

$$K_n = \frac{2\lambda}{d_f} \tag{6}$$

where d_f is fiber diameter and λ is the mean free path of gas molecules

$$\lambda = \frac{RT}{\sqrt{2}N_a \pi d_m^2 p} \tag{7}$$

where R is the gas constant, T the temperature, N_a the number of Avogadro, p the pressure and d_m the collision diameter of an air molecule ($3.7.10^{-10}$ m).

$F_{b_{i+1}}$ is the Brownian white noise excitation due to the impact of air molecules on the particle defined according to Li and Ahmadi (1992), Ounis and Ahmadi (1990), Ounis et al. (1991) as

$$F_{b_i} = \varsigma_i \sqrt{\frac{\pi S_{nn}}{\Delta t}}, \tag{8}$$

where ς_i are zero-mean, unit-variance independent Gaussian random numbers, S_{nn} is the spectral intensity (characterizing the noise intensity) defined as

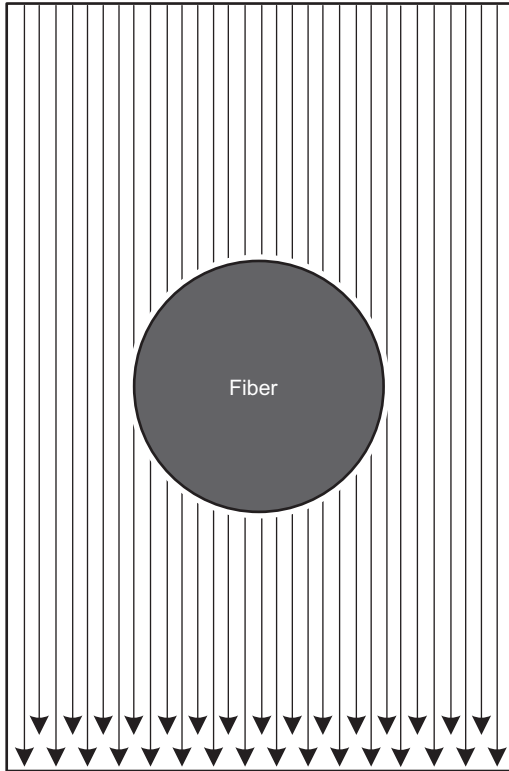$$S_{nn} = \frac{3kT\beta}{\pi d_p^3 \rho_p}, \tag{9}$$

II.5

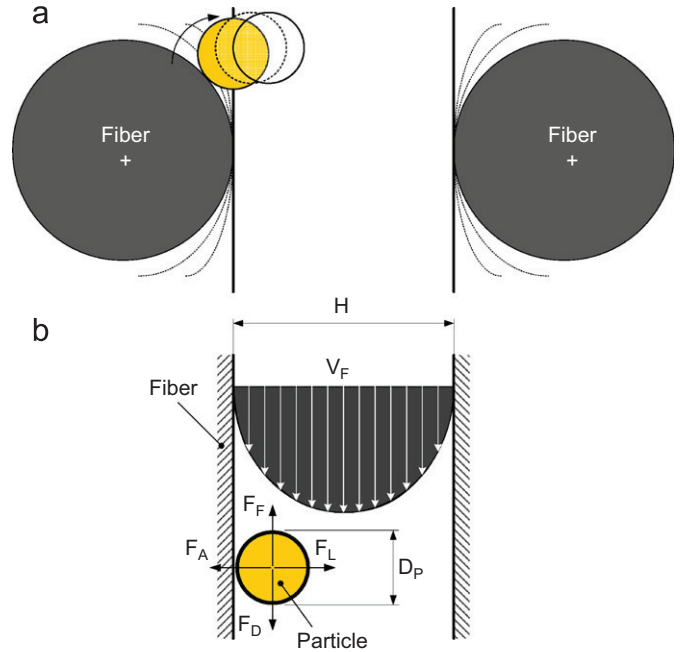**Fig. 7.** Assumed air flow field around the fiber.

Fig. 8. Visualization of the particle movement along the fiber. (a) Tube pore definition (*H*—tube diameter, *L*—tube length); (b) particle–fiber force balance visualization inside the tube pore.

where k is the Boltzmann constant and T the temperature. It should be mentioned that the particles are not allowed to escape the simulation box through the sides; if this happened, their velocity vector is mirrored to move them back inside, as suggested in Maze et al. (2007).

5. Particle–fiber interaction modeling

The force balance, suggested by Altmann and Ripperger (1997) is accommodated here (see Fig. 8) for capturing particle–fiber interactions. It is considered here that the flow through the particular pore can be viewed as the Poiseuille flow in a 2D duct, which is characterized by the gap distance, H, and its length L. In order to calculate reduced gas viscosity, η, (due to the slip) correctly at high Knudsen numbers ($K_n > 0.01$), the following viscosity definition equation proposed by McNenly et al. (2005) has been utilized for Poiseuille flows:

$$\eta = \eta'[a_0 + a_1 \arctan(a_2 K_n^{a_3})] \tag{10}$$

where η' is the gas viscosity at given pressure and temperature, $a_0 = 1.066$, $a_1 = 0.679$, $a_2 = -2.082$, $a_3 = 0.866$.

In the force balance model, four different forces are considered; the drag force, F_D, the lift force, F_L, the adhesion (van der Waals) force, F_A, and the friction force F_F, which are defined in the following way.

5.1. Drag force, F_D

Drag force, F_D, starts to act on the fiber intercepted particle due to pressure driven shear flow occurring inside the pore having average diameter H because velocity between the solid particle and the fluid starts to be different. According to theoretical and experimental work of Rubin (1977), Altmann and Ripperger
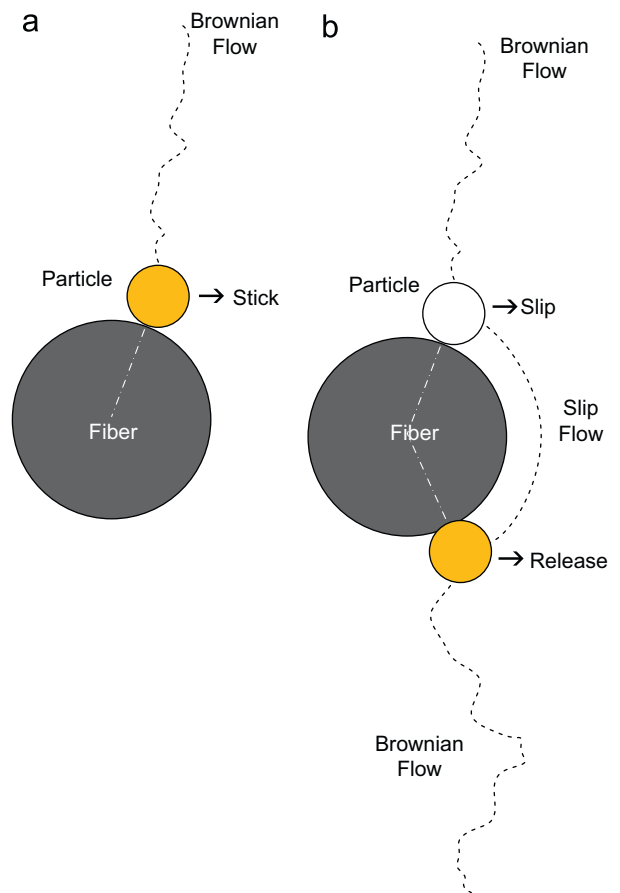

Fig. 9. Visualization of two possible particle–fiber configurations: (a) Particle sticks at the fiber and (b) particle slips along the fiber.
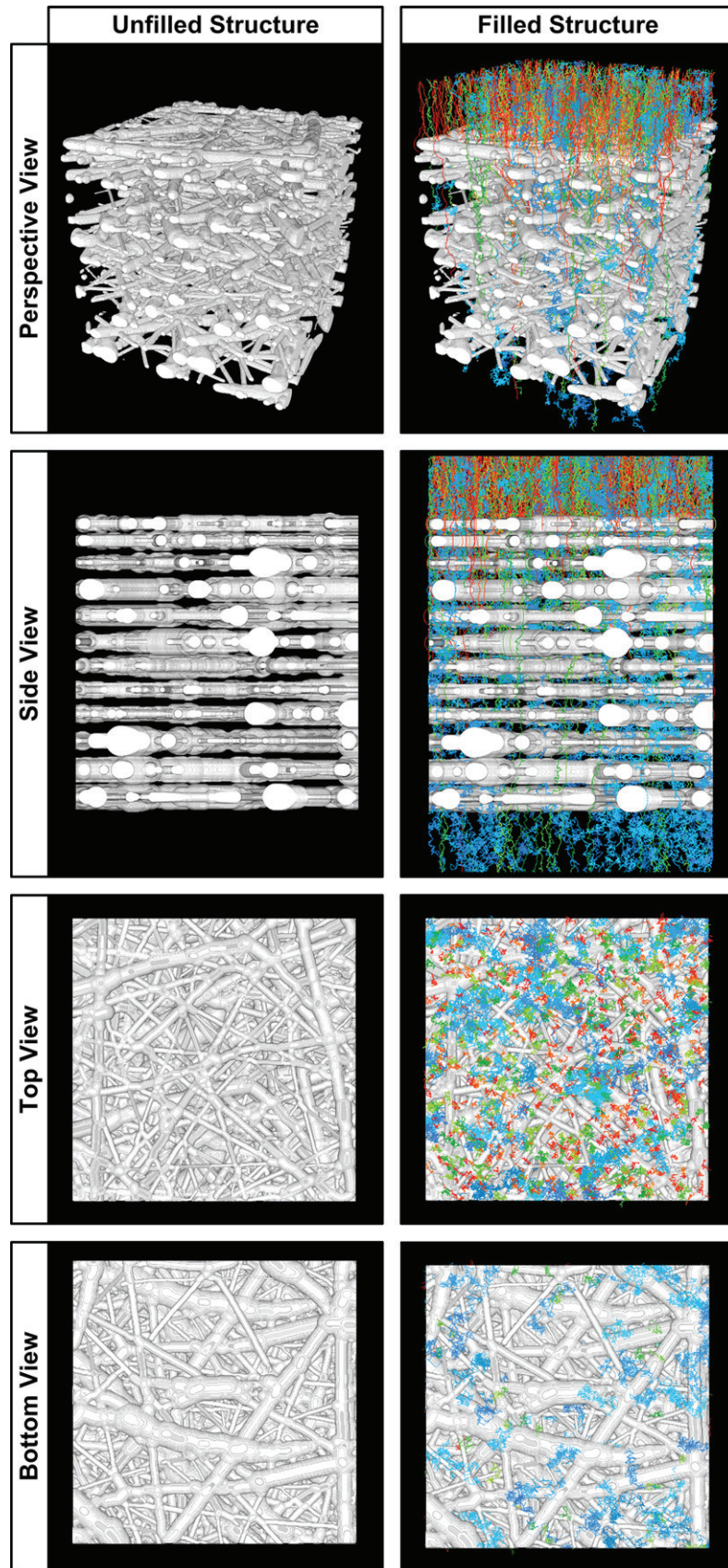
II.6

Fig. 10. Flow path lines through the medium colored by particle sizes (50 nm—blue, 200 nm—green, 500 nm—red). (For interpretation of the references to color in this figure legend, the reader is referred to the web version of this article.)

II.7

(1997), the drag force can be expressed in the following way:

$$F_D = 3.16\pi\tau_w d_p^2 \tag{11}$$

where τ_w is local fiber wall shear stress, which can be calculated from the Newtonian law as

$$\tau_w = \eta\dot{\gamma}, \tag{12}$$

where $\dot{\gamma}$ represents shear rate at the fiber wall. Note that the characteristic pore size dimension H is determined here as the perpendicular distance between the interception particle–fiber point and surrounding fiber, which represents the second part of the pore. It also should be mentioned that the assumption about the constant flow velocity field has been relaxed for the force balance calculation in order to mimic different levels of slip and drag force intensity according to actual fiber diameter (Knudsen number) dependent air viscosity.

5.2. Lift force, F_L

According to the theoretical and experimental analysis of Rubin (1977), Altmann and Ripperger (1997 and McLaughlin, 1993), the lift force is caused by the shear flow and can be calculated as follows

$$F_L = \frac{0.761\tau_w^{1.5} d_P^3 \rho_f^{0.5}}{\eta}, \tag{13}$$

where ρ_f is density of the fluid.

5.3. Adhesive force F_A

The estimation of the this force is complicated because different parameters such as particle–fiber shape, particle–fiber roughness, adhesion distance, number of contact points, etc. may influence the adhesive force strongly (Altmann and Ripperger, 1997). Neglecting the electrostatic interactions, the adhesive forces can be evaluated by calculating van der Waals force between two ideal spheres as follows

$$F_A = \frac{\hbar\overline{\omega} d_P}{32\pi a^2} \tag{14}$$

where $\hbar\overline{\omega}$ is the Lifschitz–van der Waals constant (10^{-20} J) and a is the adhesive distance (0.4 nm (Altmann and Ripperger, 1997; Brown, 1993)).

5.4. Friction force F_F

The friction force is caused by the action of the forces acting towards the fiber surface (van der Waals force F_A in this case).

$$F_F = \mu F_A \tag{15}$$

where μ is the friction coefficient ($0 < \mu < 1$).

The particle is considered to be intercepted by the fiber when the lift force is lower/equal than the adhesion force, $F_L \leq F_A$, or the drag force is lower/equal than the friction force, $F_D \leq F_F$ (see
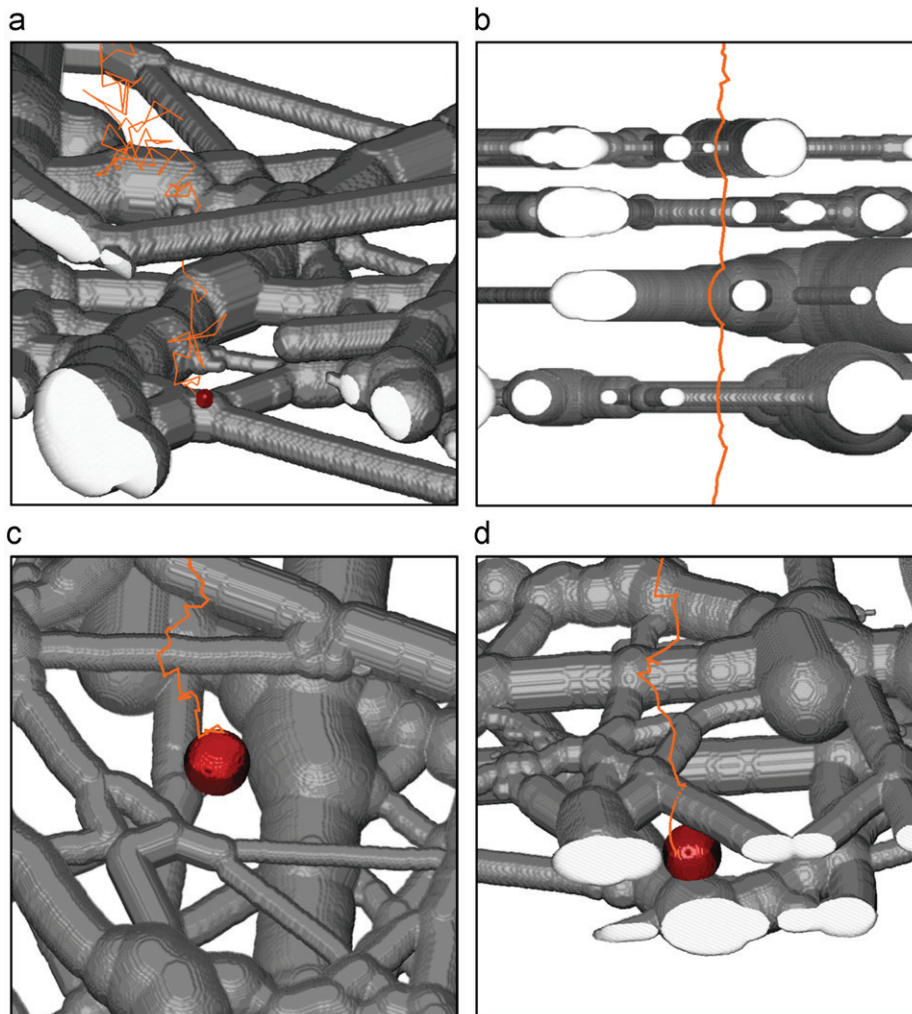

Fig. 11. Detail view of the flow path lines: (a) Captured 100 nm particle at the fiber; (b) 500 nm particle path line, which has passed the filter due to slip around the fiber; (c) sieve of the 500 nm particle at one model layer and (d) sieve of the 500 nm particle between 2 different model layers.

II.8

Fig. 9(a)). On the other hand, if the lift force is higher than the adhesion force ($F_L > F_A$) or the drag force is higher than the friction force ($F_D > F_F$), the particle starts to slip around the fiber in the perpendicular plane with respect to that fiber and the particle is always released from the fiber in the horizontally mirrored position with respect to initial sticking point between the particle and fiber as visible in Fig. 9(b). This is due to the applied assumption that the slipping particle follows the air path line, which is always released from the fiber in the horizontally mirrored position with respect to initial sticking point as depicted in Fig. 7. It also should be mentioned that particle catching due to sieving is considered when at least two connection points between fiber1–particle–fiber2 are identified during the particle motion modeling.

6. Comparison between experimental and theoretical data, parametric study and conclusions

In this part, the suggested particle filtration modeling approach will be tested. In the first step, the 3D structure model for manufactured PU filter samples according to methodology described above has been generated. Efficiency of the filter is theoretically determined by the number of particles, which can be captured inside the filter (Maze et al., 2007)

$$E = \frac{N_{in} - N_{out}}{N_{in}} \tag{16}$$

where N_{in} and N_{out} are the number of entering and exiting particles, respectively. 100 different groups of particles having diameter linearly varying from 20 to 1000 nm in logarithmic scale (1000 identical sphere particles per one group) were injected at the filter inlet ($28 \times 28\ \mu m^2$). The following reference filtration parameters (which correspond to the filtration experiment described above) have been utilized: $v_{i_f} = 0.057$ m/s, $p = 101,325$ Pa, $T = 300$ K, $\mu = 0.0025$, $\rho_p = 1000$ kg/m^3, $\eta' = 3.8\ 10^{-5}$ Pa s. Each particle has been traced through the clean filter, i.e. particle–particle interactions have been neglected, and number of exiting partic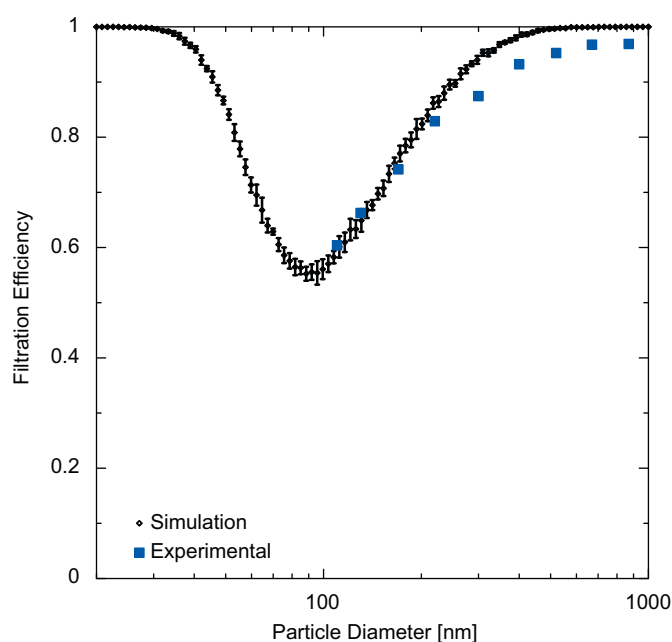les was determined in order to calculate filter capture efficiency as a function of particle size. Fig. 10 is an example of the simulation results, where a number of particle path lines having different sizes (50, 200 and 500 nm) are visualized. Detail view of the possible individual particle path lines is provided in the Fig. 11.
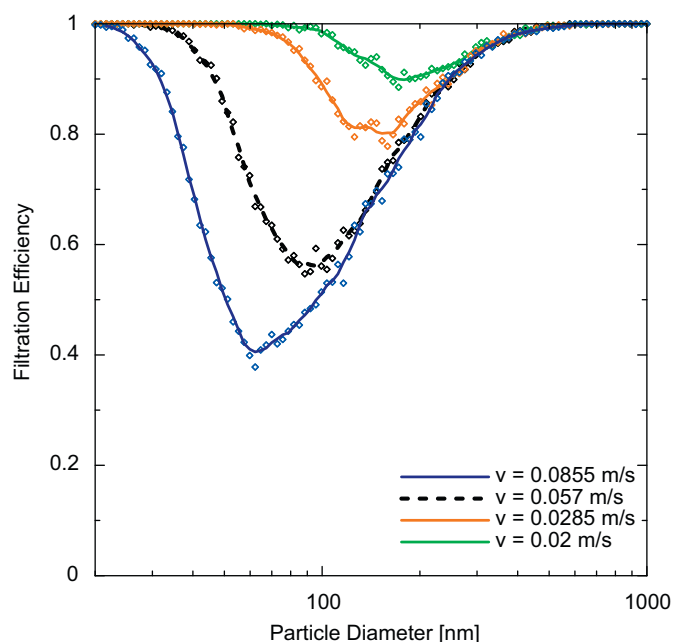

Fig. 13. Predicted effect of the air velocity on the PUR electrospinning sample filtration efficiency (mass area = 3.14 g/m^2, sample thickness = 20 μm, p = 101,325 Pa, T = 300 K, μ = 0.0025, ρ_p = 1000 kg/m^3, η' = 3.8 10^{-5} Pa s). Lines represent curve fit for particular calculated data points (running average fit with window width equal to 5).

Fig. 12. Comparison between measured and predicted filtration efficiency curves for the PUR electrospinning nonwoven sample (mass area = 3.14 g/m^2, sample thickness = 20 μm, v_{i_f} = 0.057 m/s, p = 101,325 Pa, T = 300 K, μ = 0.0025, ρ_p = 1000 kg/m^3, η' = 3.8 10^{-5} Pa s).
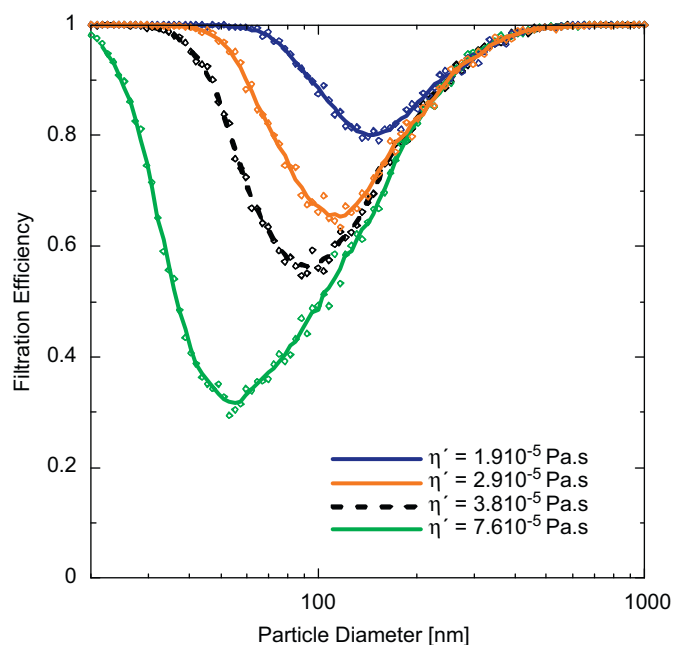

Fig. 14. Predicted effect of the air viscosity on the PUR electrospinning sample filtration efficiency (mass area = 3.14 g/m^2, sample thickness = 20 μm, v_{i_f} = 0.057 m/s, p = 101,325 Pa, T = 300 K, μ = 0.0025, ρ_p = 1000 kg/m^3). Lines represent curve fit for particular calculated data points (running average fit with window width equal to 5).
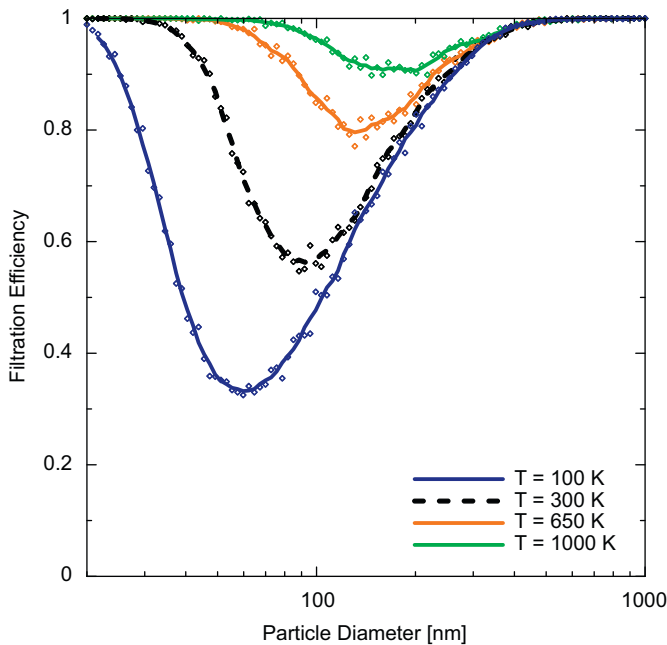
II.9

Fig. 15. Predicted effect of the air temperature on the PUR electrospinning sample filtration efficiency (mass area$=3.14$ g/m^2, sample thickness$=20$ μm, $v_{i_f}=0.057$ m/s, $p=101{,}325$ Pa, $\mu=0.0025$, $\rho_p=1000$ kg/m^3, $\eta'=3.8\ 10^{-5}$ Pa s). Lines represent curve fit for particular calculated data points (running average fit with window width equal to 5).
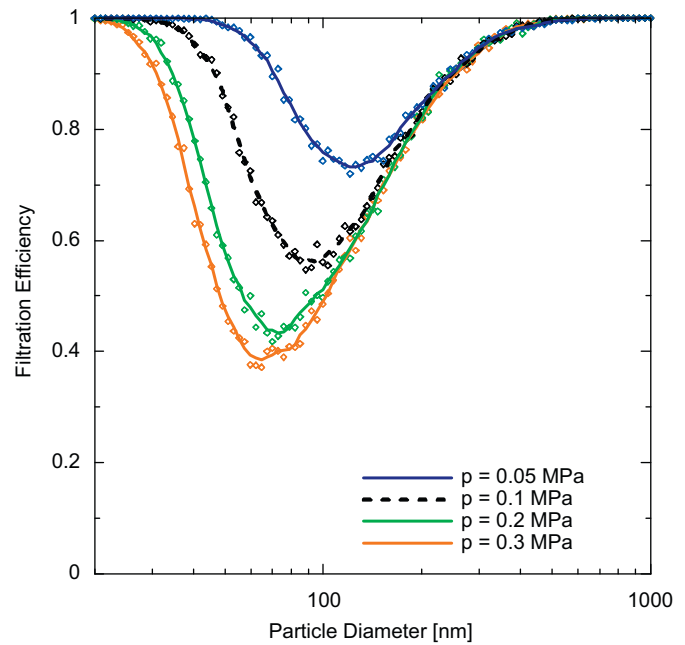

Fig. 16. Predicted effect of the air pressure on the PUR electrospinning sample filtration efficiency (mass area$=3.14$ g/m^2, sample thickness$=20$ μm, $v_{i_f}=0.057$ m/s, $T=300$ K, $\mu=0.0025$, $\rho_p=1000$ kg/m^3, $\eta'=3.8\ 10^{-5}$ Pa s). Lines represent curve fit for particular calculated data points (running average fit with window width equal to 5).

Comparison between experimentally and theoretically determined filter efficiency data for the tested sample is provided in Fig. 12. Note that simulations were repeated 10 times in order to obtain average values and standard deviations. It is nicely visible, that the model predictions are in very good agreement with the experimental data in the range of small particle sizes at which the Brownian force, rather than air flow field, dominantly influences the nanoparticles trajectory i.e. within the particle size range for which the assumption about a uniform air flow field is justifiable. Disagreement between predicted and measured filter efficiency for the large diameter particles can be explained by the error in the particle trajectory calculation, because the Brownian force vanishes in this case and air flow field starts to play the dominant role, or by the possible presence of big pores (defects) in the tested sample, which have not been SEM detected and thus not considered in the performed calculation.

In the second step, the effect of air velocity, viscosity, temperature, pressure and friction coefficient between the particle and fiber have been investigated theoretically by the proposed technique. For that purpose, the 3D structure model for the produced PU filter has been utilized. The theoretical predictions of the filtration efficiency are provided in Figs. 13–17. It can be clearly seen that increase in air velocity, viscosity and air pressure leads to filtration efficiency decrease, because of increased drag/lift forces and reduced Brownian motion intensity, whereas the increase in the air temperature and particle–fiber friction coefficient leads to filtration efficiency enhancement due to increased Brownian motion intensity and reduced particle slip, respectively, and vice versa. Clearly, the air velocity, viscosity and particle–fiber friction coefficient seems to have the highest impact on the filtration efficiency of the tested filter. In more detail, the obtained theoretical results with respect to friction coefficient effect on the filtration efficiency depicted in Fig. 17 suggests that particle–fiber surface modification can significantly influence filtration efficiency especially for particles having small size ($<$ about 200 nm in this specific case).
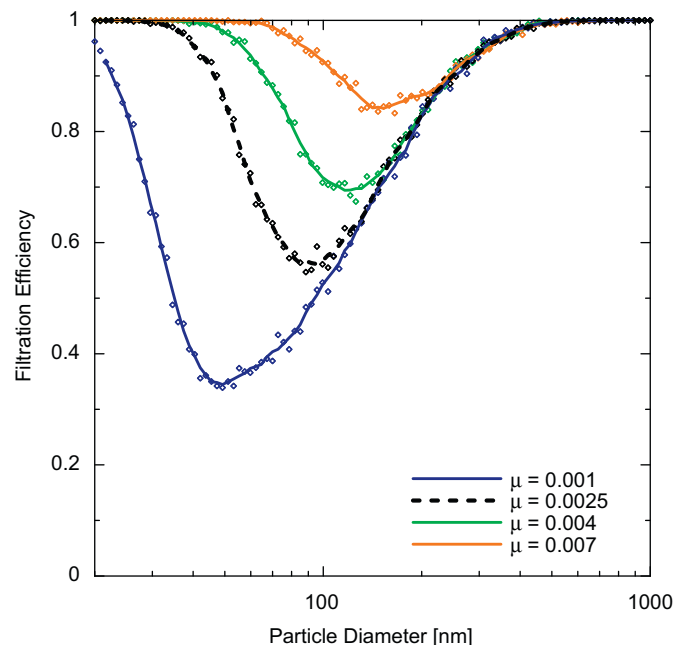

Fig. 17. Predicted effect of the friction coefficient on the PUR electrospinning sample filtration efficiency (mass area$=3.14$ g/m^2, sample thickness$=20$ μm, $v_{i_f}=0.057$ m/s, $p=101{,}325$ Pa, $T=300$ K, $\rho_p=1000$ kg/m^3, $\eta'=3.8\ 10^{-5}$ Pa s). Lines represent curve fit for particular calculated data points (running average fit with window width equal to 5).

It should also be mentioned that the predicted trends for air temperature/velocity with respect to filtration efficiency are in good quantitative agreement with previous studies (Maze et al., 2007; Thomas and Yoder, 1956; Sinclair, 1970).

II.10

7. Conclusions

In this work, a nanofiber nonwoven based PU filter has been produced using electrospinning process. A new methodology to create simple 3D structure model from SEM image of the filter has been proposed. Full 3D particle filtration modeling using such a 3D structure model representing real filter structure has been utilized considering slip/transition/free molecular flow regime, particle–fiber interactions, air/particle slip at the fiber surface, sieve and homogenous flow field. The obtained theoretical predictions for the filtration efficiency have been compared with the corresponding experimental data and good agreement between both data sets have been obtained, especially at the particle size range for which the applied model assumptions are valid. The effect of different factors such as air velocity, viscosity, temperature, pressure and particle–fiber friction coefficient has been theoretically investigated for the produced PU nanofiber based filter. It has been revealed that the change of the particle–fiber friction coefficient (which can be done by particle–surface modification for example) has one of the highest effects on the filtration efficiency (within the range of all tested parameters and their values), especially for nanoparticles having diameter less than about 200 nm for the studied conditions and filter structure. It is believed that the proposed modeling tools in this work will help to evaluate filtration efficiency of different nanofiber nonwoven based structures from their SEM images in order to provide useful guidelines for their optimization and enhancement.

Acknowledgments

References

Andrady, A.L., 2008. Science and Technology of Polymers Nanofibers. John Wiley & Sons, Inc., New Jersey.
Ashari, A., Tafreshi, H.V., 2009. A two-scale modeling of motion-induced fluid release from thin fibrous porous media. Chemical Engineering and Science 64, 2067–2075.
Altmann, J., Ripperger, S., 1997. Particle deposition and layer formation at the crossflow microfiltration. Journal of Membrane Science 124, 119–128.
Brown, R.C., 1993. Air Filtration: An integrated Approach to the Theory and Applications of Fibrous Filters. Pergamon Press, Oxford.
Fotovati, S., Tafreshi, H.V., Pourdeyhimi, B., 2010. Influence of fiber orientation distribution on performance of aerosol filtration media. Chemical Engineering and Science 65, 5285–5293.
Ghasemi-Mobarakeh, L., Semnani, D., Morshed, M., 2007. A novel method for porosity measurement of various surface layers of nanofibers mat using image analysis for tissue engineering applications. Journal of Applied Polymer Science 106, 2536–2542.
Hosseini, S.A., Tafreshi, H.V., 2010a. Modeling permeability of 3-D nanofiber media in slip flow regime. Chemical Engineering and Science 65, 2249–2254.
Hosseini, S.A., Tafreshi, H.V., 2010b. 3-D simulation of particle filtration in electrospun nanofibrous filters. Powder Technology 201, 153–160.
Ignacio, Arganda-Carreras, Rodrigo, Fernandez-Gonzalez, Arrate, Munoz-Barrutia, Carlos, Ortiz-De-Solorzano, 2010. 3D reconstruction of histological sections: application to mammary gland tissue. Microscopy Research and Technique 73, 1019–1029.
Jaganathan, S., Tafreshi, H.V., 2008. Modeling liquid porosimetry in modeled and imaged 3-D fibrous microstructures. Journal of Colloid and Interface Science 326, 166–175.
Jaganathan, S., Tafreshi, H.V., Pourdeyhimi, B., 2008. A realistic approach for modeling permeability of fibrous media: 3-D imaging coupled with CFD simulation. Chemical Engineering and Science 63, 244–252.
Li, A., Ahmadi, G., 1992. Dispersion and deposition of spherical-particles from the point sources in a turbulent chemical flow. Aerosol Science and Technology 16, 209–226.
Maze, B., Tafreshi, H.V., Wang, Q., Pourdeyhimi, B, 2007. A simulation of unsteady-state filtration via nanofiber media at reduced operating pressures. Journal of Aerosol Science 38, 550–571.
McNenly, M.J., Gallis, M.A., Boyd, I.D., 2005. Empirical slip and viscosity model performance for microscale gas flow. International Journal for Numerical Methods in Fluids 49, 1169–1191.
McLaughlin, J.B., 1993. The lift on a small sphere in wall bounded linear shear flows. Journal of Fluid Mechanics 246, 249–265.
Ounis, H., Ahmadi, G., 1990. A comparison of Brownian and turbulent-diffusion. Aerosol Science and Technology 13, 47–53.
Ounis, H., Ahmadi, G., Mclaughlin, J.B., 1991. Dispersion and deposition of Brownian particles from the point sources in a simulated turbulent channel flow. Journal of Colloid and Interface Science 147, 233–250.
Pich, J., 1966. Pressure drop of fibrous filters at small Knudsen numbers. Annals of Occupational Hygiene 9, 23–27.
Rubin, G., 1977. Widerstands und Auftriebsbeiwerte von Ruhenden Kugelformigen Partikeln in Stationaren, Wandnahen Laminaren Grenzschichten, Dissertation. TH Karlsruhe.
Sambaer, W., Zatloukal, M., Kimmer, D., 2010. The use of novel digital image analysis technique and rheological tools to characterize nanofiber nonwovens. Polymer Testing 29, 82–94.
Sinclair, D., 1970. Penetration of HEPA filters by submicron aerosols. Journal of Aerosol Science 1, 53–67.
Tafreshi, H.V., Rahman, M.S.A., Jaganathan, S., Wang, Q., Pourdeyhimi, B., 2009. Analytical expressions for predicting permeability of bimodal fibrous porous media. Chemical Engineering and Science 64, 1154–1159.
Thomas, J.W., Yoder, R.E., 1956. Aerosolsize for maximum penetration through fiberglass and sand filters. American Medical Association Archives of Industrial Health 13, 545–549.
Wang, Q., Maze, B., Tafreshi, H.V., Pourdeyhimi, B., 2007. On the pressure drop modeling of monofilament-woven fabrics. Chemical Engineering and Science 62, 4817–4821.
Wang, Q., Mazé, B., Tafreshi, H.V., Pourdeyhimi, B., 2006a. A note on permeability simulation of multifilament woven fabrics. Chemical Engineering and Science 61, 8085–8088.
Wang, Q., Maze, B., Tafreshi, H.V., Pourdeyhimi, B., 2006b. A case study of simulating submicron aerosol filtration via lightweight spun-bonded filter media. Chemical Engineering and Science 61, 4871–4883.
Zobel, S., Maze, B., Tafreshi, H.V., Wang, Q., Pourdeyhimi, B., 2007. Simulating permeability of 3-D calendered fibrous structures. Chemical Engineering and Science 62, 6285–6296.

II.11

PAPER III

3D air filtration modeling for nanofiber based filters in the ultrafine particle size range

Wannes Sambaer [1,2], Martin Zatloukal [1,2*] and Dusan Kimmer [3]

[1] *Centre of Polymer Systems, University Institute, Tomas Bata University in Zlin,*

Nad Ovcirnou 3685, 760 01 Zlin, Czech Republic

[2] *Polymer Centre, Faculty of Technology, Tomas Bata University in Zlin, TGM 275,*

762 72 Zlin, Czech Republic

[3] *SPUR a.s., T. Bati 299, 764 22 Zlin, Czech Republic*

Keywords: Nanofiber, Electrospinning, 3D simulation, Filtration modeling.

*Corresponding author: *mzatloukal@ft.utb.cz*

ABSTRACT

In this work, 3D filtration modeling utilizing realistic SEM image based 3D structure model, transition/free molecular flow regime, Brownian diffusion, particle-fiber interactions, aerodynamic slip and sieve has been proposed and used for different polyurethane nanofiber based filters. For the model validation purposes, two polyurethane nanofiber layers prepared by the electrospinning process (having identical average fiber diameter, 120nm, but different average pore size) were combined to form 2 pairs of nanofiber based filters; each pair consist of two filters having comparable mass area and thickness. Filtration efficiency characteristics of prepared filters were determined experimentally in the ultrafine particle size range (20-400 nm). It has been found that the proposed model is able to reasonably predict the measured filtration efficiency curves for all tested filter samples.

INTRODUCTION

Nanofibers based nonwovens are widely applied in different areas such as filter media, tissue engineering, personal protective clothing, cosmetic skin care, life science, nanosensors and other medical and industrial applications [1-6]. Filter media is one of the largest application group of nanofiber nonwovens due to their small fibers (having fiber diameter typically in order of tens and hundreds of nanometers), high surface area (which significantly increases their filtration efficiency), and low filtration pressure drop (due to the aerodynamics slip occurrence at the nanofiber surfaces) [7].

One of the key problem in understanding of filtration processes by using nanofiber based filters is no possibility to create representative 3D models of a real nano-porous structures by standard techniques such as Magnetic Resonance Imaging [8,9], X-ray microtomography [10,11] or Digital Volumetric Imaging (DVI) [12] due to their low resolution limit (480nm/pixel for DVI). Thus, it is not surprising that virtual idealized nanofiber mat structure models are used in filtration modeling for deeper understanding of filtration via nanofiber mats [13-17]. However, utilization of virtual idealized nanofiber mats in filtration modeling considering constant diameter along the fiber, neglecting their curvature, inhomogeneous features and possible defects may not sufficiently represent real nanofiber mats and thus, predictive capabilities of such models could be significantly reduced. In order to overcome this possible limitations, realistic SEM image based 3D structure model is proposed and used here for two pairs of nanofiber based filters composed from two polyurethane nanofiber layers (having identical average fiber diameter, 120nm, but different average pore size) prepared by the electrospinning process; each pair consist of two filters having comparable mass area and thickness. In the next step, full 3D particle filtration modeling using the 3D structure models representing real filter structures has been utilized considering transition/free molecular flow regime, Brownian diffusion, particle-fiber interactions, aerodynamic slip and sieve. The obtained theoretical predictions for the filtration efficiency have been compared with the corresponding experimental data in the ultrafine particle size range (20-400 nm).

FILTER PREPERATION AND CHARACTERIZATION

Materials

Polyurethanes (PU) are segmented polyadducts prepared from diisocyanate, polymer diol (soft segment) and chain extender (low molecular diol). Two different polyurethane solutions were used to create two types of nanofiber based layers. The first polymer solution was prepared in dimethylformamide (DMF) from polyether based aliphatic PU (HydroMed D640 from AdvanSource Biomaterials Corporation, MA, USA) and is referred in this work as *'solution A'*. The second polymer solution prepared in DMF was created from aromatic diisocyanate (4,4'methylenebis (phenylisocyanate), polyester diol (poly(3-methyl-1,5-pentanediol)-alt-(adipic, isophtalic acid) and 1,4 butanediol and is referred here as *'solution B'*. The prepared solutions were suitable for electrospinning and had a PU concentration of 16.2 wt%, for solution A and 13,8 wt.% for solution B, viscosities of 1,5 Pa.s and conductivities of 150 μS/cm.

Nanofiber Layers Preparation by Electrospinning Process

In this work, a commercially available NanoSpider^{TM} machine (Elmarco s.r.o. Liberec, Czech Republic, http://www.elmarco.com/) equipped with patented (PCT/CZ2010/000042) rotating electrode with 3 cotton cords spinning elements (see Figure 1) was used to prepare nanofiber layers from polyurethane solution A or B (entitled here as Layer A and B according to corresponding polyurethane solution type). The experimental conditions were: relative humidity 25%, temperature 24°C, high voltage applied into PU solution 75 kV, distance between electrodes 210 mm, rotational electrode speed 7 rpm and speed of viscose nonwoven supporting textile collecting nanofibers was 0.32 m/min.

Nanofiber Layers Characterization

Polyurethane nanofiber Layers A and B have been characterized by Scanning Electron Microscopy (Vega III, Tescan, Czech Republic), as visible in Figure 2. Both SEM images have been consequently used to determine fiber diameter/pore size distribution by recently proposed digital image analysis [18], see Figure 3. It is clearly visible that even if the average fiber diameter for both layers is practically the same (120 nm), the average pore size of Layer B (201 nm) is about two times larger than for Layer A (98.9 nm).

The electric potential generated on the surface of both nanofiber layers was measured by electrostatic fieldmeter Simco, model FMX-003, the Netherlands. It has been found that the surface charge potential of nanofiber Layer A and Layer B was 70 V and 90 V, respectively, i.e. practically negligible for both samples.

Nanofiber Filter Preparation and Characterization

Nanofiber Layers A and B were combined to form 2 pairs of nanofiber based filters; each pair consist of two filters having comparable mass area and thickness (see Figure 4). The filtration efficiency for the prepared nanofiber based filters was determined experimentally in the ultrafine particle range according to following procedure. Ammonium sulphate solution having concentration of 1 g/l was nebulised (AGK, PALAS, Germany), a monodisperse size fraction was selected using an Electrostatic Classifier (EC 3080, TSI, USA) and particle concentration upstream and downstream the filter (face velocity 5,7 cm/s) was recorded by a condensation particle counter (UCPC 3025 A, TSI, USA). The filtration efficiency was determined at nine mobility diameter fractions: 20, 35, 50, 70, 100, 140, 200, 280 and 400 nm. All experimental data are depicted in Figure 5 and summarized in Table 1. Note that the filtration efficiency and pressure drop measurements were repeated four times and quality factor for each filter type was calculated according to the following equation:

$$QF = -\ln(E)/\Delta p \tag{1}$$

III.5

where Δp is the pressure drop and E is the filtration efficiency at Maximum Penetration Pore Size (MPPS), which is approximately 70 nm for all four samples. The following conclusions can be formulated based on the experimental data:

- the pressure drop/filter thickness ratio remains virtually the same for all investigated filter types (i.e. the filter thickness increase by factor two results in two times higher pressure drop, compare Filter 1, 2 with Filter 3, 4 in Table 1),

- increase in filter thickness/mass area leads to increase in filtration efficiency and pressure drop,

- filters with comparable mass area and thickness containing the combination of nanofiber Layer A (having small pores) with nanofiber Layer B (having big pores) have higher filtration efficiency and lower pressure drop than corresponding filters based on the Layer B only,

- reduction in mass area and utilization of small and big pores nanofiber layers, i.e. Layer A and B, respectively, in particular filter types increases their quality factor.

3D NANOFIBER STRUCTURE MODELING

Three dimensional model of the prepared nanofiber based filter has been created from SEM sample images and mass area in the following way (see Figure 6).

In the first step, the Gaussian blur (radius equal to 5 pixels) [19] was applied to the original SEM image to minimize the major pixel noise which is represented by artificial pixel value variation. In the second step, the average threshold level has been applied for the original grayscale SEM sample image to filter the top fibers only, which results in a black/white image; the single black and white pixels representing the minor noise, were removed from the image. In the third step, nanofiber centerlines pixels (which are always connected to each other) have been calculated according the algorithm developed by Huang et al. [20]. The continuous centerline curves for each individual fiber part are determined by the grouping of those centerline pixels having less than three neighbor pixels (i.e. centerline branching or crossings are eliminated). This reduces the complexity of the 3D structure model considerably because each fiber is represented by the limited number of indexed sections which helps to recognize particle-fiber interactions during the particle filtration modeling such as particle slip path, its motion history through the filter and sieve because different fiber parts can be easily identified. In the next step, the 3D shape of each fiber section is created by the rotation of local diameter circle fitted in the white fiber area along every corresponding centerline pixel in the depth direction. It should be mentioned that in our previous work [21], the fiber structure complexity has been reduced considerably due to the assumption that each nanofiber can be viewed as the number of interconnected tubes having diameter calculated as the averaged value over the whole fiber section. In this work, this assumption is relaxed in order to take varying fiber diameter, curvature and possible defect correctly into account. The comparison between the 'old methodology' [21] and the 'improved methodology' utilized in this work is provided in Figure 7 for an identical SEM image. It is clearly visible that the improved methodology allows representing the 3D nanofiber based structure more realistically than utilization of the old methodology.

In the final step, the integer number of no overlapped model layers, N, having a square shape with minimum size of 2 times maximum pore/fiber diameter size were searched and cut off from original SEM image to satisfy the following equation:

$$\left[\left(\sum_{i=1}^{N} MA_i\right) - MA_{NL}\right]^2 = minimum \tag{2}$$

where MA_i is the calculated mass area of the ith model layer and MA_{NL} is the measured mass area of the particular nanofiber layer. The 3D model of one nanofiber layer was build up as the stack of the N model layers satisfying Eq. 2. The final 3D filter model is then given by the combination of particular nanofiber layers (i.e. Layer A and/or Layer B in this case) as visible in Figures 8-9. Importantly, the calculated filter thicknesses provided in this figure are in good correspondence with the measured filter thicknesses provided in Table 1, which justify the proposed methodology described above.

FLOW FIELD CALCULATION

Based on the Knudsen number Kn (the ratio of the gas molecules mean free path and fiber diameter), transition (0.25<Kn<10)/free molecule (Kn>10) flow regime around the fibers at low pressure conditions are considered in this work because the average fiber diameter of the modeled filters is 120nm only. Maze et al. [13] concluded that in such a case, the influence of the fibers on the flow field is negligible due to significant slip occurring at the fiber surface which satisfies to consider uniform gas flow field.

In order to calculate particle position at each time step due to drag force exerted by the flow and the Brownian forces (assuming a constant air flow), all the time intervals Δt are divided into two parts by a single random coefficient (which is constant for each particle) $U \in [0;1[$ in order to shift the Brownian motion sampling. The following solution taken from Maze et al. [13] has been utilized for these two time intervals:

For a time interval $[j\Delta t; (j+U)\Delta t]$:

$$v_{i_p}\left((j+U)\Delta t\right) = \left(v_{i_p}\left(j\Delta t\right) - v_{i_f} - \frac{F_{b_i}}{\beta}\right)e^{(-\beta U\Delta t)} + \frac{F_{b_i}}{\beta} + v_{i_f},\tag{3}$$

$$x_{i_p}\left((j+U)\Delta t\right) = \left(\frac{v_{i_p}\left(j\Delta t\right) - v_{i_f} - \frac{F_{b_i}}{\beta}}{\beta}\right)\left(e^{(-\beta U\Delta t)} - 1\right) + \left(\frac{F_{b_i}}{\beta} + v_{i_f}\right)U\Delta t + x_{i_p}\left(j\Delta t\right),\tag{4}$$

and time interval $[(j+U)\Delta t; (j+1)\Delta t]$:

$$v_{i_p}\left((j+1)\Delta t\right) = \left(v_{i_p}\left((j+U)\Delta t\right) - v_{i_f} - \frac{F_{b_{i+1}}}{\beta}\right)e^{(-\beta(1-U)\Delta t)} + \frac{F_{b_{i+1}}}{\beta} + v_{i_f},\tag{5}$$

$$x_{i_p}\left((j+1)\Delta t\right) = \left(\frac{v_{i_p}\left((j+U)\Delta t\right) - v_{i_f} - \frac{F_{b_{i+1}}}{\beta}}{\beta}\right)\left(e^{(-\beta(1-U)\Delta t)} - 1\right)$$

$$+ \left(\frac{F_{b_{i+1}}}{\beta} + v_{i_f}\right)(1-U)\Delta t + x_{i_p}\left((j+U)\Delta t\right)$$

(6)

where v_{i_f} and v_{i_p} are the fluid and particle velocities in the x, y, or z direction,

$$\beta = \frac{18\eta}{d_p^2 \rho_p C_c},$$ (7)

is the relaxation frequency of the particle, d_p and ρ_p are the particle diameter and density, η is liquid viscosity, $C_c = 1 + K_n \left(1.275 + 0.4e^{\frac{-1.1}{Kn}} \right)$ is an empirical Cunningham slip correction factor, Kn is the fiber based Knudsen number

$$Kn = \frac{2\lambda}{d_f},$$ (8)

where d_f is the fiber diameter and λ is the mean free path of gas molecules

$$\lambda = \frac{R\,T}{\sqrt{2}\,N_A\,\pi d_m^2\,p},$$ (9)

where R is the gas constant, T the temperature, N_A the number of Avogadro, p the pressure and d_m Collision diameter of an air molecule $(3.7.10^{-10}\text{m})$. F_{bi} is the Brownian white noise excitation due to the impact of air molecules on the particle defined according to [22-24] as

$$F_{b_i} = \varsigma_i \sqrt{\frac{\pi S_{nn}}{\Delta t}},$$ (10)

where ς_i are zero-mean, unit-variance independent Gaussian random numbers, S_{nn} is the spectral intensity (characterizing the noise intensity) defined as

$$S_{nn} = \frac{3kT\beta}{\pi d_p^3 \rho_p},$$ (11)

where k is the Boltzmann constant and T the temperature.

PARTICLE-FIBER INTERACTION MODELING

The force balance, suggested by J. Altmann and S. Ripperger [25] is accommodated here (see Figure 10) for capturing particle-fiber interactions. It is considered here that the flow through the particular pore can be viewed as the Poiseuille flow in a 2D duct, which is characterized by the gap distance, H, and its length L. In the force balance model, four different forces are considered; the drag force, F_D, the lift force, F_L, the adhesion (van der Waals) force, F_A, and the friction force F_F, which are defined in the following way:

Drag force, F_D

The drag force starts to act on the fiber intercepted particle due to pressure driven shear flow occurring inside the pore having average diameter H, because velocity between the solid particle and the fluid starts to be different. According to theoretical and experimental work of Rubin [26], Altman and Ripperger [25], the drag force can be expressed in the following way:

$$F_D = 3.16\pi\tau_w d_p^2,$$ (12)

where τ_w is local fiber wall shear stress, which can be calculated from the Newtonian law as

$$\tau_w = \eta\dot{\gamma},$$ (13)

where $\dot{\gamma}$ represents the shear rate the fiber wall and η is the particle Knudsen number dependent gas viscosity defined by McNenly et al. [27] as

$$\eta = \eta'\left[a_0 + a_1 \arctan\left(a_2 Kn_p^{a_3}\right)\right],$$ (14)

where η' is the gas viscosity at given pressure and temperature, a_0=1.066, a_1=0.679, a_2= -2.082, a_3= 0.866. Kn_p is particle based Knudsen number defined as $2\lambda/d_p$, where d_p is particle diameter. It should be mentioned that that the characteristic pore size dimension H for fiber wall shear rate calculation is determined here as the perpendicular distance between the interception particle/fiber point and surrounding fiber, which represents the second part of the pore. At the local particle-fiber coordinate system the tangential, F_{Dt}, and normal, F_{Dn}, components of the drag force F_D are given by

$$F_{D_t} = F_D \cos\alpha$$ (15)

and

$$F_{Dn} = F_D \sin \alpha ,$$ (16)

respectively. The α angle is defined in Figure 10.

Lift force, F_L

According to the theoretical and experimental analysis of Rubin [25,26] and [28], the lift force is caused by the shear flow and can be calculated as follows:

$$F_L = \frac{0.761 \tau_w^{1.5} d_P^3 \rho_f^{0.5}}{\eta} ,$$ (17)

where ρ_f is the fluid density. At the local particle-fiber coordinate system the tangential, F_{Lt}, and normal, F_{Ln}, components of the lift force F_L are given by

$$F_{Lt} = F_L \sin \alpha$$ (18)

and

$$F_{Ln} = F_L \cos \alpha ,$$ (19)

respectively. The α angle is defined in Figure 9.

Adhesive force F_A

The estimation of the this force is complicated because different parameters such as particle/fiber shape, particle/fiber roughness, adhesion distance, number of contact points etc. may influence the adhesive force strongly [24]. Neglecting the electrostatic interactions, the adhesive forces can be evaluated by calculating the van der Waals force between two spheres of radii R_1 and R_2 as follows [29]:

$$F_A = \frac{3\hbar\bar\omega}{4\pi} \frac{1}{6a^2} \left(\frac{R_1 R_2}{R_1 + R_2} \right) ,$$ (20)

where $\hbar\bar\omega$ is the Lifschitz-van der Waals constant (10^{-20}J) and *a* is the adhesive distance (0.4 nm [1, 25]).

III.12

Friction force F_F

The friction force is caused by the action of the normal forces acting towards the fiber surface (van der Waals force F_A, normal component of the lift force F_{Ln} and drag force F_{Dn}).

$$F_F = \mu \left(F_A + F_{Dn} - F_{Ln} \right) \tag{21}$$

where μ is the friction coefficient which is considered here to be particle Knudsen number dependent parameter (i.e. in the same way as the air viscosity, see Eq. 14)

$$\mu = \mu' \left[a_0 + a_1 \arctan \left(a_2 K_p^{a_3} \right) \right] \tag{22}$$

where μ' is the particle-fiber friction coefficient at given pressure and temperature and the function type in the square parenthesis together with all adjustable parameters are identical with those utilized in Eq. 14.

The particle is considered to be intercepted by the fiber when the lift force is lower/equal than sum of the adhesion force and the drag force, $F_{Ln} \leq F_A + F_{Dn}$ (in the normal direction), or the sum of the drag force and the lift force is lower/equal than the friction force, $F_{Dt} + F_{Lt} \leq F_F$ (in the tangent direction); see Figure 11a. On the other hand, if the sum of the adhesion force and the drag force is higher than the lift force, $F_{Ln} > F_A + F_{Dn}$ (in the normal direction), or the drag force is higher than the sum of the friction force and the lift force, $F_{Dt} + F_{Lt} > F_F$ (in the tangent direction), the particle starts to slip around the fiber in the local slip plane with respect to the particular fiber part and the particle is always released from the particular fiber part in the horizontally mirrored position with respect to initial sticking point between the particle and the particular fiber part as visible in Figure 11b. It also should be mentioned that particle catching due to sieving is considered when at least two connection points between fiber1-particle-fiber2 are identified during the particle motion modeling.

Considering the proposed slip path modeling by using the local coordinate system based force balance and geometrically complex nanofiber shapes, fully 3D character of the particle slip path through nanofiber based filters can easily be modeled as one can see in Figure 12.

PROPOSED FILTRATION MODEL TESTING

In this part, the suggested particle filtration modeling approach is tested. In the first step, the 3D structure model for all manufactured polyurethane filter samples according to methodology described above have been generated (see Figures 8-9). Efficiency of the filter is theoretically determined by the number of particles, which can be captured inside the filter [13]:

$$E = \frac{N_{in} - N_{out}}{N_{in}}, \tag{23}$$

where N_{in} and N_{out} are the numbers of entering and exiting particles, respectively. 200 different groups of particles having diameter linearly varying from 10 to 400 nm on a logarithmic scale (1000 identical particles per group) were injected in the large clean filter inlet (7.2 x 7.2 µm).

The following reference filtration parameters (which correspond to the filtration experiment described above) have been utilized for all tested filter samples: v_{if}=0.057 m/s, p=101325 Pa, T=300 K, µ'=0.02, ρ_p=1000 kg/m³, η'=3.8 10^{5}Pa s. Each particle has been traced through a clean filter, i.e. particle–particle interactions have been neglected, and number of exiting particles was determined in order to calculate the filtration efficiency.

Comparison between the predicted and experimentally determined filtration efficiency data for all four tested filter samples is provided in Figure13. It should be mentioned that simulations were repeated 10 times for each case in order to get the filtration efficiency average values and corresponding standard deviations. It is nicely visible, that the model predictions are in a fairly good agreement for all experimentally tested filters. The slight model filtration efficiency over predictions for the large particle sizes (>200 nm) can be explained by the error in the particle trajectory calculations, because the effect of the Brownian motion force vanishes in such a case and air flow field starts to play the dominant role. The minor over predictions in the filtration efficiency at small particles size range can be caused by the presence of the another forces which can in reality act on the filtered particle (electrostatic forces, general form of the van der Waals force taking the exact shape of the particle/fiber and number of connection point into account, general definition for the friction coefficient, etc.) which were

not fully taken in the filtration simulation into account. On the another hand, it should be mentioned that all theoretical predictions lies within the experimentally determined standard deviation range for the filtration efficiency, which are depicted in Figure 5 which justify the used assumptions and applied simulation methodology.

CONCLUSIONS

In this work, 3D filtration model for nanofiber based filters (utilizing particle-fiber interactions and realistic SEM image based 3D structure model) has been proposed and tested. For the model validation purposes, two polyurethane nanofiber layers prepared by the electrospinning process (having identical average fiber diameter, 120nm, but different average pore size) were combined to form 2 pairs of nanofiber based filters; each pair consist of two filters having comparable mass area and thickness. Filtration efficiency characteristics of prepared filters were determined experimentally in the ultrafine particle size range (20-400 nm). It has been found that the proposed model is able to reasonably predict the measured filtration efficiency curves for all tested filter samples. It is believed that the proposed model can be considered as a useful tool for deeper understanding and optimization the filtration processes utilizing the nanofiber based filters.

ACKNOWLEDGMENTS

REFERENCES

[1]   BROWN, R.C. *Air Filtration: An integrated Approuch to the Theory and Applications of Fibrous Filters*, Oxford: Pergamon Press 1993, 272p.

[2]   BROWN, P.J., and STEVENS, K. *Nanofiber and nanotechnology in textiles*, Cambridge: Woodhead publishing limited 2007, 528p.

[3]   ANDRADY, A.L. Science *and Technology of Polymer Nanofibers*, New Jersey, Wiley-Interscience 2008, 404p.

[4]   HUTTEN, I.M. Handbook *of Nonwoven Filter Media*, Burlington, Elsevier 2007, 473p.

[5]   HUANG, Z.M., ZHANG, Y.Z., KOTAKI, M., et al. A review on polymer nanofibers by electrospinning and their applications in nanocomposites, *Compos. Sci. Technol.* 2003, vol. 63, p.2223-2253.

[6]   KIMMER, D., VINCENT, I., PETRAS, D., FENYK, J., ZATLOUKAL, M., SAMBAER, W., SLOBODIAN, P., SALMELA, H., LEHTIMAKI, M., and ZDIMAL, V., Application of nanofibers in filtration processes, *Nanocon 2010, 2nd International Conference* 2010, p.415-422.

[7]   PODGORSKI, A., BALAZY, A. and GRADON, L. Application of nanofibers to improve the filtration efficiency of the most penetrating aerosol particles in fibrous filters, *Chem. Eng. Sci.* 2006, vol. 61, p.6804-6815.

[8]   LEHMANN, M.J., HARDY, E.H., MEYER, J., and KASPER, G. MRI as a key tool for understanding and modeling the filtration kinetics of fibrous media, *Magn. Reson. Imaging* 2005, vol. 23, no. 2, p. 341.

[9]   SCHWEERS, E. and LÖFFLER F. Realistic modeling of the behaviour of fibrous filters through consideration of filter structure, *Powder Technol.* 1994, vol. 80, no. 3, p. 191–206.

[10]   FAESSEL, M., DELISÉE, C., BOS, F. and CASTÉRA, P., 3D modelling of random cellulosic fibrous network X-ray tomography and image analysis, *Composite Sci. Tech.* 2005, vol. 65, no. 13, p. 1931–1940.

[11]   LUX, J., AHMADI, A., GOBBÉ, C. and DELISÉE, C. Macroscopic thermal properties of real fibrous materials: Volume averaging method and 3D image analysis, *Int. J. Heat. Mass. Transfer* 2006, vol. 49, no. 11-12, p. 1958-1973.

[12]   JAGANATHAN, S., TAFRESHI, H.V., POURDEYHIMI, B. Modeling liquid porosimetry in modeled and imaged 3-D fibrous microstructures, *Journal of Colloid and Interface Science* 2008, vol. 326, no. 1, p. 166-175.

[13]   MAZE, B., TAFRESHI, H.V., WANG, Q., POURDEYHIMI, B., A simulation of unsteady-state filtration via nanofiber media at reduced operating pressures, *J. Aerosol Sci.* 2007, vol. 38, no. 5, p.550-571.

[14]   HOSSEINI, S.A., and TAFRESHI, H.V. Modeling permeability of 3-D nanofiber media in slip flow regime, *Chem. Eng. Sci.* 2010, vol. 65, p.2249-2254.

[15]   HOSSEINI, S.A., and TAFRESHI, H.V., 3-D simulation of particle filtration in electrospun nanofibrous filters, *Powder Technol.* 2010, vol. 201, p.153-160.

[16]   REBAÏ, M., DROLET F., VIDAL D., VAKEIKO I., BERTRAND F. A Lattice Boltzmann Approach for Predicting the Capture Efficiency of Random Fibrous Media, Asia-Pac. *J. Chem. Eng.* 2011, vol. 6, p.26-37.

[17]   JAGANATHAN, S., TAFRESHI H.V. and POURDEYHIMI B. A realistic approuch for modeling permeability of fibrous media: 3-D imaging coupled with CFD simulation, *Chem. Eng. Sci.* 2008, vol. 63, p.244-252.

[18]   SAMBAER, W., ZATLOUKAL, M., and KIMMER, D. The use of novel digital image analysis technique and rheological tools to characterize nanofiber nonwovens, *Polym. Test.* 2010, vol. 29, p.82–94.

[19]   RUSS, J.C. *The Image Processing Handbook (fifth edition)*, CRC Press, Taylor & Francis Group 2007, 817p.

[20]   HUANG, L., WAN, G., and LIU, C. "An Improved Parallel Thinning Algorithm" in Proceedings of the Seventh International Conference on Document Analysis and Recognition (2003), p.780-78.

[21]   SAMBAER, W., ZATLOUKAL, M. and KIMMER, D. 3D modeling of filtration process via polyurethance nanofiber based nonwoven filters prepared by electrospinning process, *Chem. Eng. Sci.* 2011, vol. 66, p.613-623.

[22]   A.LI, G. AHMADI, Dispersion and deposition of spherical-particles from the point sources in a turbulent chemical flow, *Aerosol Science and Technology* 1992, vol. 16, p.209-226.

[23]   H. OUNIS and G. AHMADI, A comparison of Brownian and turbulent-diffusion, *Aerosol Science and Technology* 1990, vol. 13, p.47-53.

[24]   H. OUNIS, G. AHMADI and J.B. MCLAUGHLIN, Dispersion and deposition of Brownian particles from the point sources in a simulated turbulent channel flow, *Journal of Colloid and Interface Science* 1991, vol.47, p.233-250.

[25]   ALTMANN, J., RIPPERGER, S. Particle deposition and layer formation at the crossflow microfiltration, *J. Membrane Sci.* 1997, vol. 124, p.119-128.

[26]   RUBIN, G., Widerstands und Auftreibsbeiwerte von ruhenden kugelformigen Partikeln in stationaren, wandnahen laminaren Grenzschichten, PhD Thesis, TH Karlsruhe, Germany, 1977.

[27]   MCNENLY, M.J., GALLIS, M.A., and BOYD, I.D., Empirical slip and viscosity model performance for microscale gas flow, *Int. J. Numer. Meth. Fl.* 2005, vol. 49, p.1169-1191.

[28]   MCLAUGHLIN, J.B. The lift on a small sphere in wall-bounded linear shear flows, *J. Fluid. Mech.* 1993, vol. 246, p.249-265.

[29]   BHUSHAN, B. *Nanotribology and Nanomechanics: An Introduction*, Springer 2005, 1148p.

Table 1: Basic characteristics for all investigated filter types.

Filter Type	Mass Area [g/m²]	Thickness* [µm]	MPPS [nm]	Filtration Efficiency [%]	Pressure Drop [Pa]	Quality Factor [1/kPa]
1	0.438	3.17 ± 0.89	70	88.5 ± 1.38	123 ± 1.41	49.7 ± 3.4
2	0.447	3.44 ± 1.15	70	91 ± 2.84	96.5 ± 2.89	69.7 ± 2.22
3	0.878	6.36 ± 1.78	70	98.5 ± 3.79	225.5 ± 0.70	42.5 ± 2.12
4	0.893	6.88 ± 2.30	80	99.66 ± 5.74	190 ± 7.34	54.5 ± 3.42

* The filter thicknesses were determined from particular side SEM image views
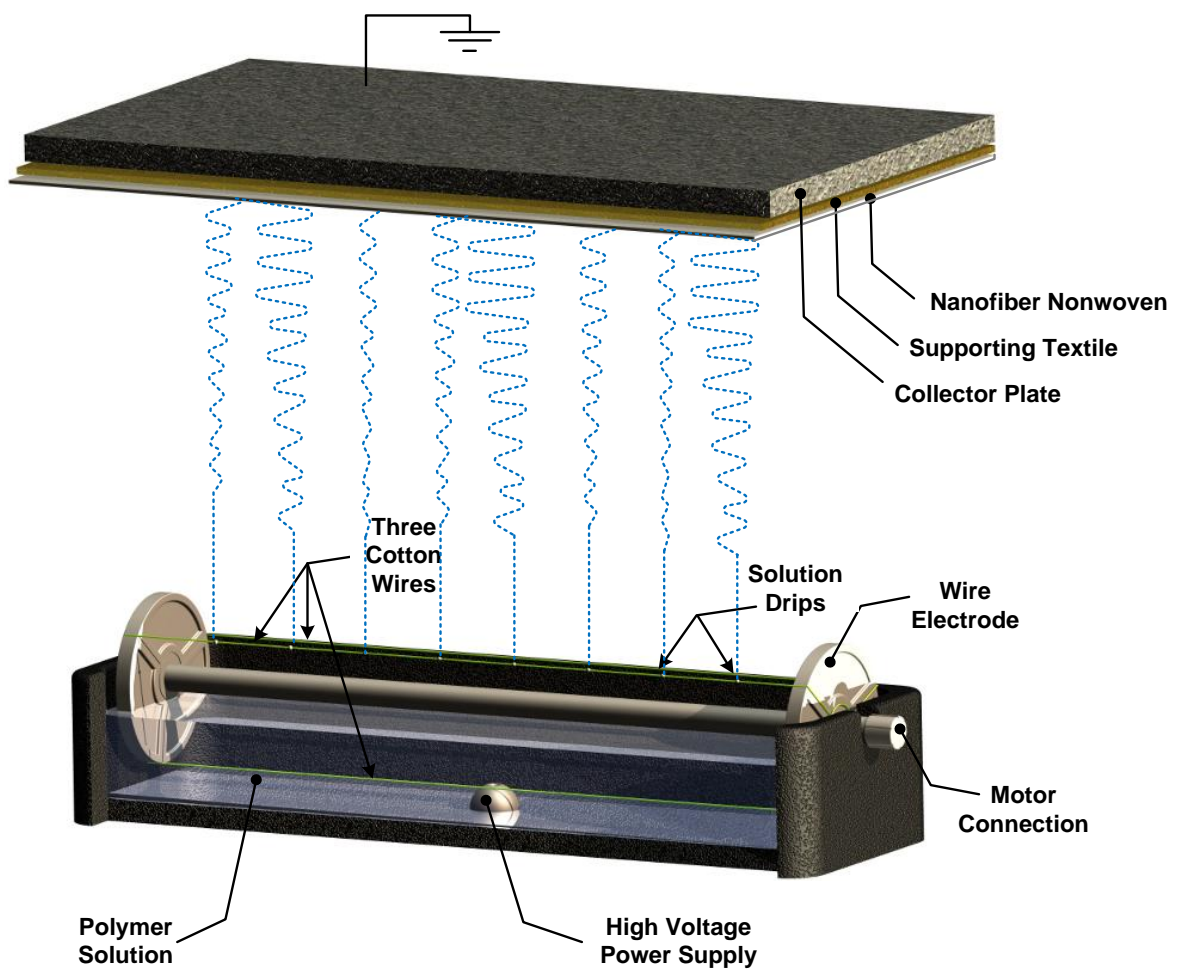
Figure 1: *Scheme of the electrospinning process using a rotating electrode with cotton cord spinning elements.*

a.

5μm

b.

5μm
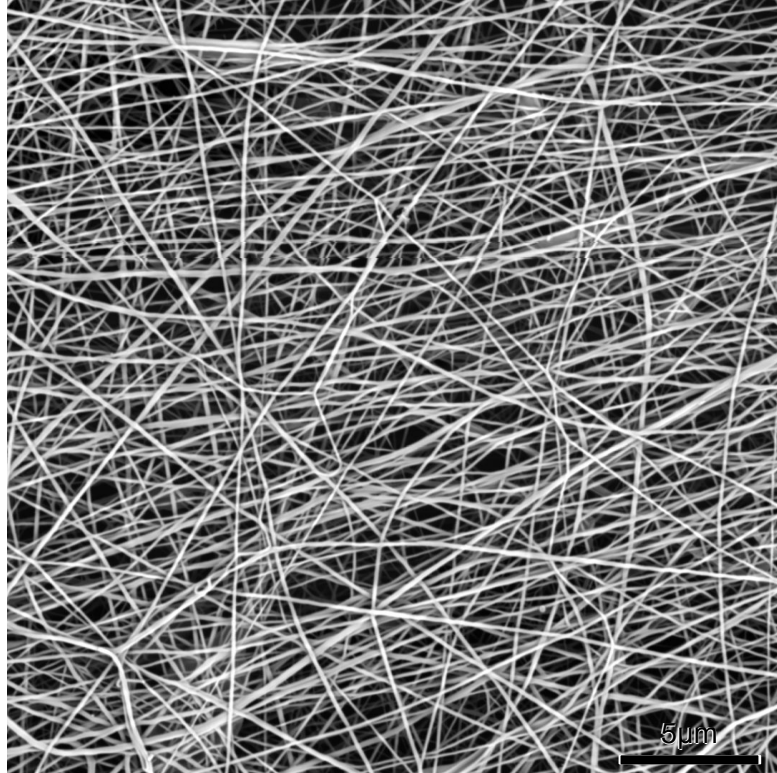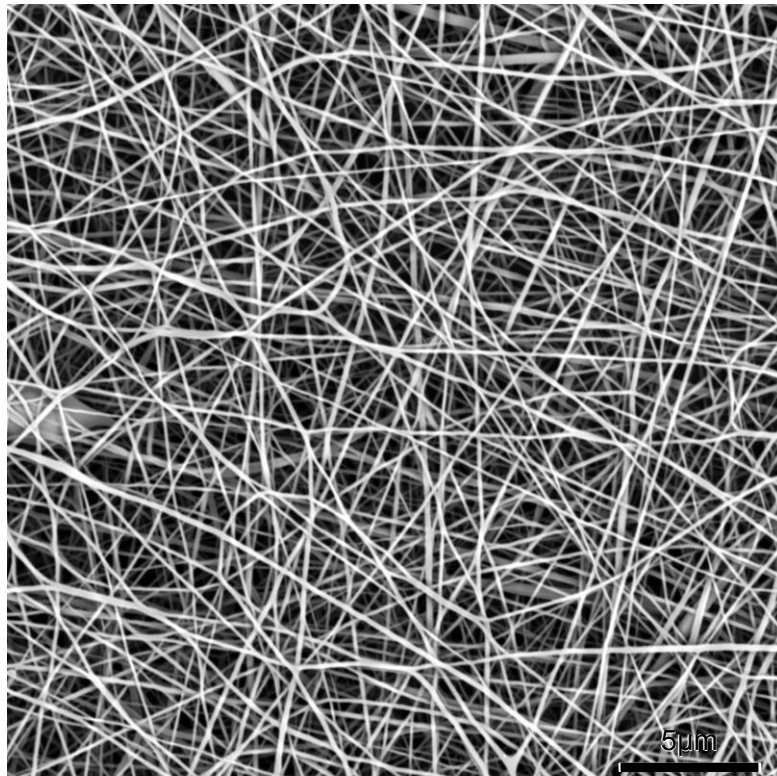
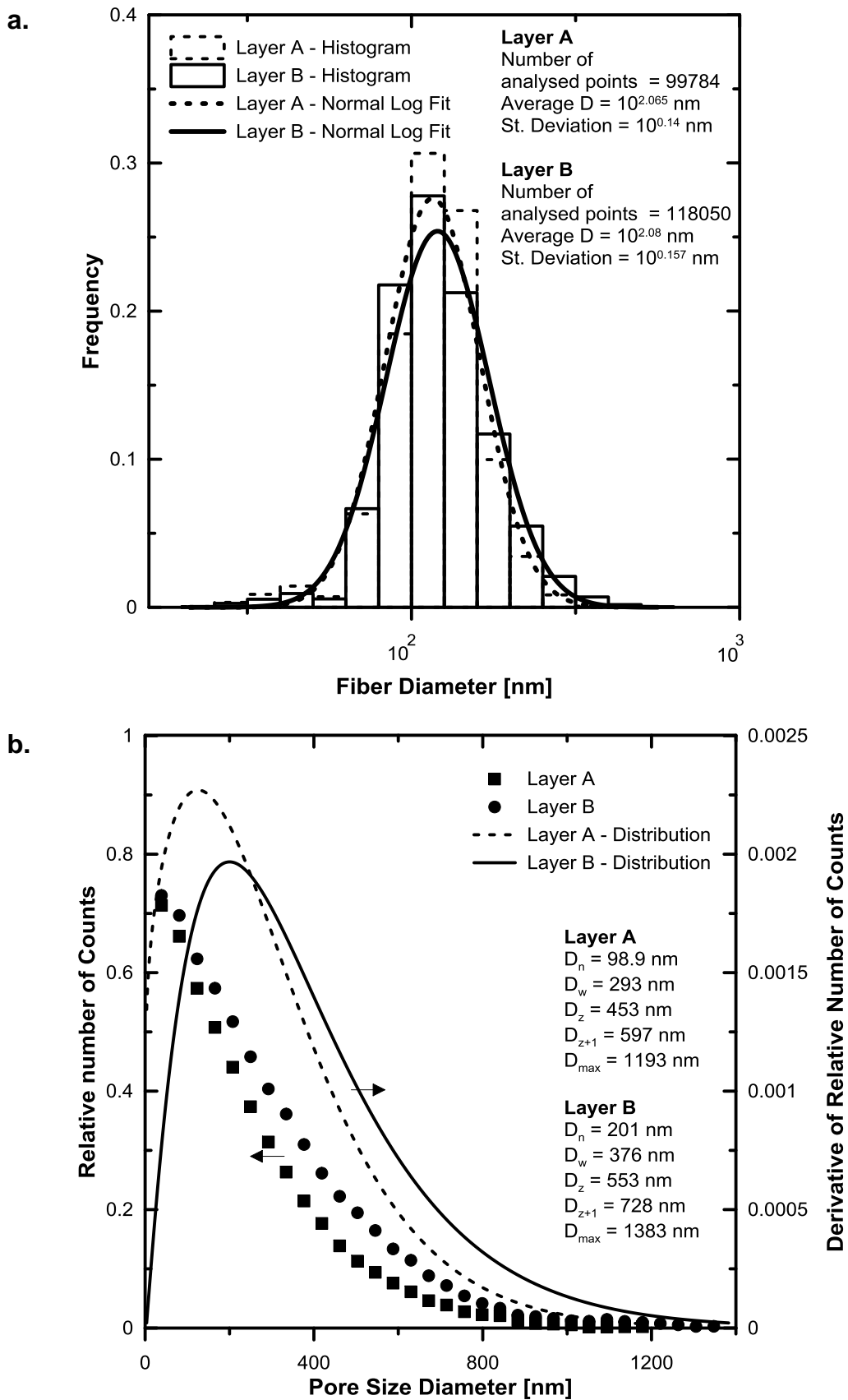*Figure 2:* *Top SEM image views for nanofiber Layer A, 2a) and Layer B, 2b), prepared by electrospinning process.*

a.

Layer A - Histogram
Layer B - Histogram
Layer A - Normal Log Fit
Layer B - Normal Log Fit

Layer A
Number of
analysed points = 99784
Average D = $10^{2.065}$ nm
St. Deviation = $10^{0.14}$ nm

Layer B
Number of
analysed points = 118050
Average D = $10^{2.08}$ nm
St. Deviation = $10^{0.157}$ nm

Frequency

Fiber Diameter [nm]

b.

Layer A
Layer B
Layer A - Distribution
Layer B - Distribution

Layer A
D_n = 98.9 nm
D_w = 293 nm
D_z = 453 nm
D_{z+1} = 597 nm
D_{max} = 1193 nm

Layer B
D_n = 201 nm
D_w = 376 nm
D_z = 553 nm
D_{z+1} = 728 nm
D_{max} = 1383 nm

Relative number of Counts

Derivative of Relative Number of Counts

Pore Size Diameter [nm]

Figure 3: Morphological characteristics for fiber nanofiber layer A and B; 3a) Fiber di-ameter distribution;3b) Pore size distribution.

Filter 1	Filter 2	Filter 3	Filter 4
layer B		layer B	
layer B	layer A	layer B	layer A
layer B		layer B	
layer B	layer B	layer B	layer B
		layer B	layer B
		layer B	
		layer B	layer A
		layer B	
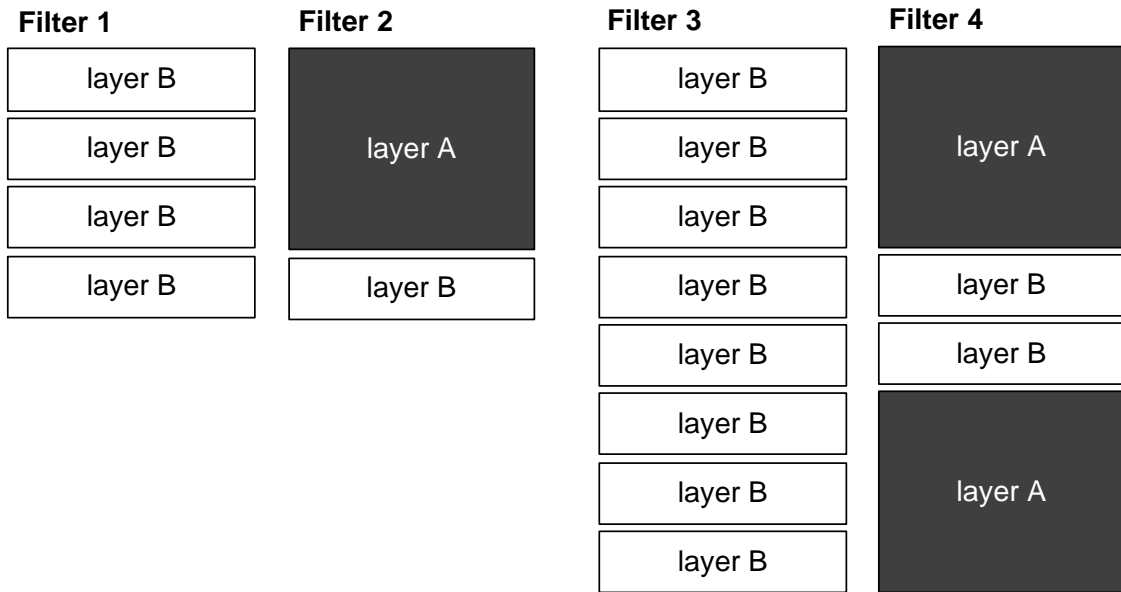
Figure 4: Structure description for all prepared nanofiber based filters.
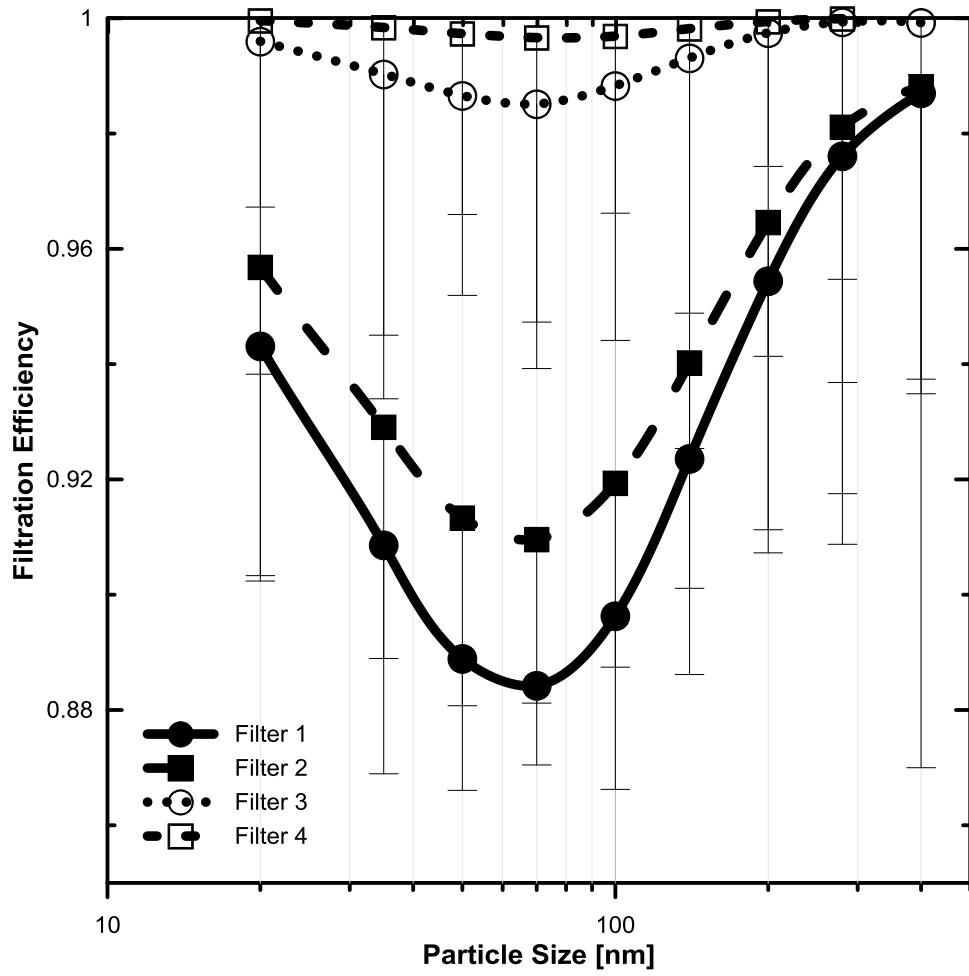
Figure 5:   *Filtration efficiency measurements for the four analyzed filters (the points represents average values whereas the error bars represents the negative standard deviation).*
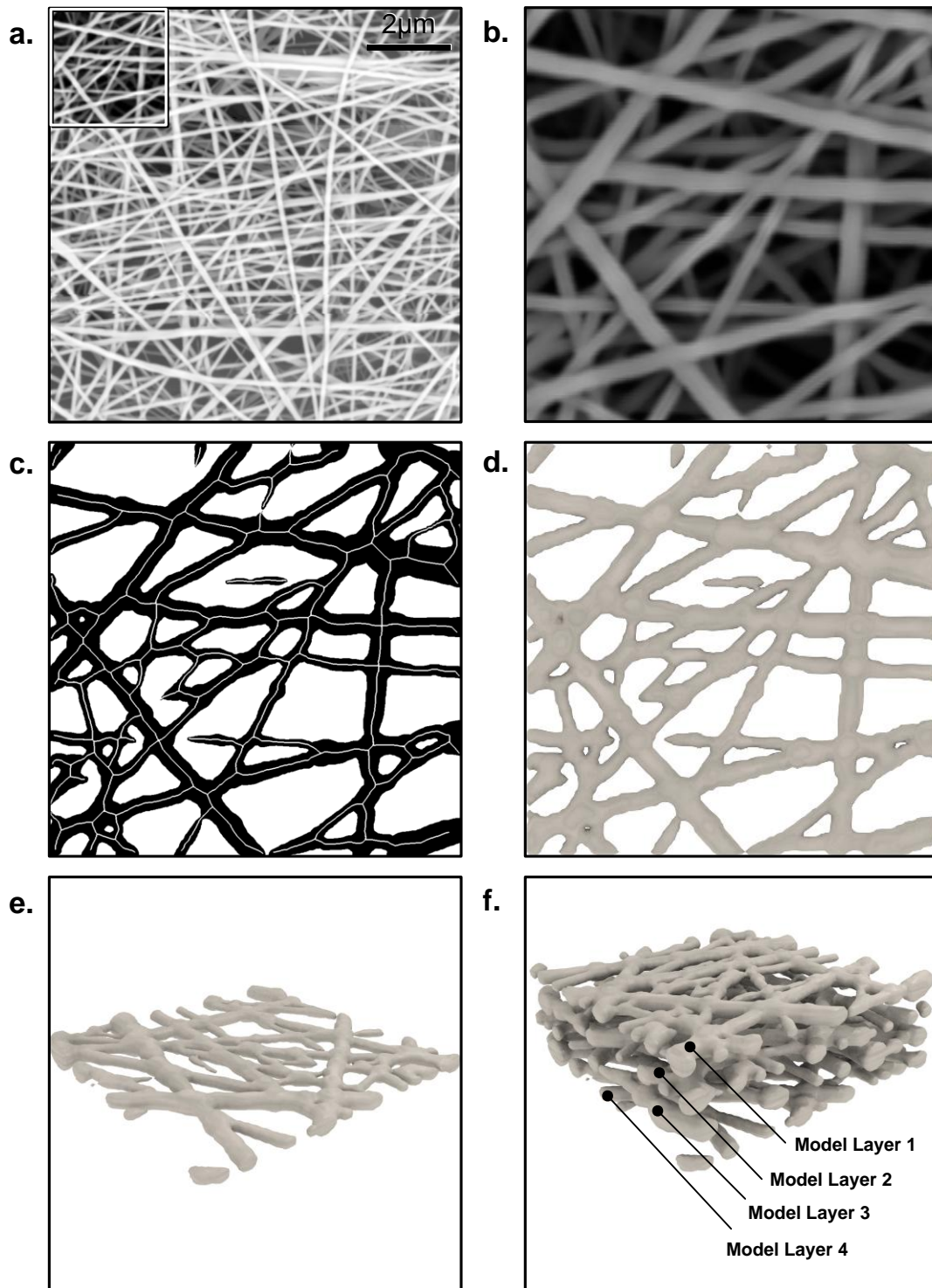
Figure 6:   3D structure model creation for particular nanofiber layer from SEM image-layer based on a SEM image; 6a) SEM top view of particular nanofiber layer; 6b) SEM top section view of particular nanofiber layer; 6c) Nanofiber center-line determination from Figure 6b); 6d) Top view of one 3D model layer; 6e) Perspective view of one 3D model layer; 6f) Full 3D model of a nanofiber lay-er.
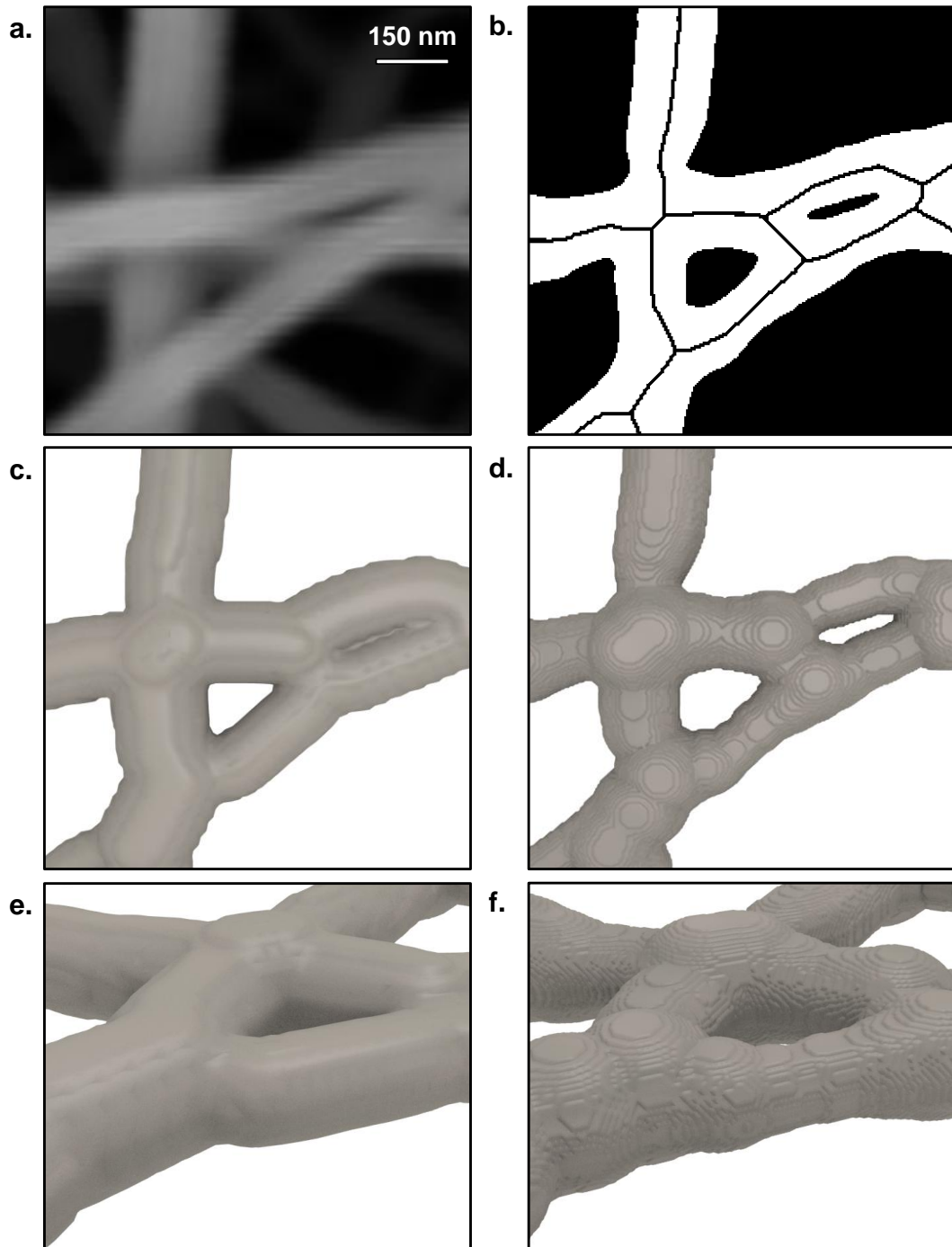
Figure 7: Comparison between old an improved methodology for the 3D layer creation from SEM image;7a) SEM image of nanofiber layer (detailed view); 7b) Nano-fiber centerlines determination from thresholded SEM image; 7c) 3D model lay-er created by using the old methodology [21] from Figure 7b); 7d) 3D model layer layer created from Figure 7b) by using the improved methodology utilized in this work; 7e) Perspective view of the image depicted in Figure 7c); 7f) Per-spective view of the image depicted in Figure 7d).

Filter 1

Calculated thickness: 2.43 *μm*

B

B

B

B

B
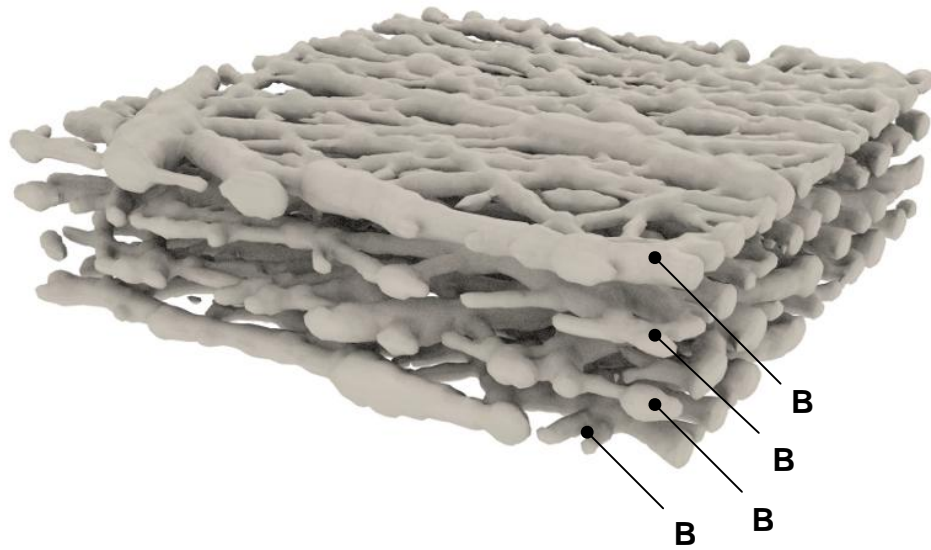
Filter 2

Calculated thickness: 2.57 *μm*

A

B
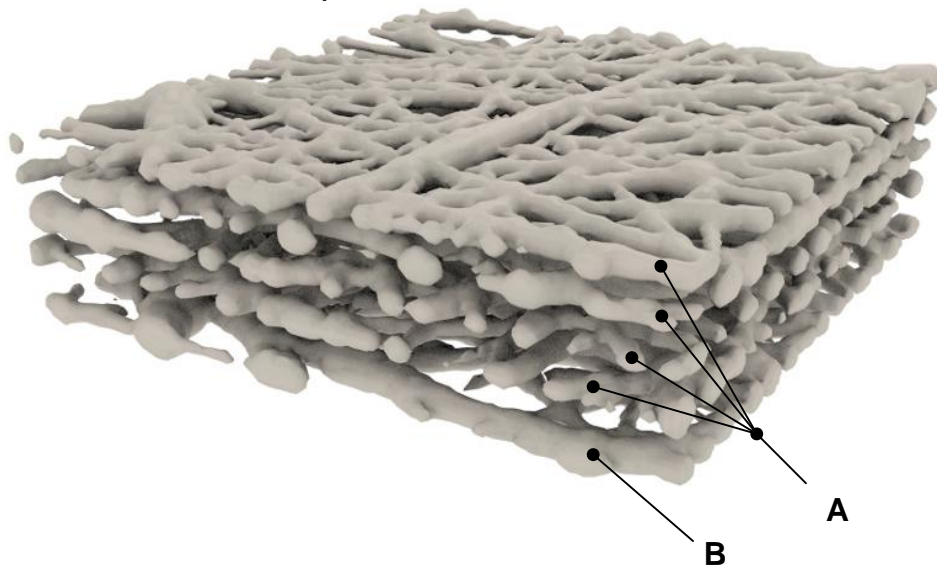
Figure 8: Full 3D structure models for Filter 1 and Filter 2.

III.28

Filter 3

Calculated thickness: 4.66 *µm*
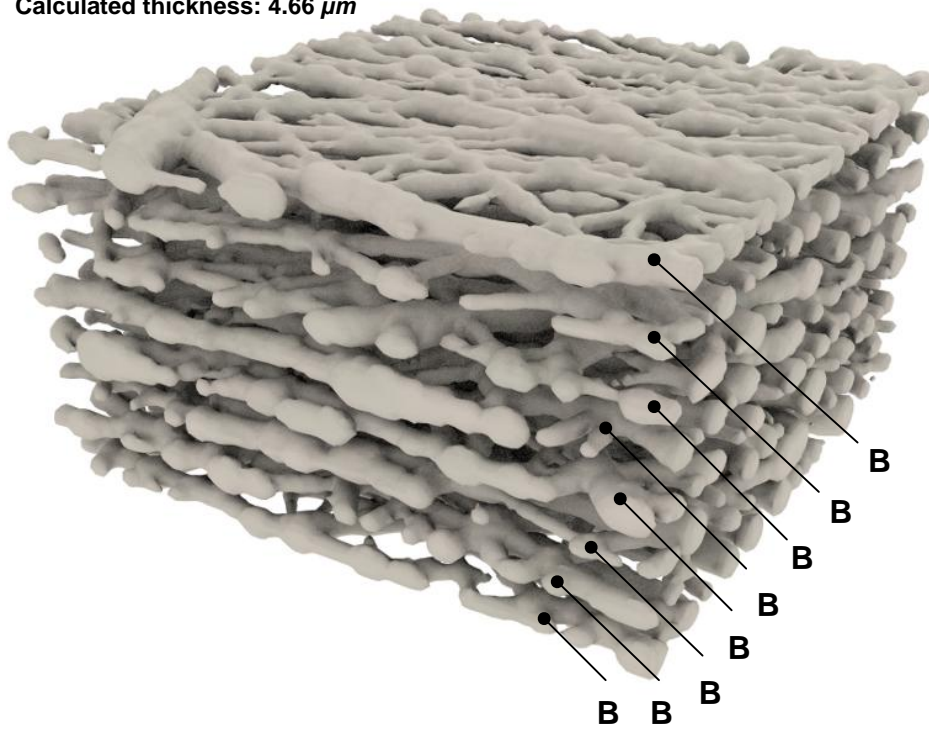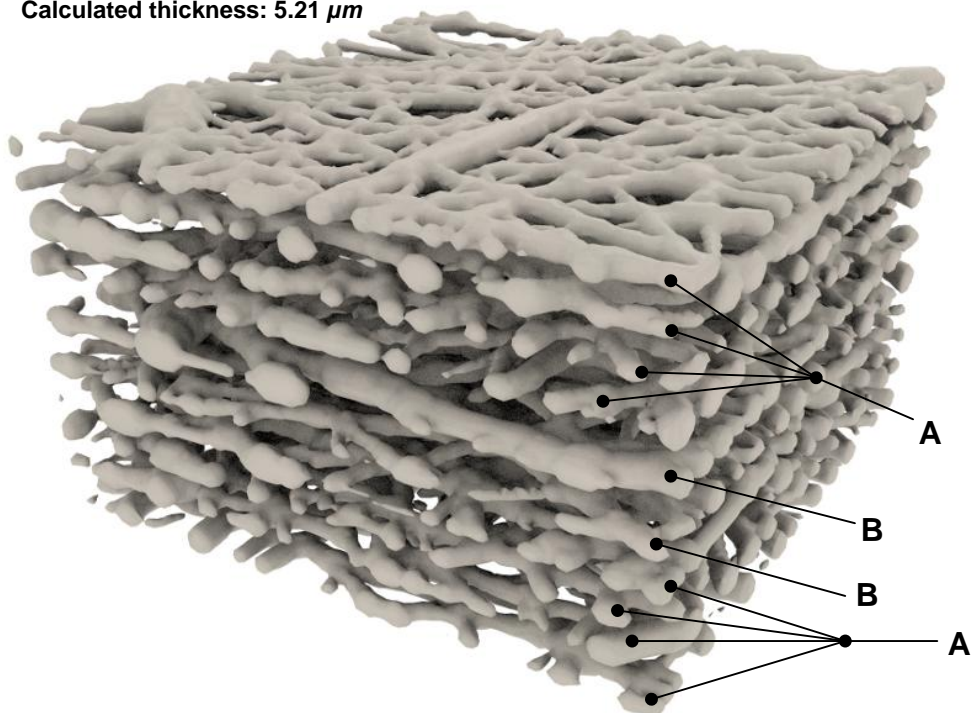

Filter 4

Calculated thickness: 5.21 *µm*

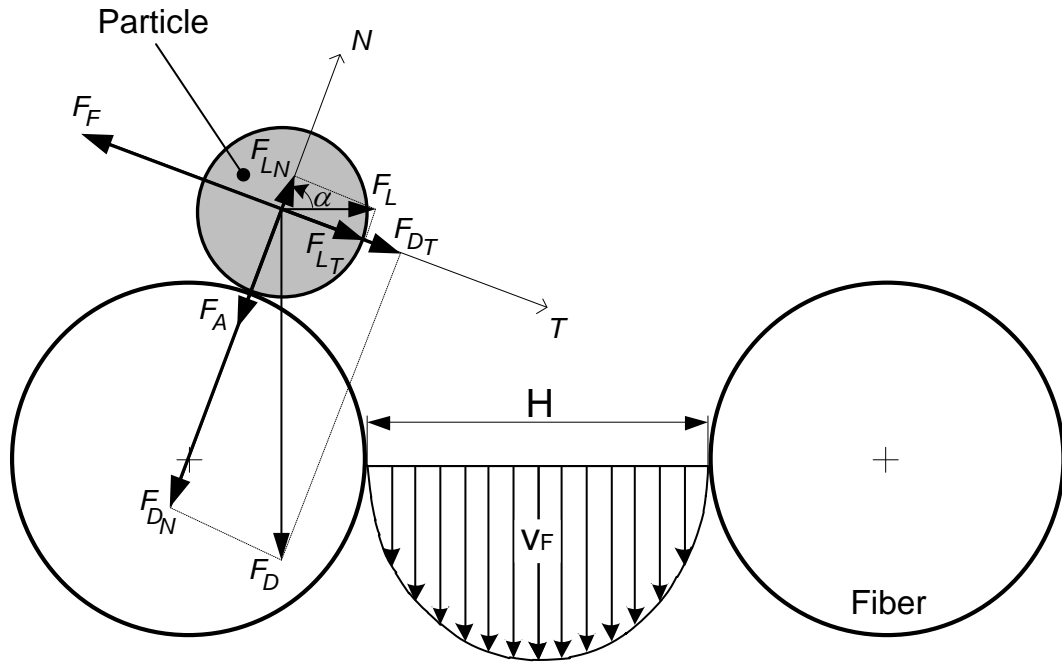*Figure 9: Full 3D structure model for Filter 3 and Filter 4.*

Figure 10: Fiber local coordinate system based force balance utilized for particle-fiber interaction modeling.
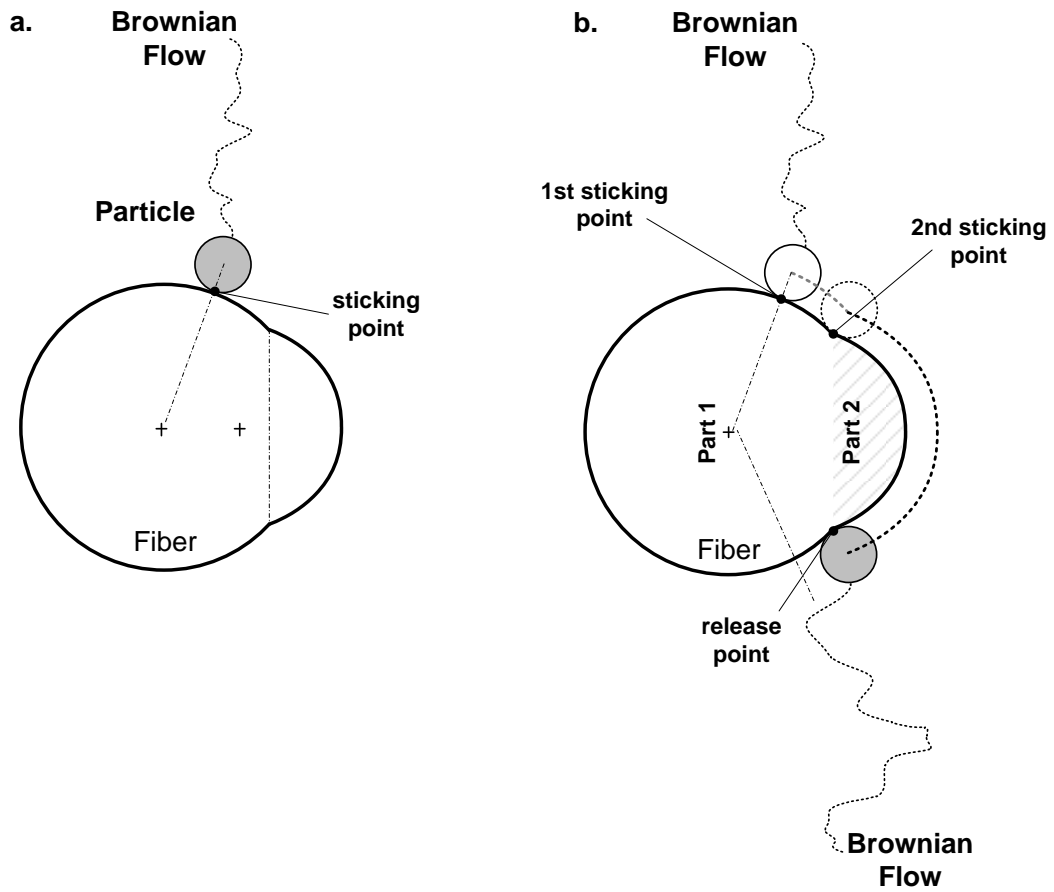
a. Brownian Flow

Particle

sticking point

Fiber

b. Brownian Flow

1st sticking point

2nd sticking point

Part 1

Part 2

Fiber

release point

Brownian Flow

Figure 11: Visualization of two possible particle-fiber configurations; 10a) Particle sticks at the fiber; 10b) Particle slips along the fiber.
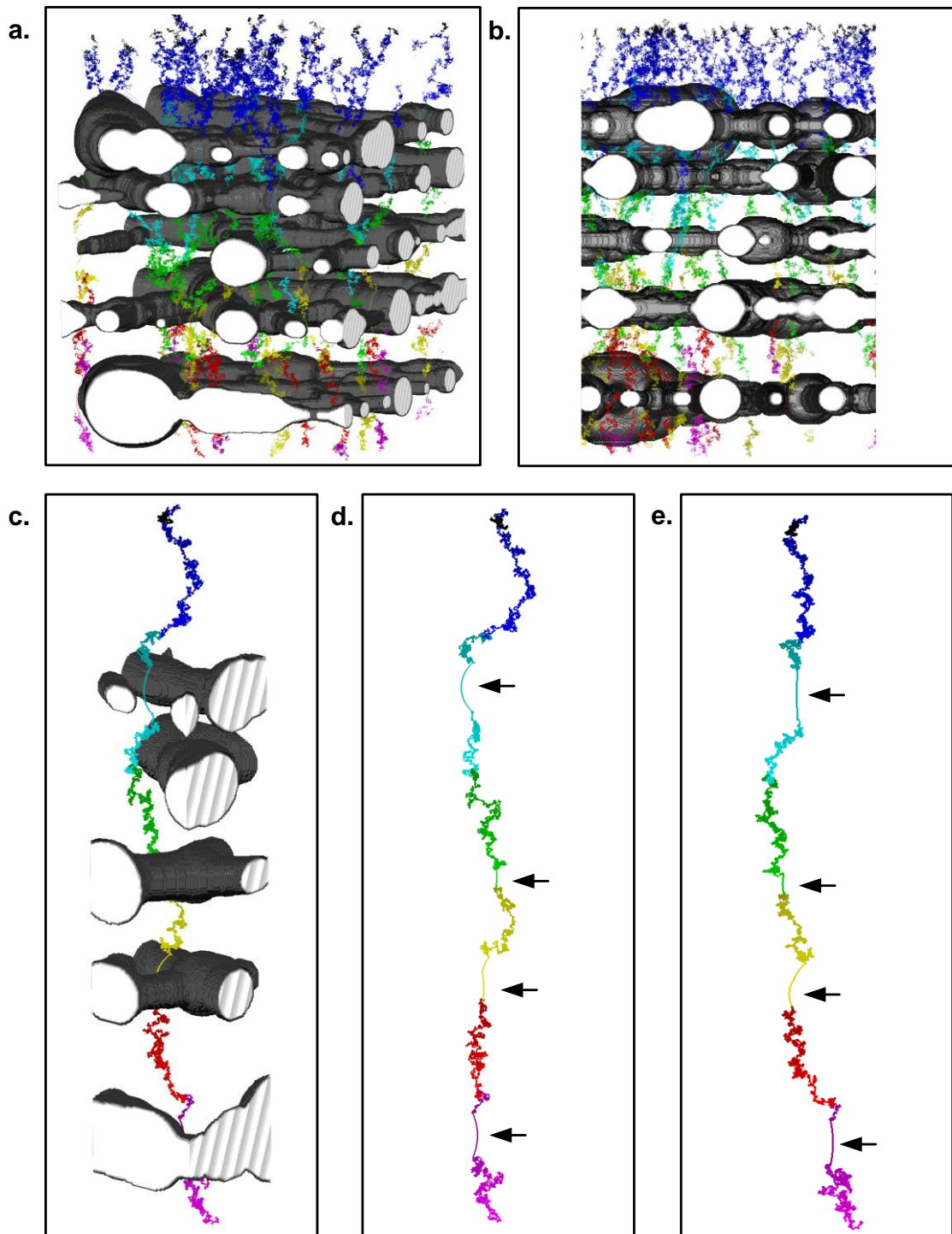
Figure 12:   Flow path lines through a part of the Filter2 for 100 nm diameter particles; 11a) Perspective view; 11b) Side view; 11c) Perspective view for one flow path line visualized with surrounding fibers; 11d) Side view visualized without surrounding fibers; 11e) Front view visualized without surrounding fibers. The arrows in Figures 11d) and 11e) indicates the slip path location.
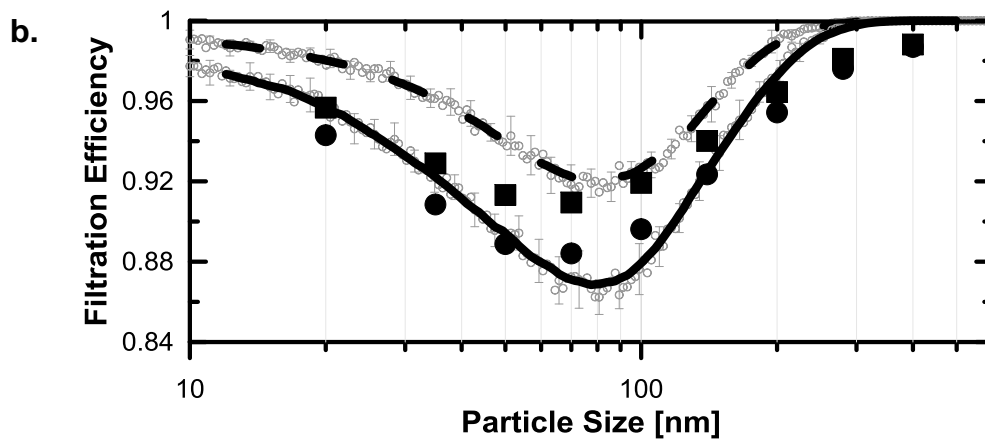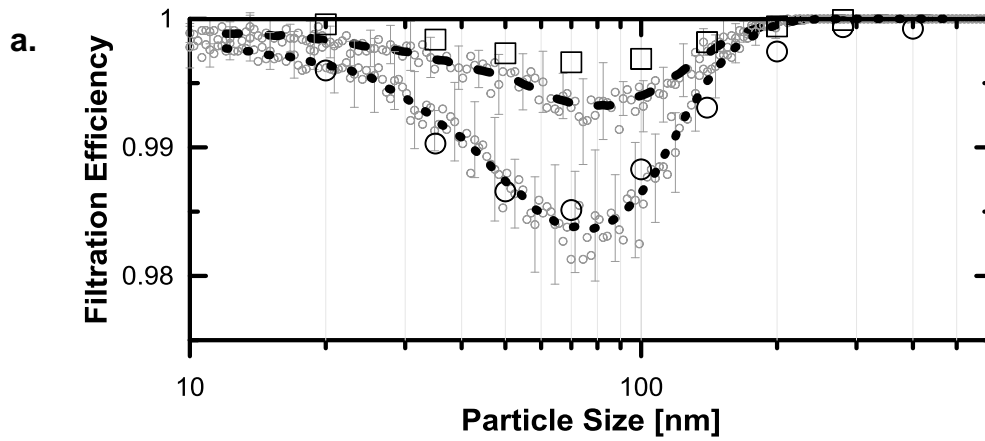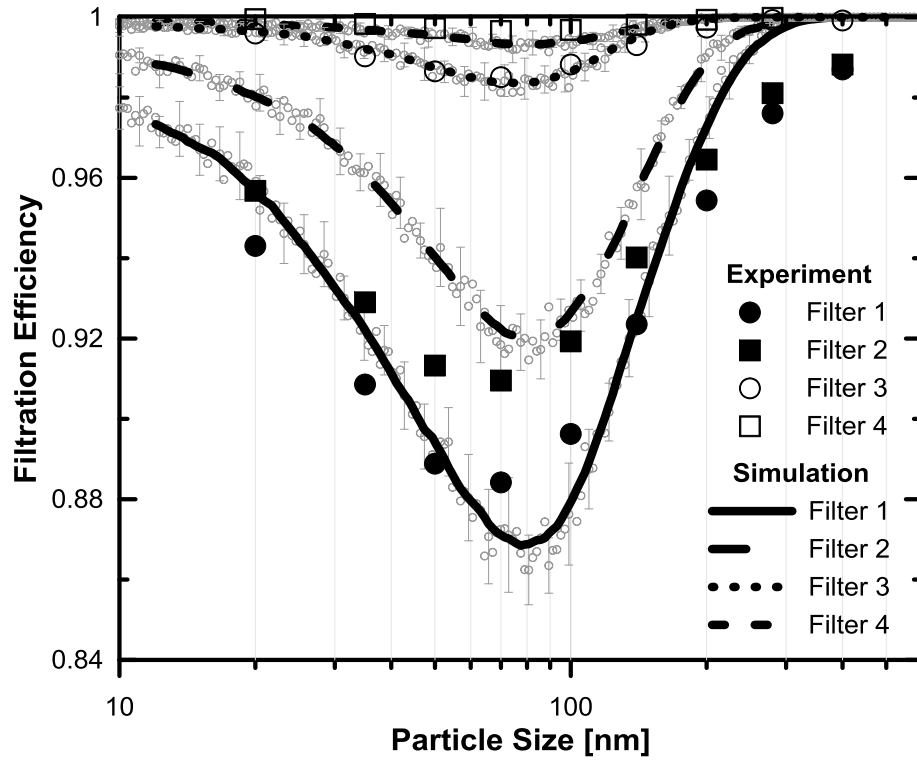
Figure 13: *Comparison between measured and predicted filtration efficiency curves for all investigated filters; 12a) Detailed view for the Filter 3 and 4; 12b) Detailed view for the Filter 1 and 2.*

PAPER IV

3D clogging modeling of polyurethane nanofiber based filters by ultrafine aerosol particles

Wannes Sambaer [1,2], Martin Zatloukal [1,2*] and Dusan Kimmer [3]

[1] *Centre of Polymer Systems, University Institute, Tomas Bata University in Zlin,*

Nad Ovcirnou 3685, 760 01 Zlin, Czech Republic

[2] *Polymer Centre, Faculty of Technology, Tomas Bata University in Zlin, TGM 275,*

762 72 Zlin, Czech Republic

[3] *SPUR a.s., T. Bati 299, 764 22 Zlin, Czech Republic*

Keywords: Nanofiber, Electrospinning, 3D simulation, Filtration modeling, Cake formation, Clogging.

*Corresponding author: mzatloukal@ft.utb.cz

ABSTRACT

Realistic SEM image based 3D filter model, transition/free molecular flow regime, Brownian diffusion, aerodynamic slip, particle-fiber and particle-particle interactions together with a novel Euclidian distance map based methodology to calculate the pressure drop has been utilized for a polyurethane nanofiber based filter prepared via electrospinning process in order to more deeply understand the filter clogging, filtration cake formation and its role on the final filter efficiency. The model predictions have been found to be in good agreement with the corresponding experimental data justifying the used assumptions. By using proposed theoretical approach for the 3D filter clogging modeling, it has been found that the decrease in the fiber-particle friction coefficient leads to higher pressure drop, lower filtration efficiency, lower quality factor and lower quality factor sensitivity to the increased collected particle mass due to deeper particle penetration in the filter and creation of smaller pores.

INTRODUCTION

Fibrous based air filters are widely used in many applications in area of pharmaceutical, medical, biology, food, semi-conductor industries and therefore it is not surprising that both experimental [1-3] and theoretical studies [4-11] dealing with their basic characteristics (such as the pressure drop and particle collection efficiency) can be found in the open literature. It has been shown theoretically and experimentally [12-13] that the particles accumulation in the filter happened in the following three stages. Firstly, particles are touched to the surface of the filter media (capillary deposition), i.e. there are particle-fiber interactions only. In the second stage, capillary deposition together with interception of already caught particles (capillary clogging) takes place, i.e. there are both, particle-fiber as well as particle-particle interactions. In the final stage, the particles are caught by the interception of other particles only, which leads to a large increase in cake growth, i.e. there are particle-particle interactions only. A number of theoretical studies considering the above described filter clogging mechanism [12-22] have already been performed for micro-fibrous filters.

Nowadays, nanofiber nonwoven based filters becomes of high interest due to their ability to reach high filtration efficiency for ultrafine particles with a low pressure drop due to aerodynamic slip around the nanofibers. Unfortunately, till now, the detailed theoretical analysis of the nanofiber based filters clogging has not been performed yet and thus, the full understanding of the filtration cake formation on the nanofiber based filters and its role on the final filter efficiency is not fully understood yet. In order to provide a better understanding of the nanofiber based filters loading process with respect to pressure drop and filtration efficiency evolution, a realistic SEM image based 3D structure model of the filter, transition/free molecular flow regime, Brownian diffusion, particle-fiber interactions, aerodynamic slip and sieve has been utilized in this work. To ensure that the utilized filtration model assumptions are valid and thus justifying the validity of its predictions, the nanofiber based filter characteristics (determined experimentally for the filter sample manufactured by the electrospinning process in this work) as well as the suitable experimental data taken

from the literature [13][23] has been used for the basic filtration model validation purpose.

FILTER PREPERATION AND CHARACTERIZATION

Materials

A polyurethane solution in dimethylformamide (DMF) based on 4,4'methylenebis(phenylisocyanate) (MDI), poly(3-methyl-1,5-pentanediol)-alt-(adipic, isophtalic acid) (PAIM) and 1,4 butanediol (BD) was synthesized in molar ratio 9:1:8 at 90°C for 5 hours (per partes way of synthesis starting with preparation of prepolymer from MDI and PAIM and followed by addition of BD and remaining quantity of MDI). The prepared solution was suitable for electrospinning process and had a PU concentration of 24.1 wt%, viscosity of 1.45 Pa.s and conductivity of 157 µS/cm (adjusted by 3 parts of citric acid and 1 part of borax).

Nanofiber Layers Preparation by Electrospinning Process

In this work, a commercially available NanoSpider[TM] machine (Elmarco s.r.o. Liberec, Czech Republic, http://www.elmarco.com/) equipped with patented (PCT/CZ2010/000042) rotating electrode with 3 cotton cords spinning elements was used to prepare nanofiber nonwoven based filter sample from polyurethane solution. The experimental conditions were: relative humidity 25 %, temperature 23.5 °C, high voltage applied into PU solution 75 kV, distance between electrodes 210 mm, rotational electrode speed 7 rpm and speed of polyester nonwoven supporting textile collecting nanofibers was 0.4 m/min. Samples for further analyses were taken from the middle part of the 40 cm wide fabric coated with layer of nanofibers.

Nanofiber Filter Characterization

A nanofiber based filter, prepared via electrospinning process, has been characterized by Scanning Electron Microscope technique (Vega 3, Tescan, Czech republic), as visible in Figure 1. The obtained SEM picture has consequently been used for the fiber diameter/pore size distribution determination by using recently proposed digital image analysis technique [24]. The obtained basic characteristics for the analyzed filter sample are summarized in Figures 2a-2b. The filter has an average

fiber diameter and average pore size equal to 133 nm and 156 nm, respectively, thickness (3.59 μm) and mass area (0.54 g/m²).

The electric potential generated on the surface of the filter was measured by electrostatic fieldmeter Simco, model FMX-003, the Netherlands. It has been found that the surface charge potential of the filter was practically negligible, equal to 70 V, i.e. there are practically no electrostatic forces, which could affect its filtration characteristics.

The filtration efficiency for the prepared nanofiber based filter was determined experimentally in the ultrafine particle range according to following procedure. An ammonium sulphate solution having concentration of 1 g/l was nebulized (AGK, PALAS, Germany), a monodisperse size fraction was selected (original particle distribution is provided in Figure 3a) using an Electrostatic Classifier (EC 3080, TSI, USA) and particle concentration upstream and downstream the filter (face velocity 5.7 cm/s) was recorded by a condensation particle counter (UCPC 3025 A, TSI, USA). The filtration efficiency, determined at nine mobility diameter fractions (20, 35, 50, 70, 100, 140, 200, 280 and 400 nm) is depicted in Figure 3b. Note that the filtration efficiency and pressure drop measurements were repeated four times and the following filtration efficiency characteristics of the filter were experimentally determined: the Maximum Penetration Pore Size (MPPS) 70 nm, the minimum filtration efficiency 98.32 %, the average pressure drop 148.5 Pa and the quality factor 27.5 kPa^{-1}, which is defined according to Eq. 1.

$$QF = -\ln(E)/\Delta p \qquad (1)$$

where Δp is the pressure drop and E is the filtration efficiency at MPPS.

FILTRATION MODEL DESCRIPTION

3D Filter Structure Model

The 3D filter model has been generated from SEM image by using recently proposed methodology [25] in order to take varying fiber diameter, curvature and possible structure defects as well as 3D features of the whole filter correctly into account. In the first step of this technique, the average threshold level is applied for the original grayscale SEM sample image to filter the top fibers only, which results in a black/white image. Secondly, nanofiber centerline pixels are calculated and the 3D shape of each fiber section is created by the rotation in the depth direction of local diameter circle fitted in the white fiber area along every corresponding centerline pixel. In the final step, the integer number of no overlapped model layers is searched, cut out from the original SEM image and stacked on each other to form the 3D filter model having the same mass area as the real filter. Figure 4 and Video 1 (see supplementary material) shows the 3D structure model for the investigated polyurethane nanofiber based filter created from the SEM image depicted in Figure 1 according to the technique described above.

Flow Field Calculation

The transition-free molecular flow regime is considered in this work due to small average fiber diameter size (133 nm) of the investigated filter for which the Knudsen number (the ratio of two times gas molecules mean free path and fiber diameter) is higher than 0.25. In such a case, particle Brownian motion and uniform gas flow field can only be considered as the result of significant air slip occurrence at the fiber surface where the influence of the fibers on the flow field is negligible as suggested by Maze et al. [7]. In such a case, the flow field is described by the set of equations, which are summarized in Table 1.

Particle-Fiber Interaction Modeling

In this work, the flow through the particular pore is viewed as the Poiseuille flow in a 2D duct (having the gap distance, H, and length L) where the drag force, F_D, the lift force, F_L, the adhesion (van der Waals) force, F_A, and the friction force F_F are considered to act between the fiber and a non-deformable spherical particle according to J. Altmann and S. Ripperger [26] (see Figure 5 and Table 2). In more detail, the *drag force, F_D*, starts to act on the fiber intercepted particle due to pressure driven shear flow occurring inside the pore having average diameter H determined here as the perpendicular distance between the interception particle/fiber point and surrounding fiber, which represents the second part of the pore. The local fiber wall shear stress, τ_w, is defined here through the Newtonian law utilizing the Knudsen number dependent air viscosity proposed by M.J. McNenly et al. [27] for Poiseuille flow. The equation for the *lift force, F_L*, which is induced by the shear flow perpendicularly to the drag force, is utilized here in the form suggested by Rubin [28], J. Altmann and S. Ripperger [26] and McLaughlin [29] based on their theoretical and experimental analysis. The estimation of the *adhesion force, F_A*, is complicated because different parameters such as particle/fiber shape, particle/fiber roughness, adhesion distance, number of contact points etc. may influence the adhesive force strongly [26]. Here, neglecting the electrostatic interactions, the adhesive forces is evaluated through the van der Waals force acting between two spheres of radii R_1 and R_2 [30]. The *friction force, F_F*, is caused by the action of the normal force, F_N, acting towards the fiber surface (i.e. sum of the van der Waals force F_A, normal component of the lift force F_{Ln} and drag force F_{Dn}) where the friction coefficient, μ, is considered here to be Knudsen number dependent parameter (i.e. in the same way as the air viscosity).

The particle is considered to be intercepted by the fiber when the lift force is lower/equal than the adhesion force, $F_L \leq F_A$, or the drag force is lower/equal than the friction force, $F_D \leq F_F$. On the other hand, if the lift force is higher than the adhesion force ($F_L > F_A$) or the drag force is higher than the friction force ($F_D > F_F$), the particle starts to slip around the fiber in the local slip plane with respect to the particular fiber part and the particle is always released from the particular fiber part in the horizontally mirrored position with respect to initial sticking point between the particle and the

IV.8

particular fiber part. It also should be mentioned that particle catching due to sieving is considered when at least two connection points between fiber1-particle-fiber2 are identified during the particle motion modeling.

Particle-Particle Interaction

In this work, the fully sticking (single touching point) boundary condition was applied for the particle-particle interaction modeling (similarly to other theoretical studies [13; 15-20; 31-33]) which can be justified for the 10nm-5µm particle size range as showed experimentally by Wang and Kasper [34] and Pawu and Braaten [35]. Under this condition, dendrites (formed by the accumulated particles during the filtration process) cannot bend or break down, see Figure 6.

PRESSURE DROP CALCULATION

In this work, the following novel methodology to calculate the pressure drop through the 3D filter model is introduced for the first time. First, the 3D filter model is divided into a number of binary slice layers (where black pixels represents pores and white pixels the fibers/particles) having the same thickness (equal to pixel resolution) as illustrated in Figures 7a-d.

Second, the Euclidian distance map (a matrix containing binary elements, where all black pore pixels are labeled with a number, visualized by a grayscale level, which is related to the shortest distance to the nearest white fiber/particle pixel) is generated for particular binary slice layer (see Figure 7e).

Third, a characteristic pore radius, Rc, for the given layer is determined according to Eq.2

$$Rc = \sqrt{\frac{scale^2 \sum_{i=0}^{n} \left(\frac{d_i}{d_{max}} \right)^2}{\pi}} \tag{2}$$

where *scale* is the pixel size, *n* is the overall number of pixels, d_i represents local distance map value for the i-th pixel, d_{max} is the maximum distance map value.

Fourth, considering that the air flow through the porous slice layer can be viewed as the Poiseuille flow in a 2D tube, the corresponding pressure drop can be calculated according to well-known Poiseuille equation

$$\Delta p = \frac{Q.8.\eta'.L}{\pi . Rc^4} \tag{3}$$

where Q is the volume flow rate of the air through the filter, L is the slice layer thickness, Rc is the characteristic pore radius defined by Eq. 2 and η' is the Knudsen number dependent gas viscosity defined by McNenly et al. [27] as:

$$\eta' = \eta \left[a_0 + a_1 \arctan \left(a_2 Kn_p^{a_3} \right) \right] \tag{4}$$

where η is the gas viscosity at given pressure and temperature, a_0=1.066, a_1=0.679, a_2= -2.082, a_3= 0.866. Kn_p is particle based Knudsen number defined as $2\lambda/d_p$, where λ is the mean free path of molecules and d_p is the particle diameter.

Finally, the overall pressure drop through the whole filter is then calculated as the sum of all individual pressure drops from each slice.

PROPOSED FILTRATION MODEL TESTING, PARAMETRIC STUDY AND CONCLUSIONS

The filtration efficiency of the filter is theoretically determined by the number of particles, which can be captured inside the filter [7]:

$$E = \frac{N_{in} - N_{out}}{N_{in}} ,$$

(5)

where N_{in} and N_{out} are the numbers of entering and exiting particles, respectively. Twenty different groups of particles having diameter linearly varying from 20 to 500 nm on a logarithmic scale (10000 identical particles per group) were injected in the large clean filter inlet (7.2 x 7.2 µm).

Polyurethane nanofiber 3D structure model, generated from the SEM image in the previous section (see Figure 4), was utilized in the filtration modeling together with the following reference filtration parameters, which are based on the performed filtration experimental work: v_{if}=0.057 m/s, p=101325 Pa, T=300 K, µ'=0.031, ρ_p=1000 kg/m³, η'=3.8 10^5Pa s. Each particle has been traced through a clean filter, i.e. particle–particle interactions have been neglected, and number of exiting particles was determined for every group in order to calculate the filtration efficiency curve. In order to get the filtration efficiency average values and corresponding standard deviations, the simulations were repeated five times.

The newly proposed Euclidian distance map based approach, introduced in the previous section, was applied for the pressure drop calculation through the filter manufactured in this work (Figure 4) as well as for another four polyurethane nanofiber based filters for which pressure drops have already been determined in our previous work (see Figure 5 in [22]).

The comparison between the predicted and experimentally determined filtration efficiency and pressure drop data for the tested filter samples is provided in Figure 8 and Figure 9, respectively. It is nicely visible, that the model predictions are in a fairly good agreement with the corresponding experimental data which justifies the used model assumptions. It is important to note that even if the utilized methodology tends to overestimate the pressure drop by 34.1%, the filter samples ordering according to pressure drop is predicted correctly as visible in Figure 9.

For the cake formation modeling, the 3D filtration model depicted in Figure 4 was randomly penetrated with 25000 particles, having the particle size distribution the same as the nebulized ammonium sulphate solution used in the experimental filtration test (see Figure 3a), considering both particle-fiber and particle-particle interactions. Other parameters and assumptions were kept the same as in the filtration efficiency/pressure drop calculation. The cake formation for 0, 750, 2500, 5000, 7500, 10000, 15000, 20000, 25000 particles on the filter tested in this work is depicted in Figure 10 and Video 2 (see supplementary material). Clearly, deposited particles form dendrites in the beginning of the filtration process (at the filter top and in through the depth) as well as at the end where predominant filter cake formation takes place, which is in good agreement with the open literature [12]. The top views of the 25000 particles filled filter structure slices from the top to the bottom and a flight through the filled filter are provided in Video 3 and Video 4, respectively (see supplementary materials), clearly shows that the predicted cake structure, formed on the analyzed nanofiber based filter, is rather porous.

The theoretically predicted evolution of the filtration efficiency and the pressure drop during the filter clogging is depicted in Figure 11. It can clearly be seen that during the first stage, corresponding to the small linear pressure drop increase, the filtration efficiency grows dramatically until the loading point of cake formation is reached (approximately until 12000 particles), causing the rate of efficiency increase to fall, which is (within the comparable particle sizes range and loading) in good agreement with the experimental work of Thomas et al. [13].

In order to more deeply understand the particle-fiber friction coefficient effect on the cake build up, filtration efficiency, pressure drop and quality factor of the nanofiber based filters, its value was varied from 0 to 0.025 in the utilized filtration model. The 3D filter model was randomly penetrated with 50000 particles, with an experimentally defined particle size distribution shown in Figure 3a. The filtration efficiency, the pressure drop and quality factor (calculated by Eq. 1) was recorded during the filter clogging as a function of the captured particle mass area for different particle-fiber frictions and the results are depicted in Figure 12. Clearly, the increase in the fiber-particle friction coefficient leads to lower pressure drop, higher filtration

efficiency and higher quality factor. On the other hand, the filter samples with higher fiber-particle friction coefficient shows much higher quality factor reduction with the increased collected particle mass in comparison with the filter samples having lower fiber-particle friction coefficient, as visible in Figure 12b. These trends can be understood through analysis of 3D views of all tested filters filled by the particles (see Figure 13), corresponding penetration particle profile inside the filters (Figure 14), filter depth dependent characteristic pore radius (Figure 15) and pressure drop profile (Figure 16) where it can be clearly seen that decrease in the particle-fiber friction coefficient leads to more deeper particle penetration in the filter, creation of smaller pores and generation of higher pressure drop in comparison with higher particle-fiber friction coefficient filters. On the other hand, the pressure drop through the filter cake is comparable for all tested filters samples due to their similar morphology as indicated in Figure 15.

CONCLUSIONS

Polyurethane nanofiber based filter has been prepared by electrospinning process having average fiber diameter and average pore size equal to 133nm and 156 nm, respectively, thickness 3.59 μm, mass area 0.54 g/m^2, maximum penetration pore size 70 nm, minimum filtration efficiency 98.32 %, average pressure drop 148.5 Pa and quality factor 27.5 kPa^{-1}.

The realistic SEM image based 3D filter model, transition/free molecular flow regime, Brownian diffusion, aerodynamic slip, particle-fiber and particle-particle interactions has been utilized for the prepared polyurethane nanofiber based filter in order to more deeply understand the filtration cake formation and its role on the final filter efficiency. The performed analysis has revealed that the cake structure formed on the analyzed nanofiber based filter is dendrites based and rather porous.

Novel, Euclidian distance map based methodology to calculate the pressure drop through the 3D filter model has been proposed and tested with corresponding experimental data. It has been found that even if the utilized theoretical approach tends to over predict the pressure drop by approximately 35%, the filter samples ordering according to pressure drop is predicted correctly.

Based on the performed theoretical analysis, it has been revealed that the decrease in the fiber-particle friction coefficient leads to higher pressure drop, lower filtration efficiency, lower quality factor and lower quality factor sensitivity to the increased collected particle mass due to more weaker particle penetration in the filter, creation of bigger pores and generation of lower pressure drop in comparison with lower particle-fiber friction coefficient filters. Moreover, it has been revealed that even if the particle-fiber friction coefficient is different, the cake morphology is very similar.

ACKNOWLEDGMENTS

LIST OF SYMBOLS

β	[-]	Relaxation frequency of the particle
$\dot{\gamma}$	[s^{-1}]	Shear rate at the fiber wall
ζ_i	[-]	Zero-mean
η	[Pa s]	Fluid viscosity
η'	[Pa s]	Knudsen number dependent fluid viscosity
λ	[m]	Mean free path of gas molecules
ρ_p	[kg/m³]	Particle density
τ_w	[N/m²]	Local fiber wall shear stress
μ	[-]	Kn number dependent particle-fiber friction coefficient
μ'	[-]	Particle-fiber friction coefficient
Δt	[sec]	Time step
Δp	[Pa]	Pressure drop
a	[m]	Adhesive distance (0.4×10^{-9} m)
a_0	[-]	Constant 0=1.066,
a_1	[-]	Constant 1=0.679
a_2	[-]	Constant 2= -2.082
a_3	[-]	Constant 3= 0.866
C_c	[-]	Cunningham slip correction factor
d_i	[m]	Local distance map value
d_{max}	[m]	Maximum distance map value
d_f	[m]	Fiber diameter
d_p	[m]	Particle diameter
d_m	[m]	Collision diameter of an air molecule ($3.7.10^{-10}$ m)
E	[-]	Filtration efficiency at MPPS
f	[-]	Parameter for friction reduction as a function of Kn_p
F_A	[N]	Adhesion force
F_{bi}	[N]	Brownian white noise excitation
F_D	[N]	Drag force

F_F	[N]	Friction force
F_L	[N]	Lift force
F_N	[N]	Normal force
$\hbar\bar{\omega}$	[J]	Lifschitz-van der Waals constant (10^{-20} J)
j	[-]	Integer
k	[J/K]	Boltzmann constant ($1.380\,6504\times10^{-23}$ J/K)
Kn	[-]	Knudsen number
Kn_p	[-]	Particle diameter based Knudsen number
L	[m]	Slice Thickness
n	[-]	Overall number of pixels
N_a	[mol^{-1}]	Number of Avogadro (6.02214179×10^{23} mol^{-1})
N_{in}	[-]	Number of entering particles
N_{out}	[-]	Number of exiting particles
p	[Pa]	Pressure
Q	[m³/s]	Volume flow rate
QF	[kPa^{-1}]	Quality factor
R	[J K^{-1}mol^{-1}]	Gas constant (8.314472 J mol^{-1} K^{-1})
R_1	[m]	Sphere radius 1
R_2	[m]	Sphere radius 2
R_C	[m]	Characteristic Poresize
scale	[m/px]	Pixel resolution
S_{nn}	[W m^{-2} sr^{-1}Hz^{-1}]	Spectral intensity
T	[K]	Temperature
U	[-]	Single random coefficient $U \in [0; 1[$
v_{if}	[m/s]	Fluid velocity in x, y, or z direction
v_{ip}	[m/s]	Particle velocity in x, y, or z direction

REFERENCES

[1]   LEUNG, W.W.F., Hung C.H. and YUEN P.T. Experimental Investigation on Continuous Filtration of Sub-Micron Aerosol by Filter Composed of Dual-Layers Including a Nanofiber Layer, *Aerosol Sci. Tech.* 2009, vol. 43, no. 12, p. 1174-1183.

[2]   LEUNG, W.W.F., Hung C.H. and YUEN P.T. Effect of face velocity, nanofiber packing density and thickness on filtration performance of filters with nanofibers coated on a substrate, *Sep. Purif. Technol.* 2010, vol. 71, no.1, p.30-37.

[3]   PODGORSKI, A., BALAZY A. and GRADON L. Application of nanofibers to improve the filtration efficiency of the most penetrating aerosol particles in fibrous filters, *Chem. Eng. Sci.* 2006, vol. 61, p.6804-6815.

[4]   HOSSEINI S.A. and TAFRESHI H.V. Modeling particle filtration in disordered 2-D domains: A comparison with cell models, *Sep. Purif. Technol.* 2010, vol. 74, p.160-169.

[5]   ZHOU B., TRONVILLE P. and RIVERS R. Generation of 2-Dimensional Models for CFD Simulation of Fibrous Filter Midea with Binder, *Fibers and Polymers* 2009, vol. 10, no. 4, p.526-538.

[6]   SAMBAER W., ZATLOUKAL M. and KIMMER D. 3D modeling of filtraion process via polyurethane nanofiber based nonwoven filters prepared by electrospinning process, *Chem. Eng. Sci.* 2011, vol. 66, p.613-623.

[7]   MAZE B., TAFRESHI H.V., WANG Q., POURDEYHIMI B. A simulation of unsteady-state filtration via nanofiber media at reduced operating pressures, *J. Aerosol Sci.* 2007, vol. 38, no. 5, p.550-571.

[8]   HOSSEINI S.A. and TAFRESHI H.V. Modeling permeability of 3-D nanofiber media in slip flow regime, *Chem. Eng. Sci.* 2010, vol. 65, p.2249-2254.

[9]   HOSSEINI S.A. and TAFRESHI H.V. 3-D simulation of particle filtration in electrospun nanofibrous filters, *Power Technol.* 2010, vol. 201, p.153-160.

[10]   REBAÏ, M., DROLET F., VIDAL D., VAKEIKO I., BERTRAND F. A Lattice Boltzmann Approach for Predicting the Capture Efficiency of Random Fibrous Media, *Asia-Pac. J. Chem. Eng.* 2011, vol. 6, p.26-37.

[11]   JAGANATHAN, S., TAFRESHI H.V. and POURDEYHIMI B. A realistic approach for modeling permeability of fibrous media: 3-D imaging coupled with CFD simulation, *Chem. Eng. Sci.* 2008, vol. 63, p.244-252.

[12]   ELMOE, T.D., TRICOLI A., GRUNWALDT J, PRATSINIS S. Filtration of nanoparticles: Evolution of cake structure and pressure-drop, *J. Aerosol Sci.* 2009, vol. 40, p.965-981.

[13] THOMAS, D., PENICOT P., CONTAL P., LECLERC D. and VENDEL J. Clogging of fibrous filters by solid aerosol particles: Experimental and modelling study, *Chem. Eng. Sci.* 2001, vol. 56, p.3549-3561.

[14] BILLINGS, C.E. Effects of particle accumulation in aerosol filtration, *PhD Thesis*, California Institute of Technology, Pasadena, USA, 1966, 220p.

[15] KANAOKA, C., and HIRAGI S. Pressure drop of air filter with dust load, *J. Aerosol Sci.* 1990, vol. 21, p.127-137.

[16] WITTEN, T., SANDER L. Diffusion-limited aggregation, *Physical Review Letters* 1983, vol. 27, p.5686.

[17] PAYATAKES, A.C. and GRADON L. Dendritic deposition of aerosol by convective Brownian diffusion for small, intermediate and high particle Knudsen numbers, *American Int. Chem. Eng. J.* 1980, vol. 26, p.443-454.

[18] CHEUNG, C.S., CAO Y.H. and YAN Z.D. Numerical Model for particle deposition and loading in electret filter with rectangular split-type fibers, *Computation Mechanics* 2005, vol. 35, no. 6, p.449-458.

[19] KANAOKA, C., HIRAGI S. and TANTHAPANICHAKOON T. Stochastic simulation of the agglomerative deposition process of aerosol particles on an electret fiber, Powder *Technol.* 2001, vol. 118, no. 1-2, p.97–106.

[20] HUANG, B., TURTON R., PARK J., FAMOURI P, and BOYLE E.J. Dynamic model of the riser in circulating fluidized bed, *Powder Technol.* 2006, vol. 163, no. 1-2, p. 23-31.

[21] KARADIMOS, A. and OCONO R. The effect of the flow field recalculation on fibrous filter loading: a numerical simulation, *Powder Technol.* 2003, vol. 137, p.109-119.

[22] CHANG, Y., HUANG, Y., LUO Z. and ZHANG G. A study on particle deposition morphology within a constricted tube in the presence and absence of the detachment mechanism, *Sep. Purif. Technol.* 2008, vol. 63 p.566-576.

[23] SAMBAER, W., ZATLOUKAL, M. Determination of Pressure Drop and Filtration Efficiency of Filled Nanofiber Based Filters by using 3D Filtration Model, *Recent Advances in Fluid Mechanics, Heat & Mass Transfer and Biology - Proc. of the 9th WSEAS Int. Conf. on FLUIDS'12, 9th WSEAS Int. Conf. on HMT'12, 9th WSEAS Int. Conf. on MABE'12*, pp. 144-149.

[24] SAMBAER, W., M. ZATLOUKAL M. and KIMMER D. The use of novel digital image analysis technique and rheological tools to characterize nanofiber nonwovens, *Polym. Test.* 2010, vol. 29, p.82–94.

[25] SAMBAER, W., ZATLOUKAL, M., KIMMER, D. 3D Air Filtration Modelling for Nanofiber Based Filters in the Ultrafine Particle Size Range, *AIP Conference Proceedings* 2011, vol. 1375.

[26] ALTMANN, J., RIPPERGER, S. Particle deposition and layer formation at the crossflow microfiltration, *J. Membrane Sci.* 1997, vol. 124, p.119-128.

[27] MCNENLY, M.J., GALLIS, M.A., and BOYD, I.D., Empirical slip and viscosity model performance for microscale gas flow, *Int. J. Numer. Meth. Fl.* 2005, vol. 49, p.1169-1191.

[28] RUBIN, G., Widerstands und Auftreibsbeiwerte von ruhenden kugelformigen Partikeln in stationaren, wandnahen laminaren Grenzschichten, PhD Thesis, TH Karlsruhe, Germany, 1977.

[29] MCLAUGHLIN, J.B. The lift on a small sphere in wall-bounded linear shear flows, *J. Fluid. Mech.* 1993, vol. 246, p.249-265.

[30] BHUSHAN, B. *Nanotribology and Nanomechanics: An Introduction*, Springer 2005, 1148p.

[31] MÄDLER L., LALL A.A. and FRIEDLANDER S.K. One-step aerosol synthesis of nanoparticle agglomerate films: Simulation of film porosity and thickness, *Nanotechnology* 2006, vol. 17, no. 19, p. 4783–4795.

[32] RODRÍGUEZ-PÉREZ D., CASTILLO J.L. and ANTORANZ J.C. Relationship between particle deposit characteristics and the mechanism of particle arrival, *Physical Review* Letters 2005, vol. 72, no. 2, p. 021403-1–021403-9.

[33] PRZEKOP, R., GRADON, L. Deposition and Filtration of Nanoparticles in the Composites of Nano- and Microsized Fibers, *Aerosol Science and Technology* 2008, vol. 42, p. 483-493.

[34] WANG H.C. and KASPER G. Filtration efficiency of nanometer-size aerosol-particles, *J. Aerosol Sci.* 1991, vol. 22 , no. 1, p. 31–41.

[35] PAWU K.T. and BRAATEN D.A. New perspectives on rebound and re-entrainment processes, *Aerosol Sci. Tech.* 1995, vol. 23 , no. 1, p. 72–79.

Table 1: Brownian motion equations.

Equation Type	Equation	No.
Velocity in time interval [jΔt; (j+U)Δt]	$$v_{i_p}\big((j+U)\Delta t\big)=\left(v_{i_p}(j\,\Delta t)-v_{i_f}-\frac{F_{b_i}}{\beta}\right).$$ $$e^{(-\beta U\Delta t)}+\frac{F_{b_i}}{\beta}+v_{i_f}$$	(1)
Velocity in time interval [(j+U)Δt; (j+1)Δt]	$$v_{i_p}\big((j+1)\Delta t\big)=\left(v_{i_p}\big((j+U)\Delta t\big)-v_{i_f}-\frac{F_{b_{i+1}}}{\beta}\right).$$ $$e^{(-\beta(1-U)\Delta t)}+\frac{F_{b_{i+1}}}{\beta}+v_{i_f}$$	(2)
Position in time interval [jΔt; (j+U)Δt]	$$x_{i_p}\big((j+U)\Delta t\big)=\left(\frac{v_{i_p}(j\,\Delta t)-v_{i_f}-\dfrac{F_{b_i}}{\beta}}{\beta}\right)$$ $$\big(e^{(-\beta U\Delta t)}-1\big)+\left(\frac{F_{b_i}}{\beta}+v_{i_f}\right)U\Delta t+x_{i_p}(j\Delta t)$$	(3)
Position in time interval [(j+U)Δt; (j+1)Δt]	$$x_{i_p}\big((j+U)\Delta t\big)=\left(\frac{v_{i_p}(j\,\Delta t)-v_{i_f}-\dfrac{F_{b_i}}{\beta}}{\beta}\right)$$ $$\big(e^{(-\beta U\Delta t)}-1\big)+\left(\frac{F_{b_i}}{\beta}+v_{i_f}\right)U\Delta t+x_{i_p}(j\Delta t)$$	(4)
Relaxation frequency of the particle	$$\beta=\frac{18\eta}{d_p^2\,\rho_p\,C_c}$$	(5)

Cunningham slip correction factor	$C_c = 1 + K_n \left(1.275 + 0.4e^{\frac{-1.1}{Kn}} \right)$	(6)
Knudsen number	$K_n = \dfrac{2\lambda}{d_f}$	(7)
Mean free path of gas molecules	$\lambda = \dfrac{R\,T}{\sqrt{2}\,N_a\,\pi d_m^2\,p}$	(8)
Brownian white noise excitation	$F_{b_i} = \varsigma_i \sqrt{\dfrac{\pi S_{nn}}{\Delta t}}$	(9)
Spectral intensity	$S_{nn} = \dfrac{3kT\beta}{\pi d_p^3 \rho_p}$	(10)

Table 2: Particle-Fiber interaction equations.

Equation Type	Equation	No.
Drag force	$F_D = 3.16\pi\tau_w d_p^2$	(11)
Wall shear stress	$\tau_w = \eta\dot{\gamma}$	(12)
Reduced gas viscosity	$\eta = \eta'\left[a_0 + a_1 \arctan\left(a_2 Kn^{a_3}\right)\right]$	(13)
Lift force	$F_L = \dfrac{0.761\tau_w^{1.5} d_P^{3} \rho_f^{0.5}}{\eta}$	(14)
Adhesion force	$F_A = \dfrac{1.25\,\pi\,\hbar\,\bar{\omega}}{6a^2}\left(\dfrac{R_1 R_2}{R_1 + R_2}\right)$	(15)
Friction force	$F_F = \mu\,F_{N_{tot}}$	(16)
Friction coefficient	$\mu = \mu'\,f$	(17)
Parameter as a function of Kn	$f = a_0 + a_1 \arctan\left(a_2 Kn_d^{a_3}\right)$	(18)
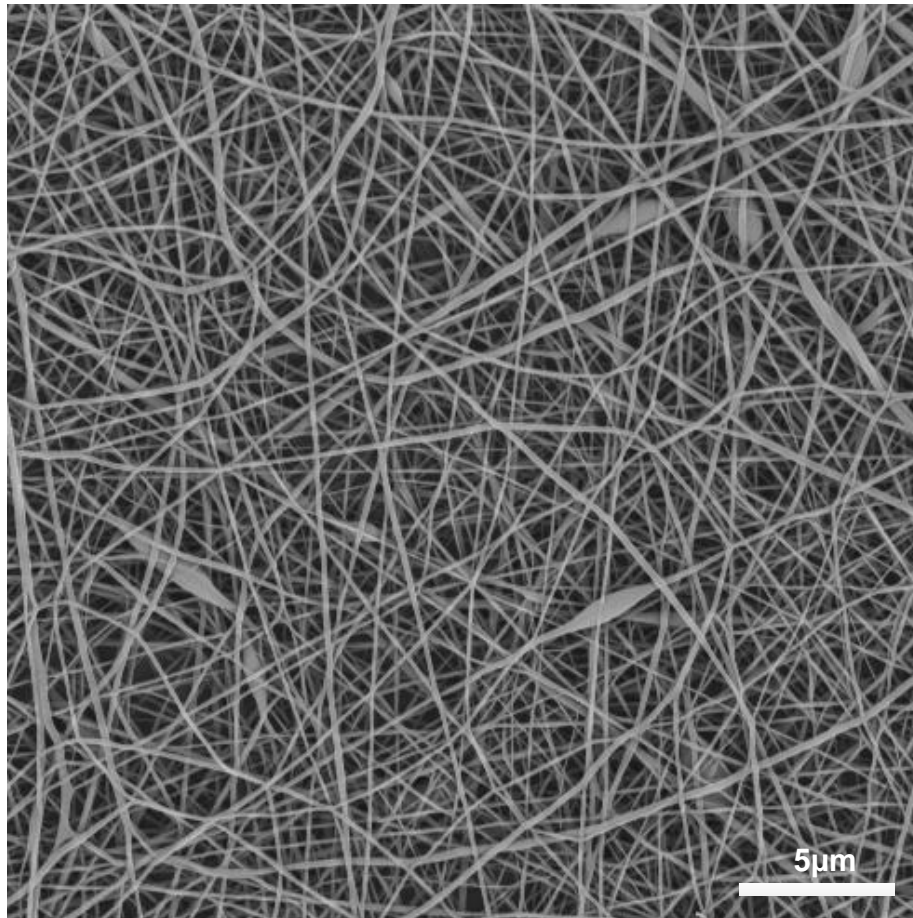
Figure 1: SEM image of the manufactured nanofiber based nonwoven filter.

a.

Pore Size Statistics
D_{avg} = 156 nm

b.

Fiber Diameter Statistics
Data points used = 65546
Diameter = $10^{2.124 \pm 0.13}$ nm
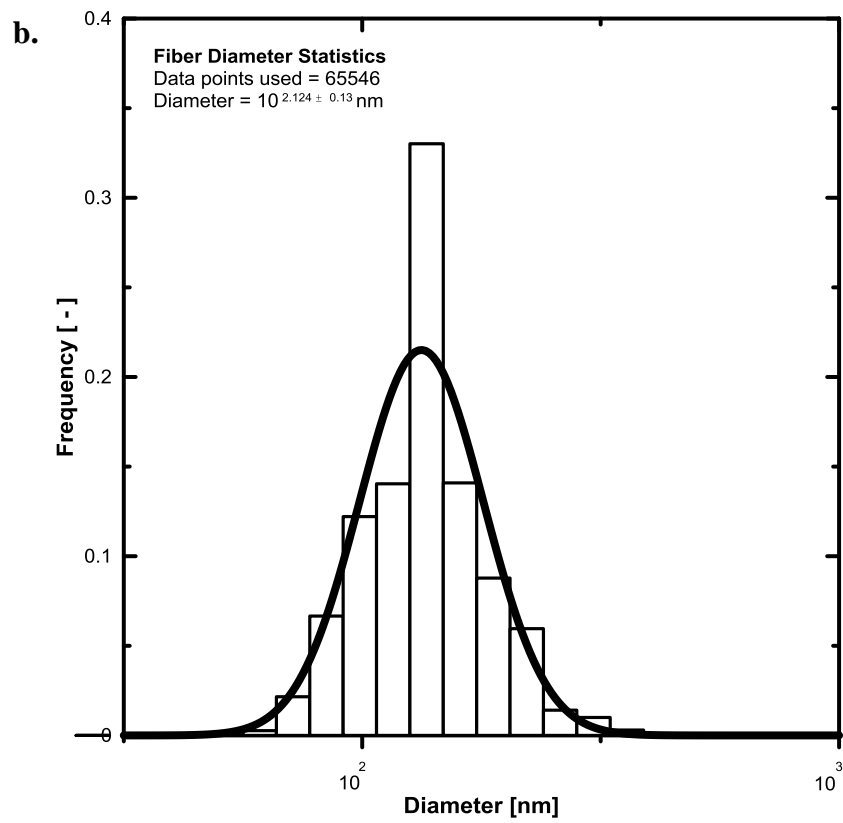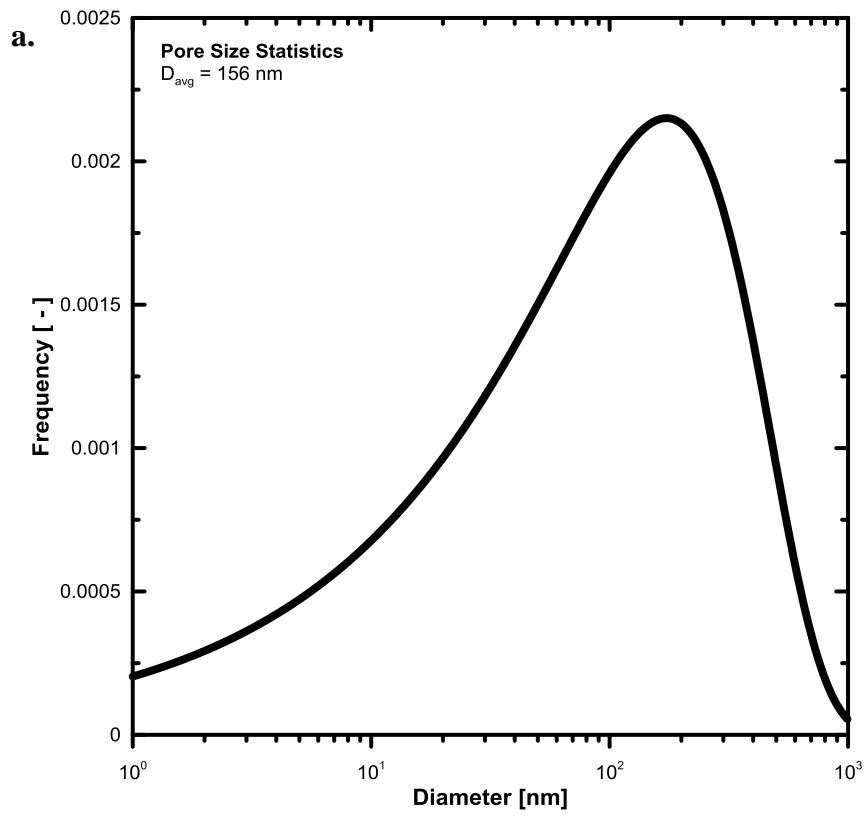
Figure 2: Pore size (a.) and fiber diameter (b.) distribution of the analyzed filter.

IV.26
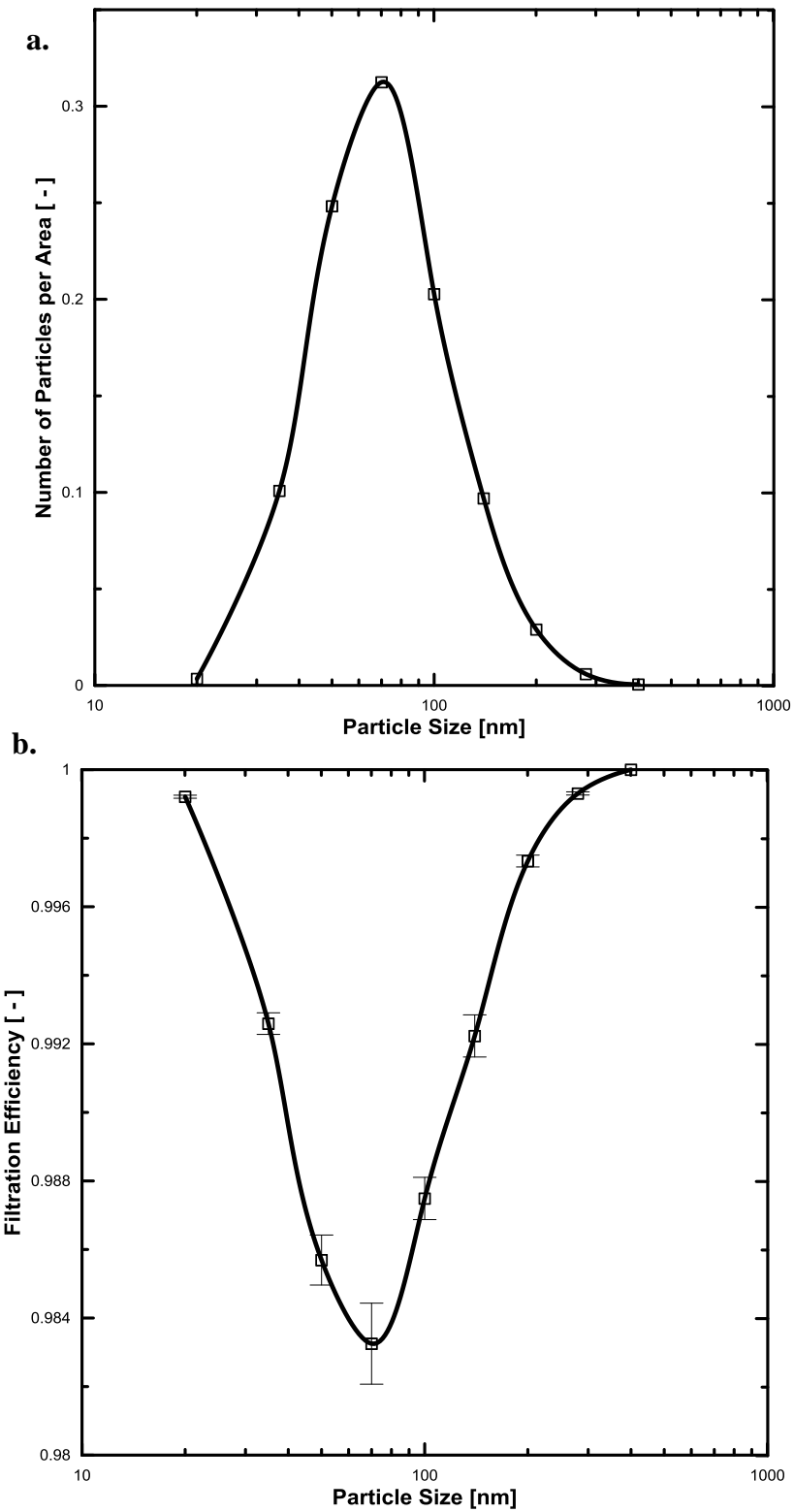
Figure 3: a: The particle size distribution of the nebulized ammonium sulphate solution.
b: Experimentally determined filtration efficiency of the manufactured filter.

IV.27

Perspective View
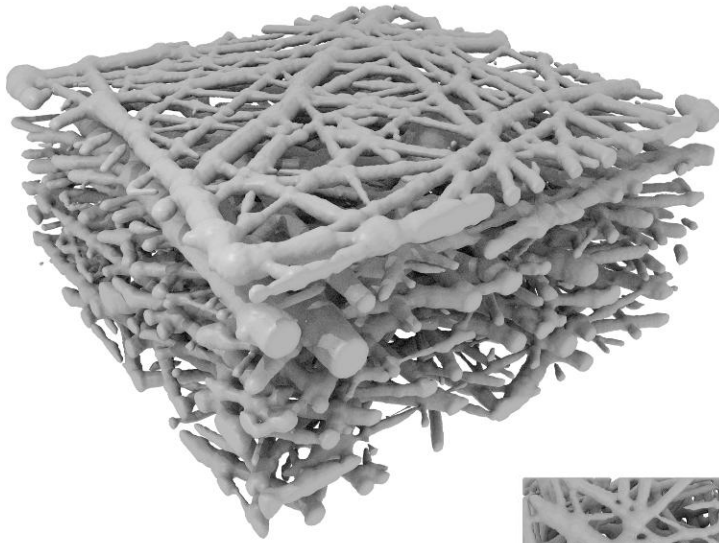
Top View
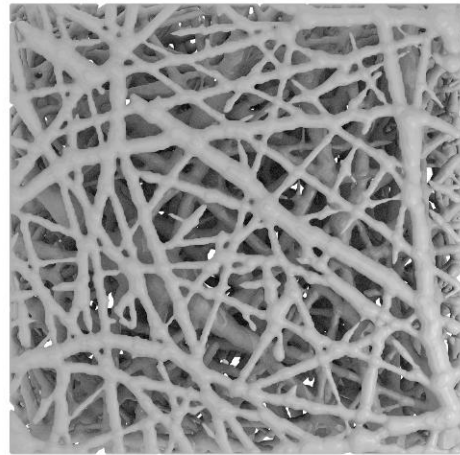
Side View
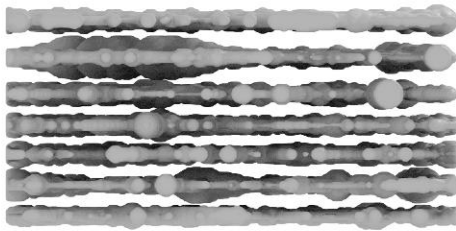
Figure 4: Full 3D structure model of the manufactured filter.
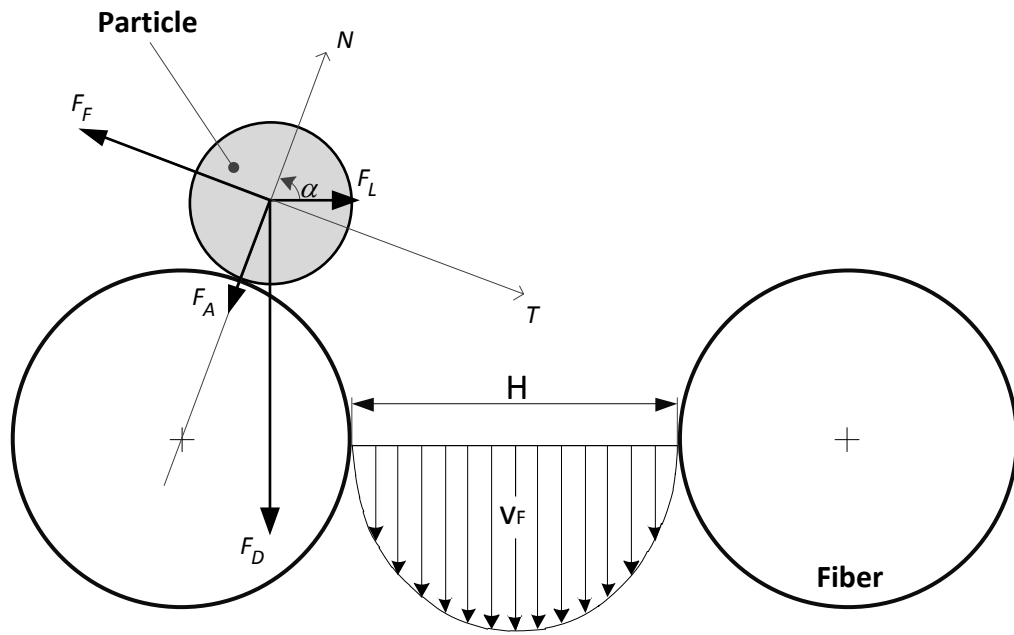
Figure 5: Fiber local coordinate system based force balance utilized for particle-fiber interaction modeling.

IV.29
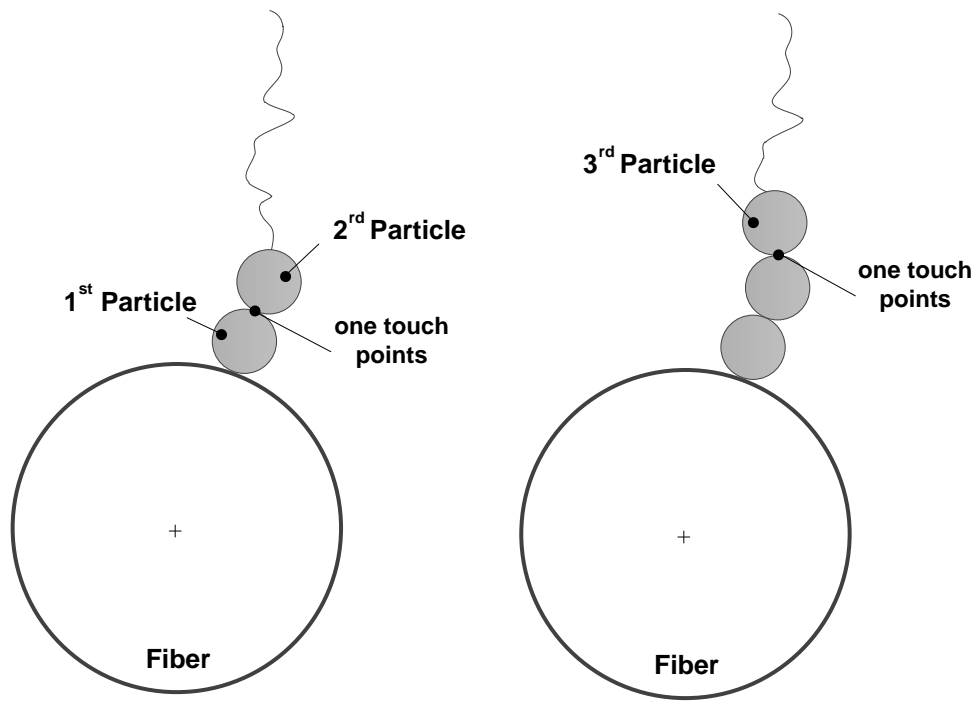
Figure 6: Description of the applied single touching point boundary condition for the particle-particle interaction modeling.
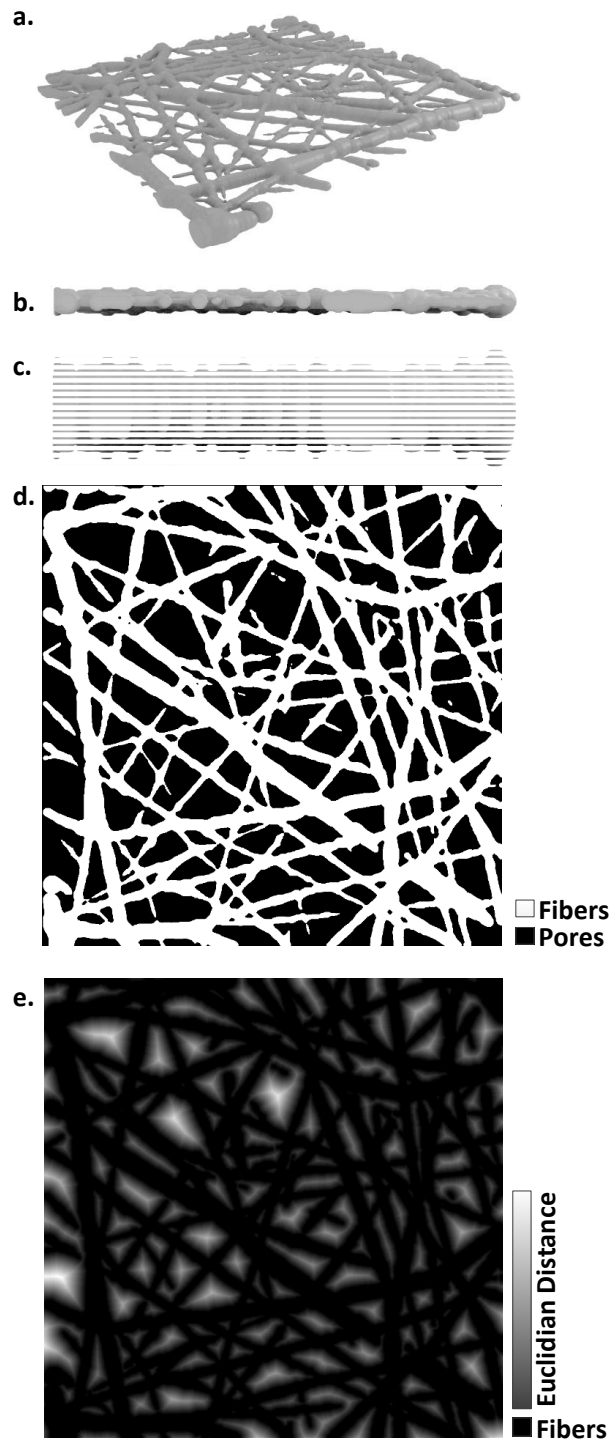
Figure 7: Description of the Euclidian distance map generation for particular filter slice layer. 7a) Perspective view of the 3D filter model, 7b) Side view of the 3D filter model. 7c) Binary slice layers. 7d) Top view of the one binary slice layer. 7e) Euclidian distance map for the one slice layer.
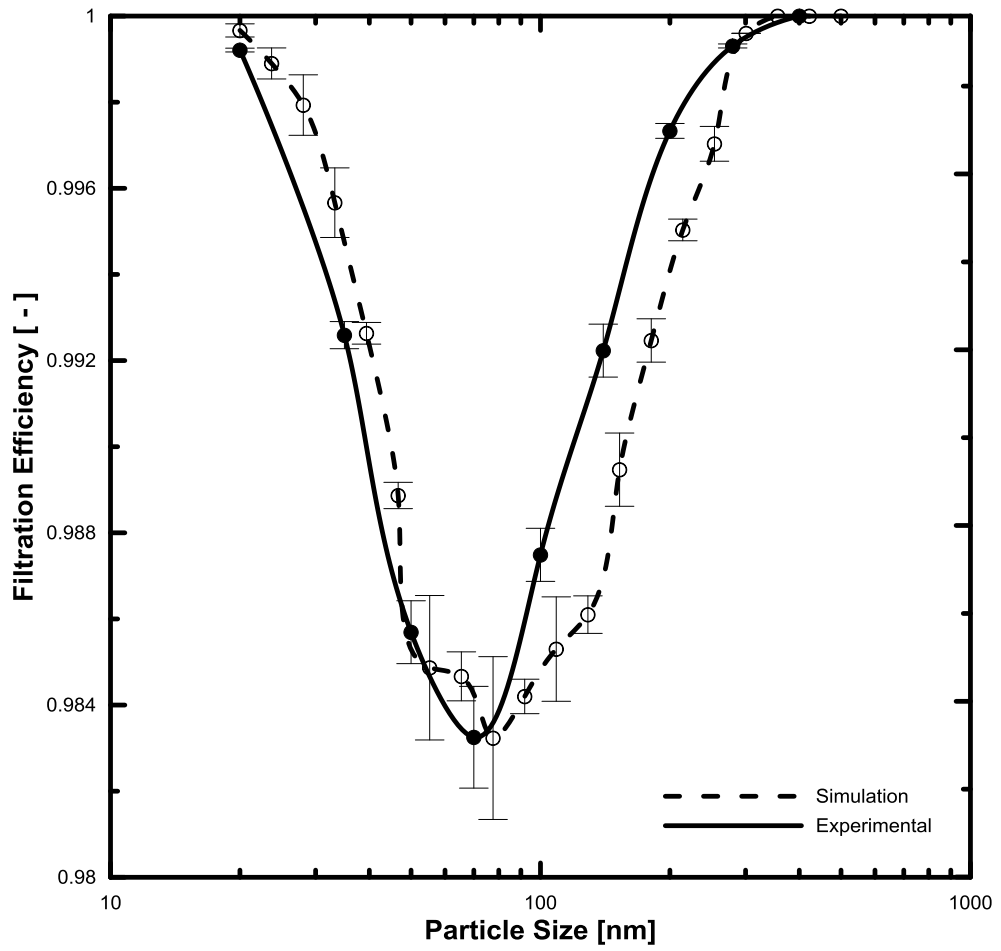
Figure 8: Comparison between measured and predicted filtration efficiency curves for the manufactured filter.
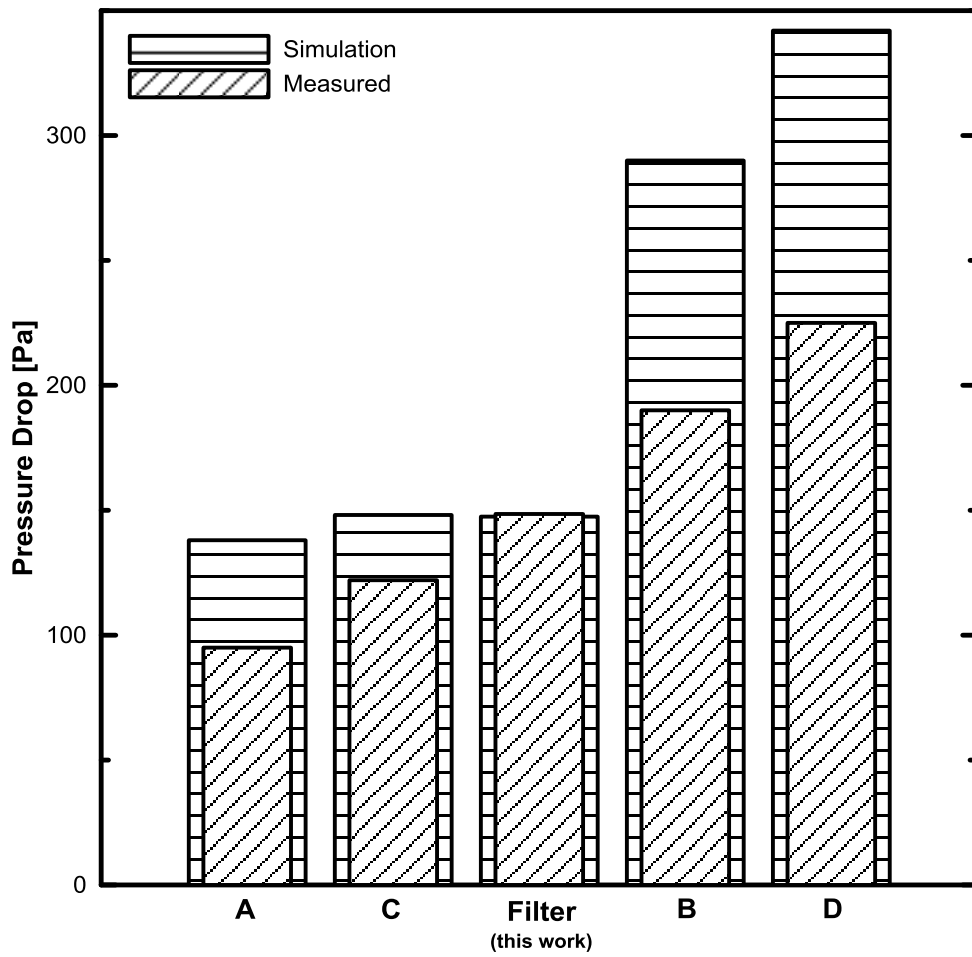
Figure 9: Comparison between measured and predicted pressure drops for different nanofiber based filters.
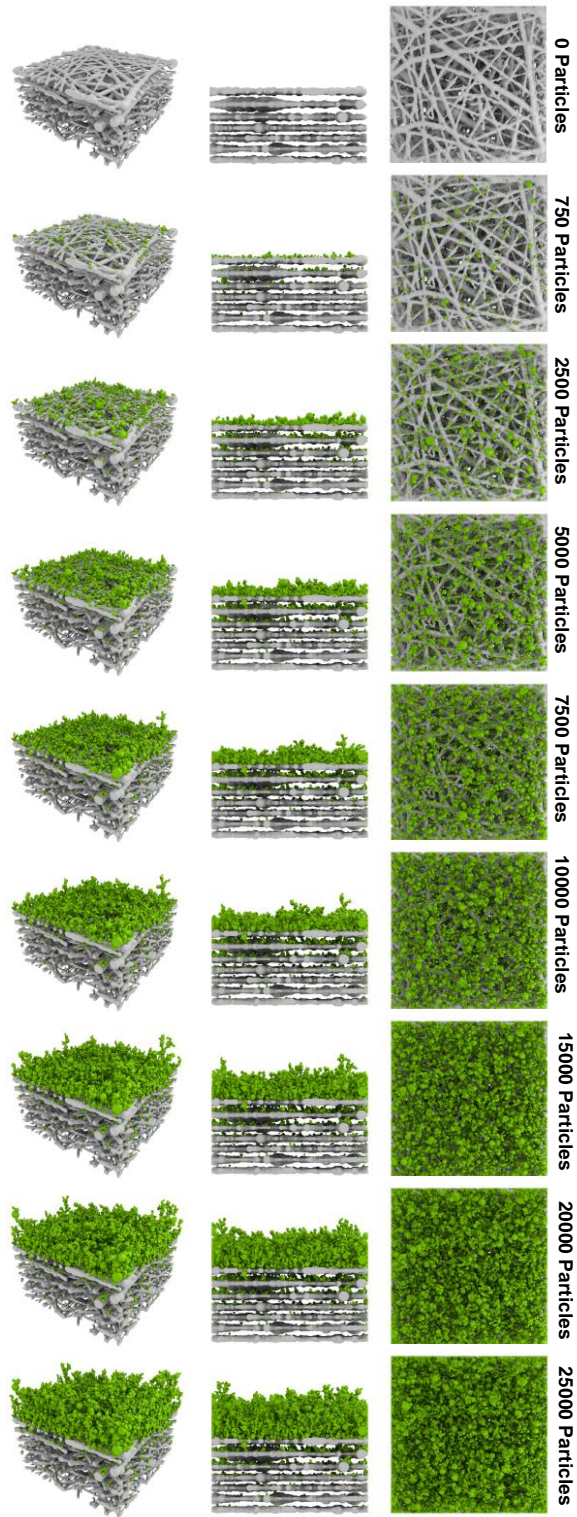
Figure 10: The cake filtration modeling for different number of particles (left – perspective view, middle - side view, right – top view).
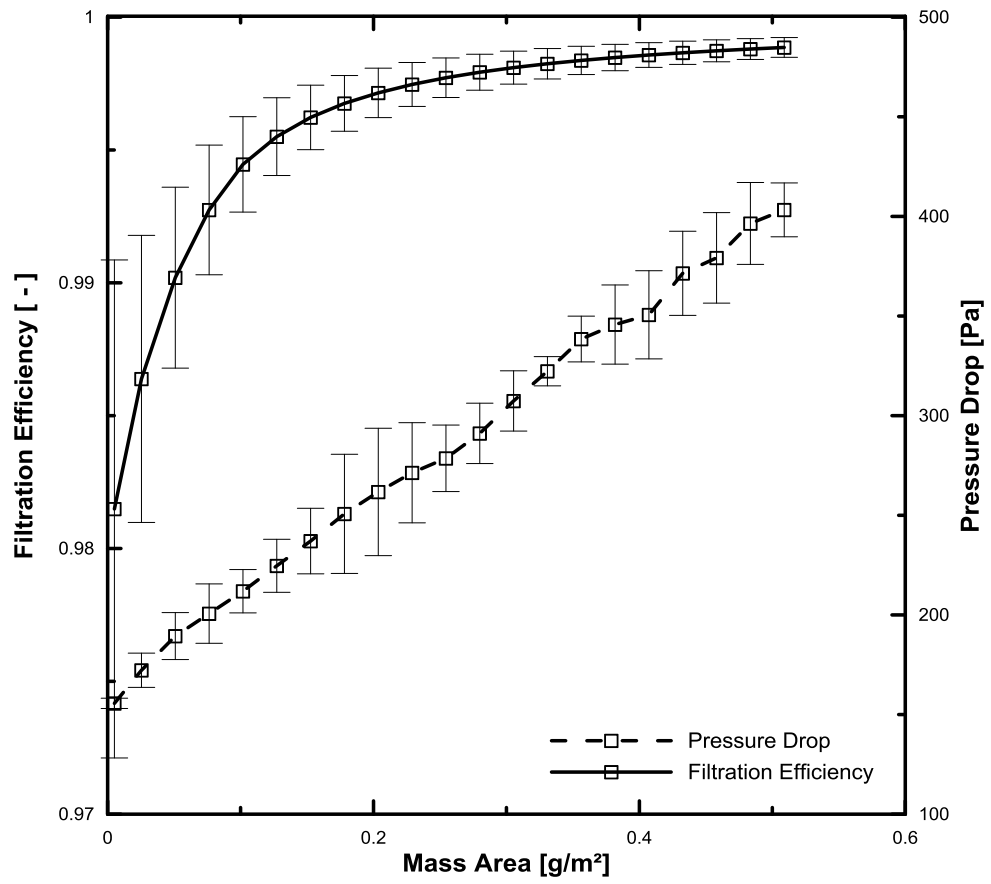
IV.34

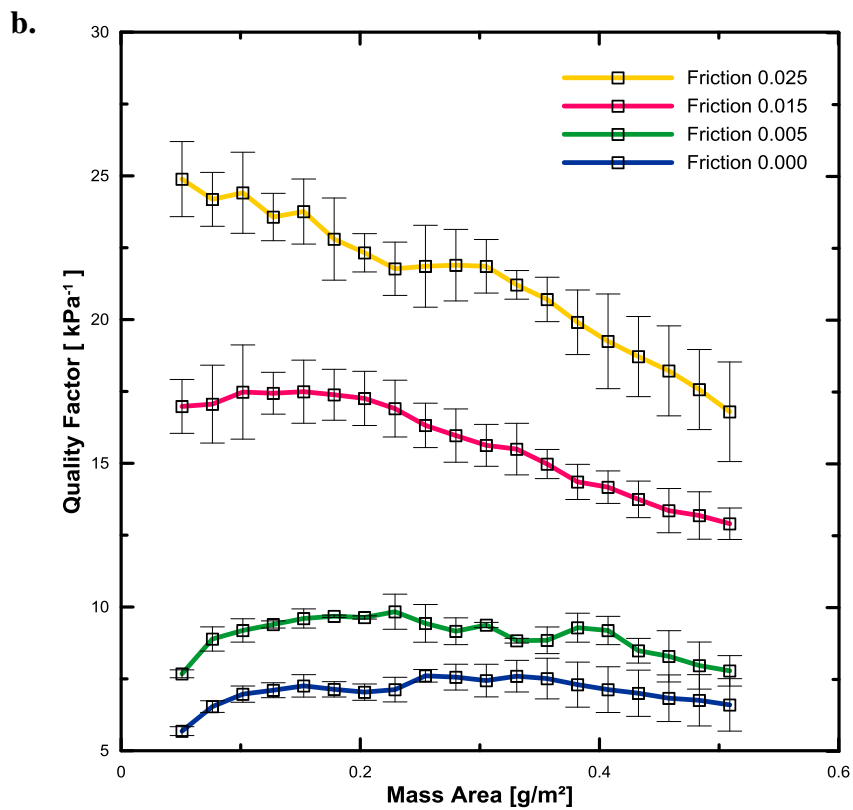*Figure 11: Evolution of filter efficiency and pressure drop during particle clogging.*
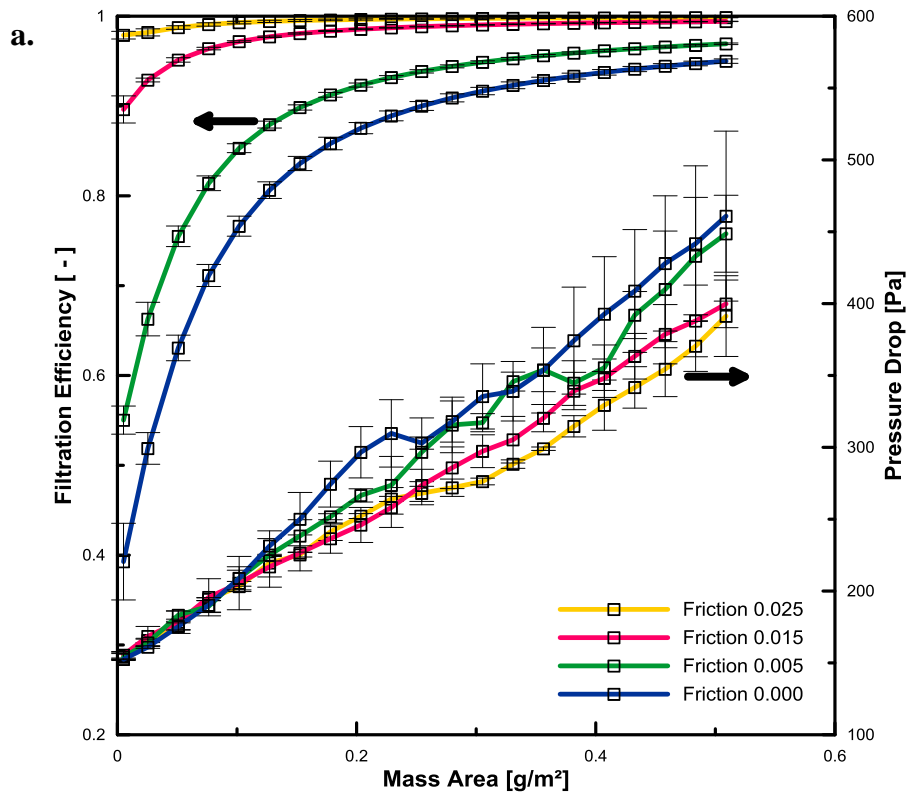
Figure 12: The effect of particle-fiber friction coefficient on basic filtration characteristics during particle clogging. 12a) Filtration efficiency and pressure drop. 12b) Quality factor.
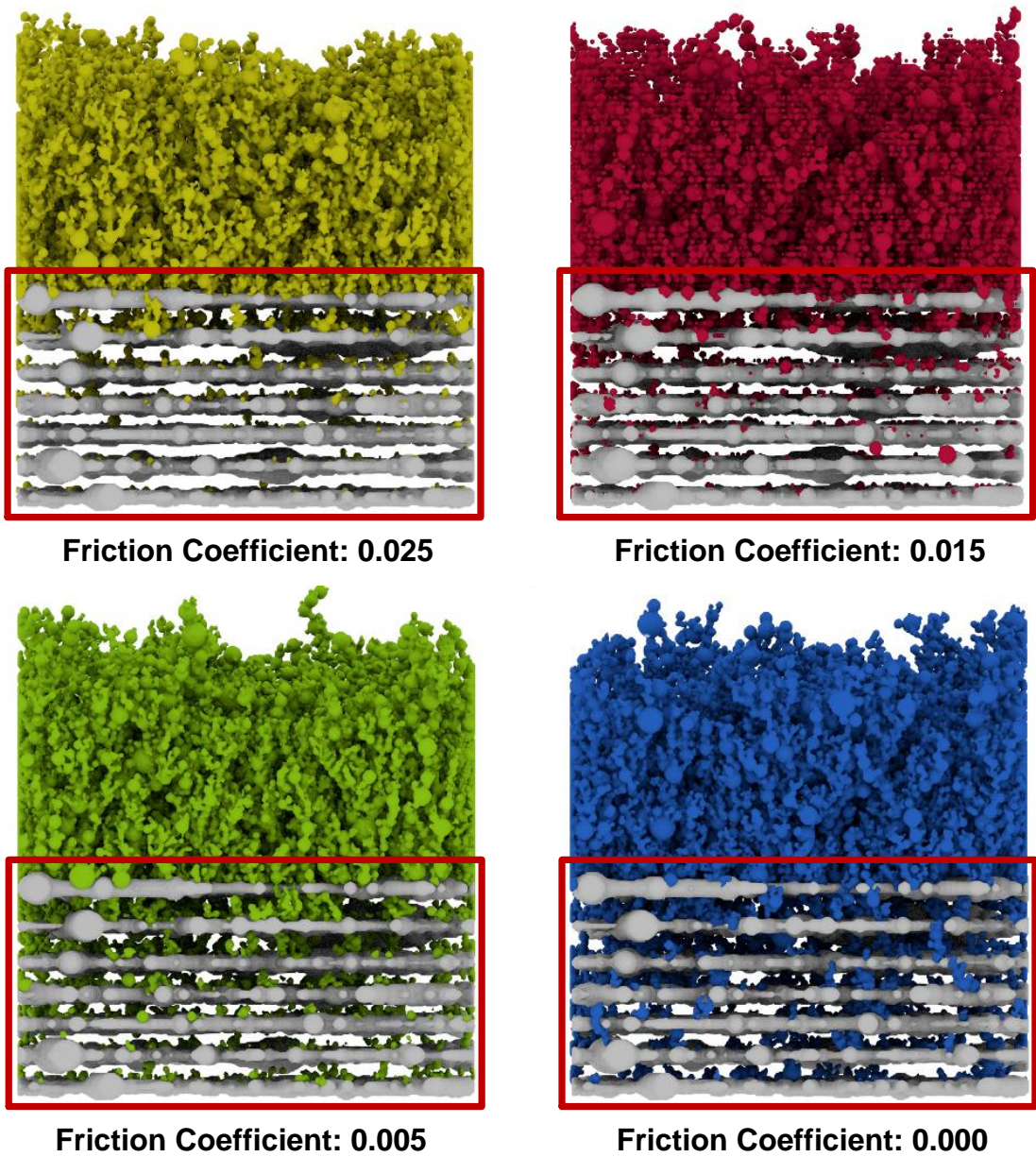
Friction Coefficient: 0.025

Friction Coefficient: 0.015

Friction Coefficient: 0.005

Friction Coefficient: 0.000

Figure 13: The effect of particle-fiber friction coefficient on particle penetration in the filter and cake build up for 50 000 particles.
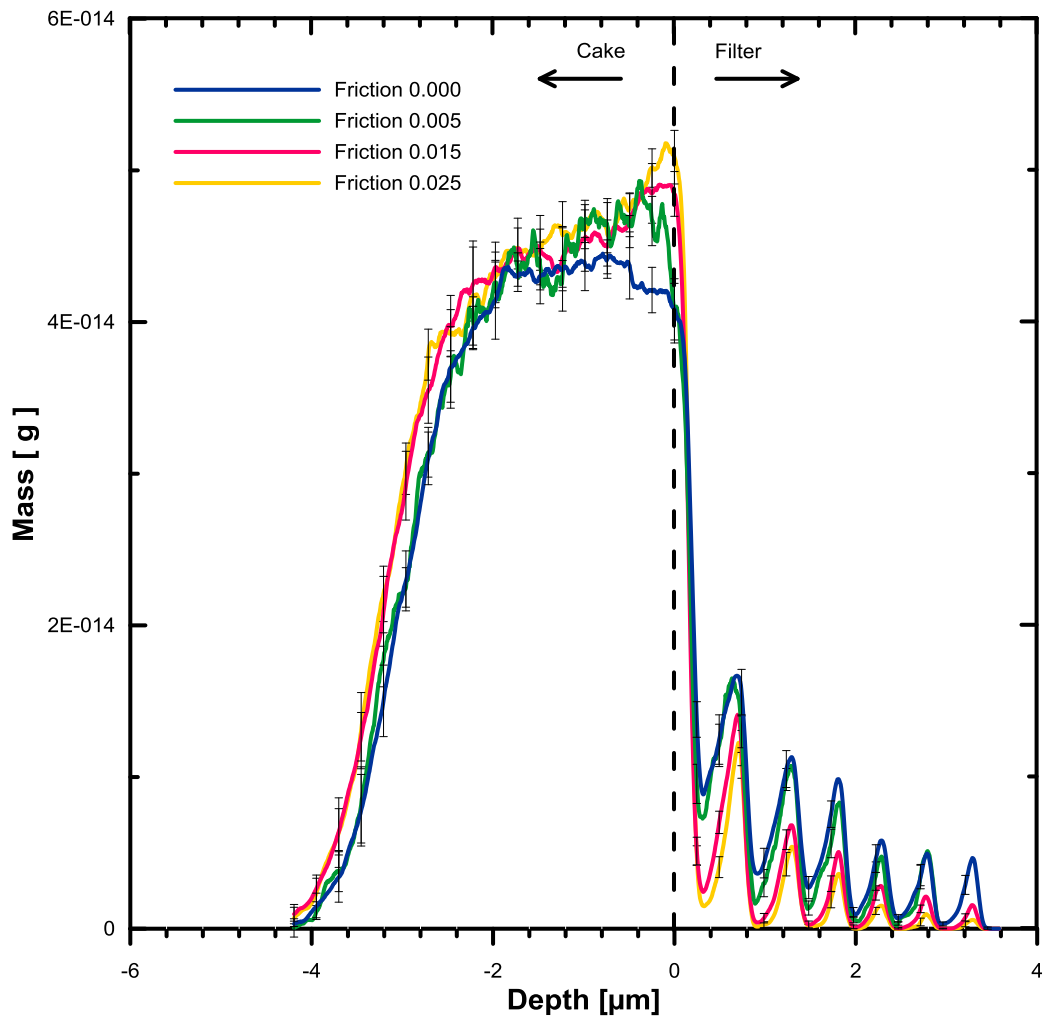
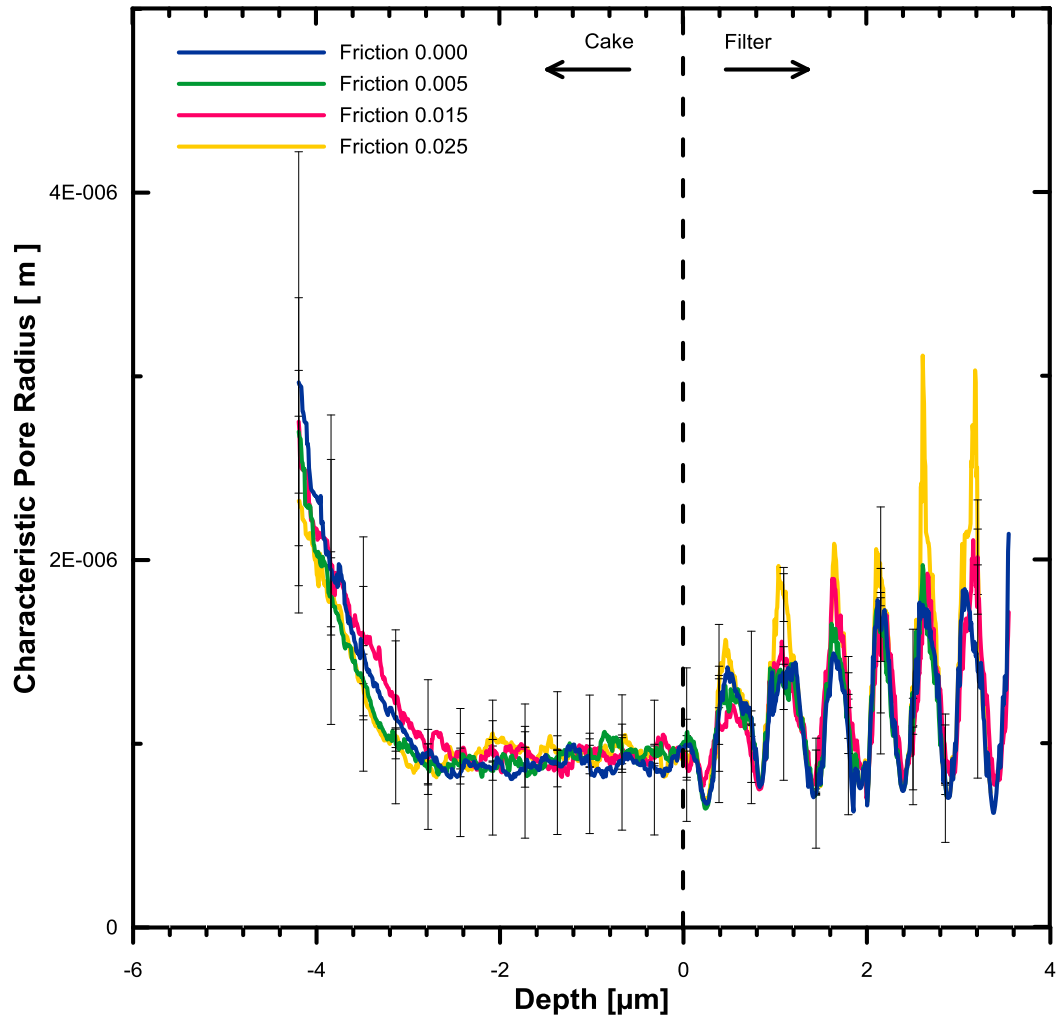*Figure 14: Effect of particle-fiber friction coefficient on the penetration particle profile inside the filter.*

IV.38

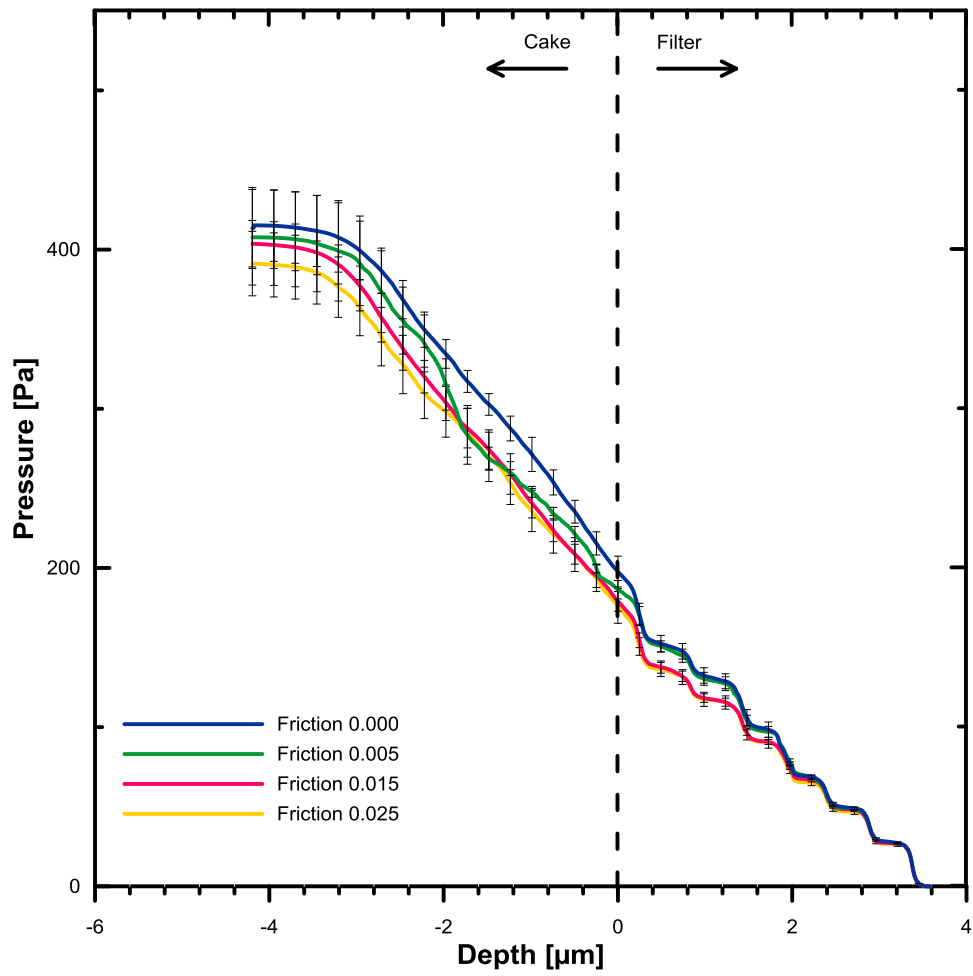*Figure 15: Effect of particle-fiber friction coefficient on the filter depth dependent characteristic pore radius.*

IV.39

Figure 16: Effect of particle-friction coefficient on the pressure drop profile.

CURRICULUM VITAE

Personal Information

Name:	*Wannes*
Surname:	*Sambaer*
Nationality:	*Belgian*
Date of Birth:	*5th September 1985*
Place of Birth:	*Roeselare (Belgium)*
E-mail:	*wannessambaer@gmail.com*

Working Activities

Since 2012	*Junior Researcher at the Tomas Bata University in Zlin, Czech Republic*
2011	*Part-time employer at the Tomas Bata University in Zlin, Czech Republic*

Education and Academic Studies

Since 2008	*Tomas Bata University in Zlin,* *Faculty of Technology,* *Polymer Centre,* *Doctoral Student,* *Zlin, Czech Republic*
2008 (4 months)	*Study stay at Tomas Bata University in Zlin,* *Faculty of Technology,* *Zlin, Czech Republic*
2006-2008	*KHBO (Katholieke Hogeschool Brugge Oostende),* *IW&T Department,* *Master Student,* *Oostende, Belgium*
2003-2006	*KHBO (Katholieke Hogeschool Brugge Oostende),* *IW&T Department,* *Bachelor Student,* *Oostende, Belgium*

Projects:

- *Grant GA AV ČR IAA200600703 "Investigation of flow behavior for a novel class of metallocene-based polymers"(2007-2011)–member of research team.*

- *Grant GA ČR 103/09/2066 "Analysis and development of constitutive equations for description of non-Newtonian fluids" (2009-2013) – member of research team.*

- *Grant GA ČR P108/10/1325 "Applied rheology for advanced polymer processing" (2010-2014) – member of research team.*

- *Internal Grant UTB IGA/3/FT/10/D "Modelling of the vortex development during polymer extrusion process" (2010) – project leader.*

- *Ministry of Education, Youth and Sports of the Czech Republic project MSM 7088352101 "Multifunctional composite systems based on natural and synthetic polymers" (2005-2011) – member of research team.*

- *Internal Grant UTB IGA/2/FT/11/D "Investigation of negative die drool phenomenon during polymer extrusion" (2011) – member of research team.*

Publications abstracted on Web of Science and Scopus databases:

- SAMBAER, W., ZATLOUKAL, M., KIMMER, D. 3D modeling of filtration process via polyurethane nanofiber based nonwoven filters prepared by electrospinning process, *Chemical Engineering Science* 2011, vol. 66, no.4, p. 613-623.

- SAMBAER, W., ZATLOUKAL, M., KIMMER, D. The use of novel digital image analysis technique and rheological tools to characterize nanofiber nonwovens, *Polymer Testing* 2010, vol. 29, no. 1, p. 82-94.

- SAMBAER, W., ZATLOUKAL, M., KIMMER, D. 3D Air Filtration Modelling for Nanofiber Based Filters in the Ultrafine Particle Size Range, *AIP Conference Proceedings* 2011, vol. 1375, p. 230-323, ISSN: 0094-243X.

- KIMMER, D., VINCENT, I., FENYK, J., PETRAS, D., ZATLOUKAL, M., SAMBAER, W., ZDIMAL, V., Morphology of nano and micro fiber structures in ultrafine particles filtration, *AIP Conference Proceedings* 2011, vol. 1375, p. 295-311, ISSN: 0094-243X.

- SAMBAER, W., ZATLOUKAL, M., KIMMER, D. The use of novel digital image analysis technique and rheological tools to characterize nanofiber nonwovens, *AIP Conference Proceedings* 2009, vol. 1152, p. 312-322, ISSN: 0094-243X.

- KIMMER, D., VINCENT, I., PETRAS, D., FENYK, J., ZATLOUKAL, M., SAMBAER, W.,SLOBODIAN, P., SALMELA, H., LEHTIMAKI, M., ZDIMAL, V., Application of nanofibers in filtration processes, *Nanocon 2010, 2nd international conference*, p. 415-422, Olomouc, Czech Republic, 2010, ISBN: 978-80-87294-19-2.
- SAMBAER, W., ZATLOUKAL, M., KIMMER, D. Investigation of Filtration Efficiency of Nanofiber Based Filters in Ultrafine Particles Range during Cake Formation, *Recent Advances in Fluid Mechanics, Heat & Mass Transfer and Biology - Proc. of the 9th WSEAS Int. Conf. on FLUIDS'12*, p. 138-143, Boston, USA, 2012, ISBN: 978-1-61804-067-1.
- SAMBAER, W., ZATLOUKAL, M., KIMMER, D. Determination of Pressure Drop and Filtration Efficiency of Filled Nanofiber Based Filters by using 3D Filtration Model, *Recent Advances in Fluid Mechanics, Heat & Mass Transfer and Biology - Proc. of the 9th WSEAS Int. Conf. on FLUIDS'12*, p. 144-149, Boston, USA, 2012, ISBN: 978-1-61804-067-1.
- SAMBAER, W., ZATLOUKAL, M., KIMMER, D. 3D modeling of Filtration Process Through Polymeric Nanofiber Based Nonwovens, *69th Annual Technical Conference of the Society of Plastics Engineers 2011, ANTEC 2011, Conference Proceedings*, vol. 2, p. 1149-1154, Boston, USA, 2011, ISBN: 978-161782960-4.
- SAMBAER, W., ZATLOUKAL, M., KIMMER, D. Advanced characterization of nanofiber based nonwovens, *68th Annual Technical Conference of the Society of Plastics Engineers 2010, Conference Proceedings*, vol. 1, p. 779-783, Orlando, USA, 2010, ISBN: 978-161738660-2.
- ZATLOUKAL, M., SAMBAER, W., LIBOTTE, A. Understanding and quantification of die drool phenomenon during polypropylene extrusion process, *67th Annual Technical Conference of the Society of Plastics Engineers 2009, Conference Proceedings*, vol. 3, p. 1572-1577, Chicago, USA, 2009, ISBN: 978-161567327-8.

Awards

Nomination Young Talent 2006 Electro-mechanic

Coauthor of 2009 ANTEC Best Paper Award in the Society of Plastic Engineers' (SPE) Extrusion Division.

SUPPLEMENTARY MATERIAL